Employing Aspherical Silica Microparticles as a Drug Delivery System for the Specific Repolarization of Human Lung Macrophages

Dissertation
zur Erlangung des Grades
des Doktors der Naturwissenschaften
der Naturwissenschaftlich-
Technischen Fakultät der
Universität des Saarlandes

von
Salma Al-Fityan

Saarbrücken

2023

Tag des Kolloquiums: 07.11.2023

Dekan: Univ.-Prof. Dr. Ludger Santen

Berichterstatter: Prof. Dr. Alexandra K. Kiemer
Prof. Dr. Marc Schneider

Vorsitz: Prof. Dr. Claus-Michael Lehr

Akad. Mitarbeiter: Dr. Matthias Engel

Abstract

Macrophages are involved in various diseases including tumors, chronic inflammatory diseases like asthma. The extremely heterogeneous population including proinflammatory (M1) type, which is active against pathogens and suppresses tumor growth, and tumor-associated macrophages (TAMs), that have a likeness to the regulatory and anti-inflammatory (M2) macrophages, facilitate tumor growth. We aimed to employ aspherical silica microparticles (µRs) as a targeted drug delivery system to deliver polyinosin:polycytidylic acid (poly(I:C)) to reprogram TAM macrophages into M1 macrophages.

Within 20 minutes, µRs were taken up by primary human macrophages based on flow cytometry and live-cell microscopy-based analysis. TAM macrophages took up more µRs than M0 and M1 macrophages. Poly(I:C)-loaded µRs increased mRNA expression of proinflammatory genes and extracellular M1 markers in TAM and M0 macrophages. Extracellular M2 markers were reduced. However, unloaded µRs also repolarize macrophages toward M1 phenotype. Unloaded µRs activated pattern recognition receptors (PRRs) to a small extent. Employing C57BL/6 wild-type and NLRP3 knockout bone marrow-derived macrophages (BMMs) showed that NLRP3 inflammasome is involved in the inflammatory activation.

Zusammenfassung

Makrophagen sind an verschiedenen Krankheiten wie Tumoren und chronischen Entzündungskrankheiten wie Asthma beteiligt. Die äußerst heterogene Population umfasst proinflammatorische (M1) Makrophagen, die gegen Krankheitserreger aktiv sind und das Tumorwachstum unterdrücken, und tumorassoziierte Makrophagen (TAMs), die den regulatorischen und entzündungshemmenden (M2) Makrophagen ähneln und das Tumorwachstum fördern. Unser Ziel war es, asphärischen Silica-Mikropartikeln (µRs) als gezieltes Drug-Delivery-System einzusetzen, um Polyinosin:Polycytidylsäure (Poly(I:C)) zu verabreichen und TAM Zellen in M1-ähnliche Zellen umzuprogrammieren.

Innerhalb von 20 Minuten wurden die µRs von primären humanen Makrophagen aufgenommen, wie die Durchflusszytometrie und Live-Cell-Mikroskopie ergaben. TAM Makrophagen nahm mehr µRs auf als M0- und M1-Makrophagen. Poly(I:C)-beladene µRs, erhöhten die mRNA-Expression entzündungsfördernder Gene und die extrazellulären M1-Marker in TAM und M0-Makrophagen. Extrazellulären M2-Marker wurden reduziert. Unbeladene µRs repolarisieren jedoch in Richtung des M1-Phänotyps. Unbeladene µRs aktivierten in geringem Umfang Patteren-Recognition-Rezeptor (PRRs). Die Verwendung von C57BL/6-Wildtyp und NLRP3-Knockout Knochenmark-abgeleitete Makrophagen (BMMs) zeigte, dass das NLRP3-Inflammasom an der entzündlichen Aktivierung beteiligt ist.

1 Introduction

1.1 Innate immune system

Beside from the anatomical and physiological barriers, the human immune system comprises both innate and adaptive immunity and consists of both cellular and humoral components (**Figure 1**). All components must be functioning properly to provide optimal protection against pathogens. The cells of the innate immune system, such as macrophages, represent the first line of defense against invaders. These cells have strong phagocytic properties and are equipped with pattern recognition receptors (PRRs) which allow them to identify and eliminate microorganisms through the recognition of common patterns expressed by various pathogens, known as pathogen-associated molecular patterns (PAMPs) or damage-associated molecular patterns (DAMPs). In addition, macrophages produce effector molecules such as cytokines, which help to regulate the immune response and facilitate communication between immune cells (Kirchenbaum et al., 2019; Swanson et al., 2019; Turvey and Broide, 2010).

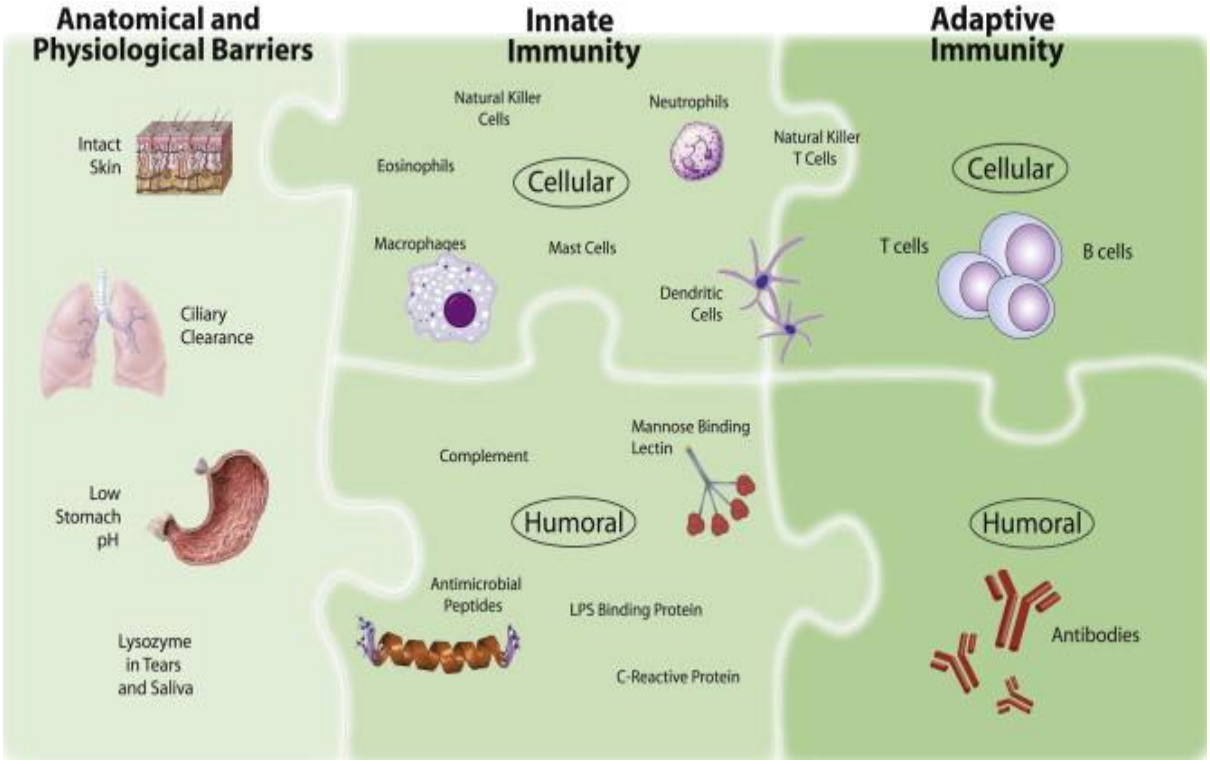

Figure 1. Human immune system (Turvey and Broide, 2010). The human immune system includes three parts: Anatomical and physiological barriers and innate and adaptive immunity. Innate and adaptive immunity consists of cellular and humoral components.

Toll-like receptors (TLRs) belong to the family of PRRs. TLR1/2 and TLR2/6, which are expressed on the cell surface, are activated by lipoproteins. Lipopolysaccharide (LPS) is a well-characterized agonist for TLR4, and flagellin is a well-known agonist for TLR5. TLR3, TLR8, and TLR9, which are localized in the endosome, are activated by viral infections (O'Neill et al., 2013).

NLRP3 inflammasome

In response to PRR activation, inflammatory mechanisms are induced to eliminate pathogens and repair tissue damage after injuries. Inflammasomes, like the NOD-, LRR- and pyrin domain-containing protein 3 (NLRP3) inflammasomes, are part of the

inflammatory pathway.

The activation of the NLRP3 inflammasome has been described as occurring through three mechanisms in mammalian cells: Canonical, non-canonical, and one-step NLRP3 inflammasome activation. Canonical NLRP3 inflammasome activation leads in the first step, after activation with PAMPs, among others, to form pro-caspase-1 and pro-interleukin 1 beta (pro- IL-1β). The second step is the activation of different signals through PAMPs or DAMPs like particulate, crystals and ATP leading to the complete activation of the NLRP3 inflammasome, resulting in caspase-1 formation and the release of interleukin 1 beta (IL-1β) and IL18, and inducing pyroptosis. Non-canonical NLRP3 activation occurs through cytosolic LPS binding to mouse caspase 11, human caspase 4, and caspase 5. One-step NLRP3 inflammasome activation results in IL-1β secretion without a second step, as occurs through TLR activation (Swanson et al., 2019).

1.2 Poly(I:C)

The TLR3 agonist polyinosinic:polycytidylic acid (poly(I:C)) is a synthetic double-stranded ribonucleic acid ((ds)RNA). Poly(I:C) binding imitates a viral infection by activating the endosomal TLR3. Due to its inflammatory effect, it has been tested in pre-clinical experiments and clinical trials to promote the immune response against cancer. Poly(I:C) has been shown to induce the secretion of pro-inflammatory cytokines and chemokines in glioblastoma cells, both untransfected and transfected or nano-complexed. To avoid systemic side effects and increase bioavailability, several drug-delivery methods have been investigated. It was shown that combination of poly(I:C) with different tumor therapy enhance his effect, which was even higher by cytosolic targeting (De Waele et al., 2021).

Transfection of poly(I:C) increased the inflammatory response at least 100-fold in HMDMs rather than by addition to cells (Reimer et al., 2008). In addition, several nanoparticle drug-delivery systems like arginine-based nano complexes were tested to repolarize macrophages toward an M1-like phenotype. It was shown that nanoparticle-formulation increase an M1-like repolarization (Dacoba et al., 2020).

1.3 Macrophages

Macrophages belong to the innate immune system and are present in all tissues as the first immune cells during embryonic development. They are highly plastic cells that can exhibit different morphologies and functions depending on the microenvironment and the organ they inhabit (Wynn et al., 2013).

The fetal liver and yolk sac are the origin of tissue-resident macrophages, while circulating monocytes can be recruited to form monocyte-derived macrophages (**Figure 2**). In contrast to tissue-resident macrophages, monocyte-derived macrophages have limited proliferation ability (Yamasaki and Eeden, 2018).

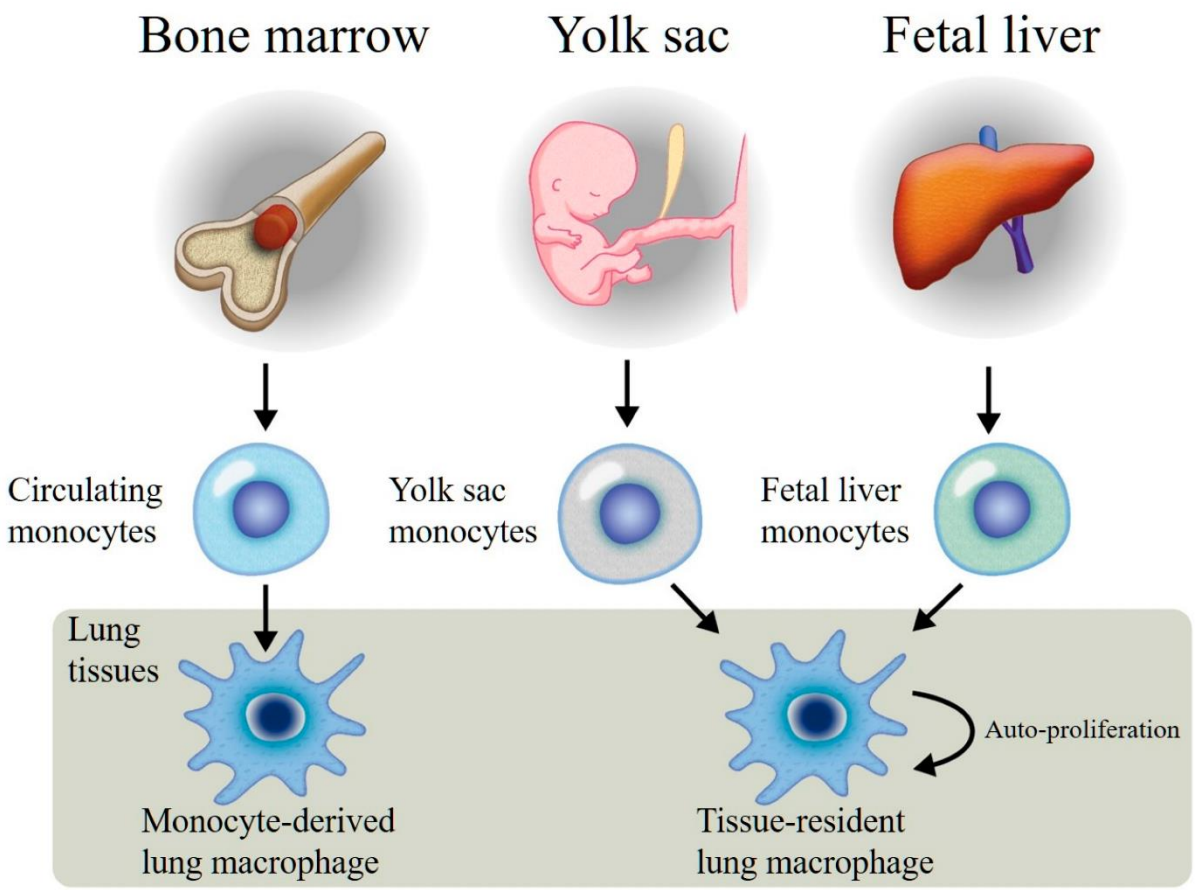

Figure 2. The origin of macrophages located in tissue (here in lung tissue) and their proliferation ability (Yamasaki and Eeden, 2018). Tissue-resident macrophages are derived from the yolk sac and fetal liver monocytes, whereas monocyte-derived macrophages are derived from bone marrow.

1.3.1 Polarization and function

Macrophages can polarize into different phenotypes depending on the stimuli present in the microenvironment. Various macrophage subpopulations have been discovered *in vivo* (Chambers et al., 2021; Guilliams and van de Laar, 2015) (**Figure 3**). Macrophages isolated from different tissues show high heterogeneity, as they express different gene and protein profiles. This diversity allows for specific functions, such as migration, phagocytosis, tissue remodeling, and pathogen killing. It has been shown that *in vitro* macrophage stimulation with various stimuli resulted in generation of distinct macrophage subtypes, as determined by gene expression and surface marker analysis (Xue et al., 2014). Monocytes differentiate into macrophages by incubation in a cell culture medium supplemented with colony stimulating factor (M-CSF). For investigation purposes, macrophages are polarized by applying certain stimuli (Hoppstädter et al., 2021; Seif et al., 2016). M1 macrophages are typically produced by adding LPS and interferon-gamma (IFNG), while M2 macrophages are generated with interleukin 4 (IL4) or interleukin 10 (IL10). TAMs are generated *in vitro* by employing a tumor-conditioned medium (TCM) that is closer to the *in vivo* situation and the microenvironment than using one cytokine only. TCM contains several stimuli produced by the cultured tumor cells (Edin et al., 2013).

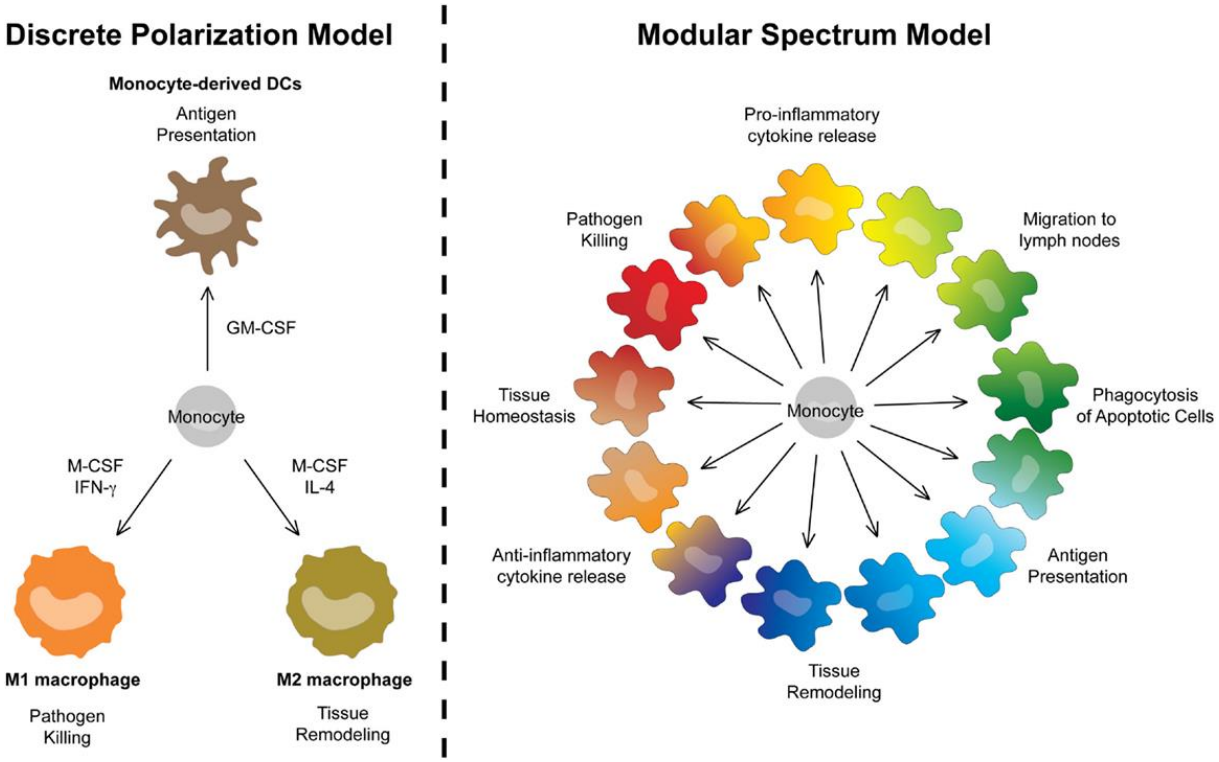

Figure 3. Macrophage generation from monocyte, polarization, and function (Guilliams and van de Laar, 2015). (left) Monocyte differentiation into dendritic cells (DCs) or macrophages. Simplified macrophage classification divides macrophages into M1 and M2 macrophages. (right) The modular spectrum model represents macrophage possible phenotypes more closely.

Macrophages have crucial roles in maintaining normal physiology in different organs. They are involved in pathogen phagocytosis, cytokine release, tissue homeostasis, tissue remodeling, and wound healing. However, it has been found that macrophages can promote diseases like atherosclerosis, fibrosis, and cancer depending on the stimuli present in the microenvironment (Wynn et al., 2013). In addition, macrophages have been reported to be involved in the progression of aging (Franceschi et al., 2000; Valbuena Perez et al., 2020).

1.3.2 Tumor-associated macrophages (TAMs)

Investigations of the tumor microenvironment have indicated that macrophages are highly present and promote tumor growth. Therefore, macrophages found in the tumor microenvironment are called tumor-associated macrophages (TAMs). The polarization of TAMs represents a plastic phenotype that is mainly described as resembling M2 macrophages, but it has been reported that TAMs may also have M1 properties (Chávez-Galán et al., 2015; Zhou et al., 2020). TAM protein expression can be used as a biomarker for diagnostic and prognosis for cancer treatment (**Figure 4**). Targeting TAMs in tumor therapy has been tested in clinical experiments, and therapeutic strategies can include killing, inhibiting their recruitment, and reprogramming (Yang and Zhang, 2017).

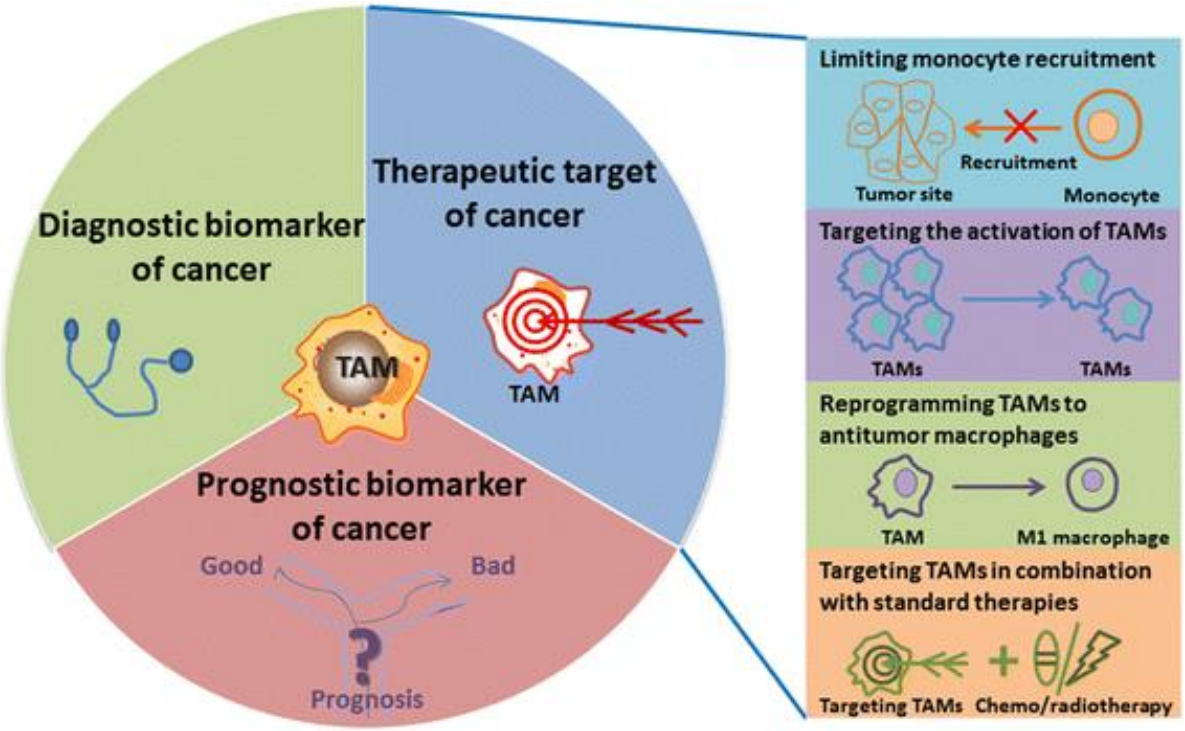

Figure 4. TAMs are a biomarker for diagnostics and prognosis and a therapeutic target for cancer (Yang and Zhang, 2017). Four therapeutic strategies are indicated: Inhibit monocyte recruitment, inactivate, reprogram, or target TAMs in combination with standard therapies.

For research purposes, macrophages can be polarized in vitro into TAM macrophages. TAM macrophages are generated by applying a tumor-conditioned medium (TCM) to primary human monocyte-derived macrophages (HMDMs) for a specific time like the incubation with the A549 cell line supernatant (Hoppstädter et al., 2021). The suitability of polarized HMDMs as *in vitro* TAM model was confirmed by comparing the gene expression and the high similarity that have been found (Hoppstädter et al., 2021). The polarization status can be investigated by analyzing gene and protein expression, as the macrophage phenotype shapes the expression profile. It was also indicated that the frequently used THP-1 cells as *in vitro* macrophage model is not suitable as TAM model due to high differences in the expression of critical genes (Al-Fityan et al., 2023).

1.3.3 Gene and marker expression in macrophage phenotypes

The gene expression of different *ex vivo* human and murine macrophage phenotypes has been analyzed, especially using single-cell sequencing (Bajpai and Lavine, 2019; Nahrendorf et al., 2007). Cells are isolated from tissues, sorted using flow cytometry, and gene and marker expression analyses are performed. In addition, expression is analyzed after *in vitro* macrophage generation, polarization, and repolarization (Edin et al., 2013). Macrophages have been found to express different surface proteins depending on the specific microenvironment in which they reside. The activation of these proteins can result in the expression of specific genes. For instance, inflammatory cytokines genes like *IL-1,* and *TNF* are described to be highly expressed in M1 macrophages, while the immune-suppressive cytokine *IL10* is described to be highly expressed in M2 macrophages, as determined by gene expression and surface marker analysis. Thus, macrophage gene and marker expression profiles allow for phenotype identification. Accordingly, the effect of compounds on macrophage polarization can be identified by gene and marker expression analysis (Liu et al., 2014).

Marker expression have also been used to identify macrophage phenotypes. CD80, CD86, and HLA-DR are known to be highly expressed in the M1 macrophage phenotype, while CD14 and CD163 are highly expressed in M2 and TAM macrophage phenotypes (Edin et al., 2013; Palmieri et al., 2017; Ringleb et al., 2018). Bulk-RNA-sequencing has indicated that *ex vivo* TAMs express lower cholesterol concentrations, which *in vitro* TAM macrophages resemble, in contrast to the *in vitro*-generated M2 phenotypes (Hoppstädter et al., 2021). Additionally, it has been indicated that *in vitro*-generated TAM macrophages resemble the M2 phenotype.

1.3.4 Role of macrophages in lung diseases

The pulmonary system is responsible for providing the body with oxygen, but the lung tissue is vulnerable to pollution and pathogens due to its direct exposure to air, which can lead to various lung diseases (Yamasaki and Eeden, 2018). Macrophages, which are present in lung tissue, serve as the first line of defense against pathogens. In addition, pulmonary macrophages are involved in inflammatory pulmonary diseases such as asthma and chronic obstructive pulmonary disease (COPD) and play a vital role in particle clearance and the production of pro-inflammatory cytokines, activating adaptive immune cells. Prolonged exposure to a pro-inflammatory environment can cause tissue damage and the progression of inflammation (Boorsma et al., 2013; Yamasaki and Eeden, 2018). It has been reported that lung cancer and chronic obstructive pulmonary disease often coexist and are associated with poor prognoses (Dai et al., 2017).

Lung cancer was the prime cause of cancer-related deaths and possessed the second highest incidence worldwide in 2020 (**Figure 5**). One of the reasons for its poor prognosis may be the late detection of lung cancer. Lung cancer can be classified into two main types: Small cell lung cancer (SCLC) and non-small cell lung cancer (NSCLC). NSCLC accounts for approximately 80-85% of lung cancer cases (Sedighzadeh et al., 2021). Smoking is a common cause of lung cancer, responsible for approximately 85-90% of cases. In addition to environmental factors, genetic factors also play a role in the development of lung cancer (Romaszko and Doboszyńska, 2018). Macrophages, which make up as much as 50% of solid tumor mass, have been shown to initiate and promote cancer as a response to chronic inflammation (Anfray et al., 2019; Wynn et al., 2013). It has been shown that a major part of macrophages in human NSCLC was monocyte-derived macrophages (Leader et al., 2021)

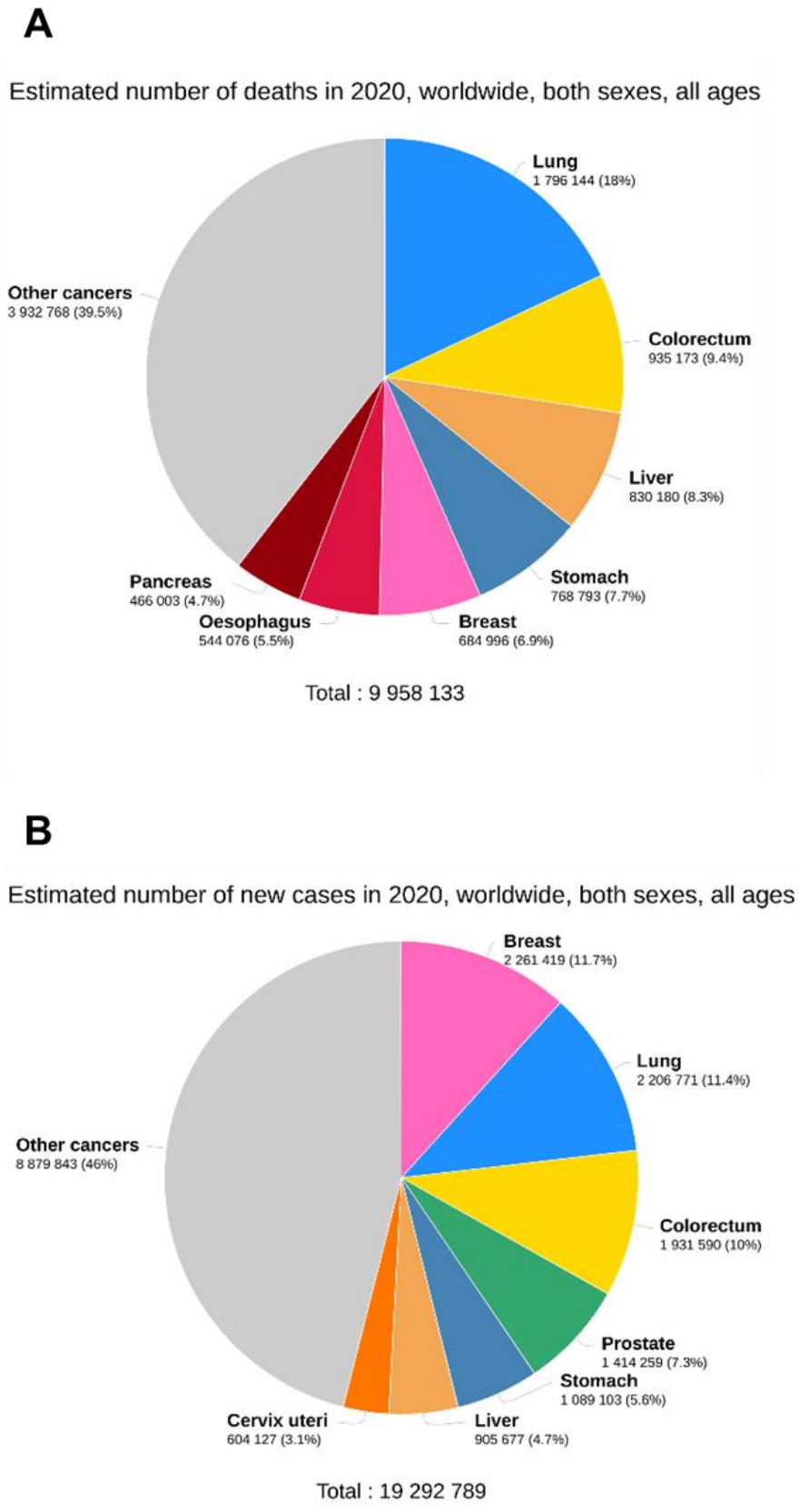

Figure 5. Cancer death (A) and incidence (B) worldwide in 2020 (GLOBOCAN 2020 study was visualized by Global Cancer Observatory (https://gco.iarc.fr)).

1.4 Specific TAM targeting

Local pulmonary drug delivery through inhalation offers numerous advantages, including the avoidance of systemic side effects, lower drug concentration, and higher bioavailability (Paranjpe and Müller-Goymann, 2014). One strategy for targeting macrophages in the lung tissue, particularly TAMs, involves reducing their number through methods such as killing TAMs or inhibiting their recruitment (Anfray et al., 2019). Monocytes are recruited, for example, as a response to specific signals by chemokines, e.g., C-C motif chemokine ligand 2 (CCL2), which binds to C-C motif chemokine receptor 2 (CCR2). For example, monocyte recruitment can be decreased by inhibiting the chemokine CCL2 and its receptor CCR2. Another strategy is to repolarize them towards an M1-like phenotype by activating inflammatory pathways, e.g., by TLR agonists. Specific cell targeting can also be achieved by targeting highly expressed proteins such as CSF1R and CD40, or by utilizing the phagocytic properties of macrophages. (Ovais et al., 2019; Sedighzadeh et al., 2021).

1.5 Nano- and microparticles as drug delivery system

As described previously, a specific macrophage targeting strategy using nanoparticles and microparticles is a common approach to reduce side effects and increase bioavailability (Paranjpe and Müller-Goymann, 2014). The advantages of particles as a drug delivery system include good absorption, the ability to overcome biological barriers, and the potential for specific targeting and targeted drug release. Studied as potential sources for nanoparticles are inorganic materials like gold, silver, iron, and silica, as well as liposomes and polymers (Jang et al., 2021). As a result, several clinically approved cancer nanomedicines have been reported. In particular, the use of liposomes and other nanomaterials like polyethylene glycol and iron oxide has been prevalent (Salvioni et al., 2019). For instance, poly(lactic-co-glycolic) acid microparticles loaded with dexamethasone have been taken up by macrophages and repolarized toward an M1 phenotype (Wofford et al., 2019a; Wofford et al., 2019b).

TAM targeting has gained particular importance as an interesting strategy for cancer therapy. Different TAM targeting strategies have been discussed, including preventing recruitment and repolarization (Guilbaud et al., 2019).

The shape, material, and size of particles can all affect their safety, uptake, and biological effects (Salvioni et al., 2019) (**Figure 6**). Therefore, it is important to carefully test each formulation type for both safety and effectiveness.

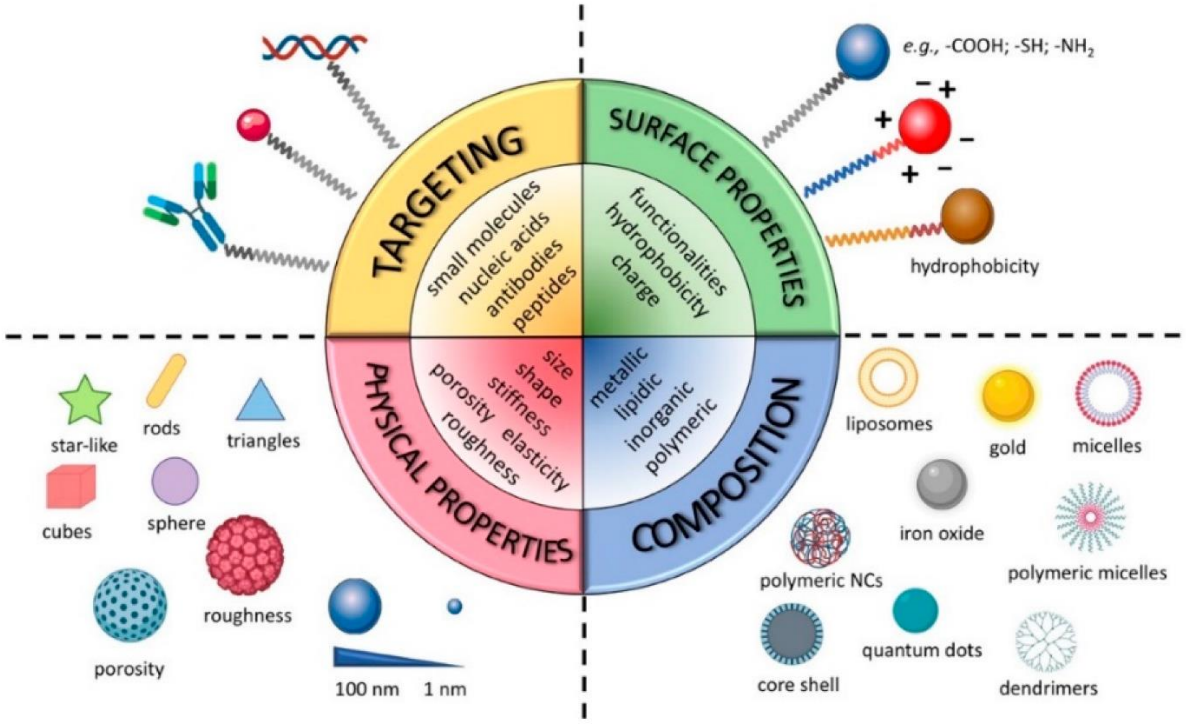

Figure 6. Particle properties and their effect on the organism (Salvioni et al., 2019). Pulmonary delivery of aspherical cylindrical silica microparticles (µRs) has been reported as a novel drug delivery system for the specific targeting of macrophages (Fischer et al., 2021b) (**Figure 7**). It has been shown that murine alveolar macrophages of the MH-S cell line and in BALB/c mice, which were isolated after pulmonary application, took up µRs (Möhwald et al., 2017) but not alveolar epithelial cells (A549) unless they were disintegrated during the incubation time into nanoparticles. Disintegration is the dismantling of the micro-rods into nanoparticles or fragments (Tschernig et al., 2018).

The µRs have been loaded with small interfering RNA (siRNA) and curcumin (Fischer et al., 2021b) or with siRNA alone (Fischer et al., 2021a), and have shown potential for shifting differentiated THP-1 cells toward an anti-inflammatory phenotype by measuring TNF secretion levels. In addition, cytotoxicity of µRs was investigated using an MTT assay in A549 and differentiated THP-1 cells. PMA-differentiated THP-1 cells were incubated with up to 300 µg/mL µRs for 48 h, whereas the viability was about 80%. Moreover, no differences in viability were detected between loaded and unloaded µRs (Fischer et al., 2021b). Thus, the µR uptake by differentiated THP-1 cells and possibility to repolarize the THP-1 cells whereby the cell viability remained.

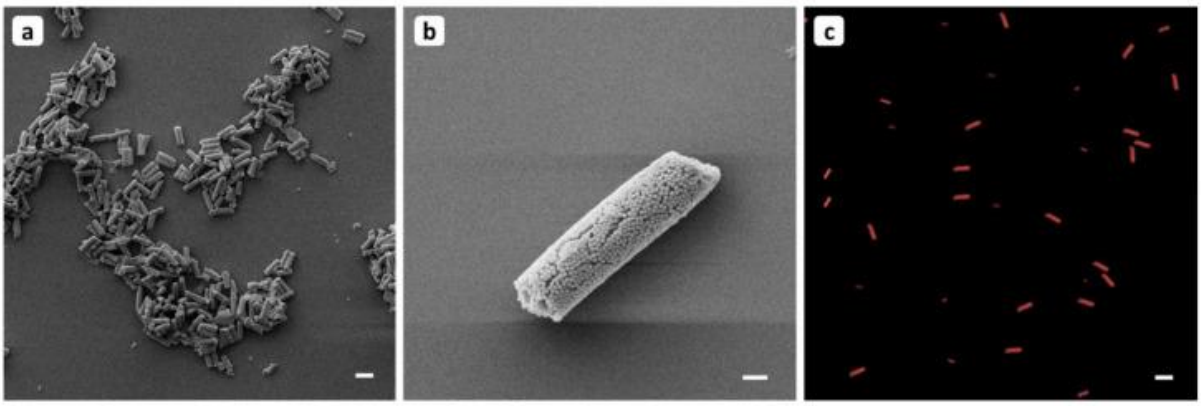

Figure 7. Images of aspherical cylindrical silica microparticles (µRs) functionalized with rhodamine B employing **(A, B)** scanning electron microscope and **(C)** CLSM (Fischer et al., 2021b).

1.6 Endotoxin contamination

Endotoxin contamination is a critical concern in cell culture, as it can induce inflammatory cell activation and pyroptosis, potentially masking the biological effects of materials (Li et al., 2017b; Swanson et al., 2019). Endotoxin can bind to the surface of microparticle materials or be integrated into the formulation during manufacturing (Li et al., 2017a; Li et al., 2017b). This is particularly important for highly sensitive cells like human monocyte-derived macrophages (HMDMs), derived from human peripheral blood mononuclear cells (PBMC), which are known to respond to as little as 0.006 ng/ml (0.0014 EU/ml) of LPS (Hartmann and Krieg, 1999).

There are three endotoxin detection tests recommended in the European Pharmacopoeia: the rabbit pyrogen test, the Limulus amebocyte lysate test (LAL test) (gel-clot formation, turbidimetric, and chromogenic), and the monocyte activation test. The monocyte activation test is unspecific and based on inflammation induction. A relatively new method recommended in the European Pharmacopoeia is the fluorescent-based recombinant Factor C method, which is based on an enzymatic reaction and has a high sensitivity of 0.005 EU/ml.

The LAL test is a standard method for detecting endotoxins, but previous research has shown that even accepted endotoxin detection methods must be carefully evaluated for their reliability when testing micro- and nanoparticles (Kucki et al., 2014; Li and Boraschi, 2016; Li et al., 2017a). Particles can interfere with gel formation, enzyme reactions, absorption, and fluorescence measurements, so it is important to carefully test each endotoxin detection method for each type of particle.

In search for a suitable method for detecting endotoxins, reporter cell lines have been employed as an unspecific bioassay (Li and Boraschi, 2016; Li et al., 2017b; Smulders et al., 2012). These cells are designed to express a PRR gene and a secreted embryonic alkaline phosphatase (SEAP). Reporter cell lines expressing a defined set of PRRs are sensitive to PAMP and DAMP agonists. Reporter cell lines can be used to detect the activation of PRRs like TLR4 and TLR2, which leads to the secretion of SEAP in the cell supernatant. The concentration of SEAP can be determined by absorption measurement, which correlates with the concentration of the agonist.

1.7 Aim of the present work

The aim of this study was to assess the potential of µRs as a drug delivery system for targeted delivery of poly(I:C) to repolarize macrophages towards an M1-like phenotype (**Figure 8**). This repolarization, particularly of TAMs, may be beneficial in the treatment of diseases such as lung cancer by promoting inflammation-mediated suppression of cancer.

To achieve this goal, we examined the uptake of the empty drug delivery system by unpolarized HMDMs. Additionally, we evaluated the effect of poly(I:C)-loaded µRs on the polarization of M0 and TAM HMDMs to an M1-like phenotype. We also investigated the role of toll-like receptors (TLRs) and the NLRP3 inflammasome in µRs-induced effects.

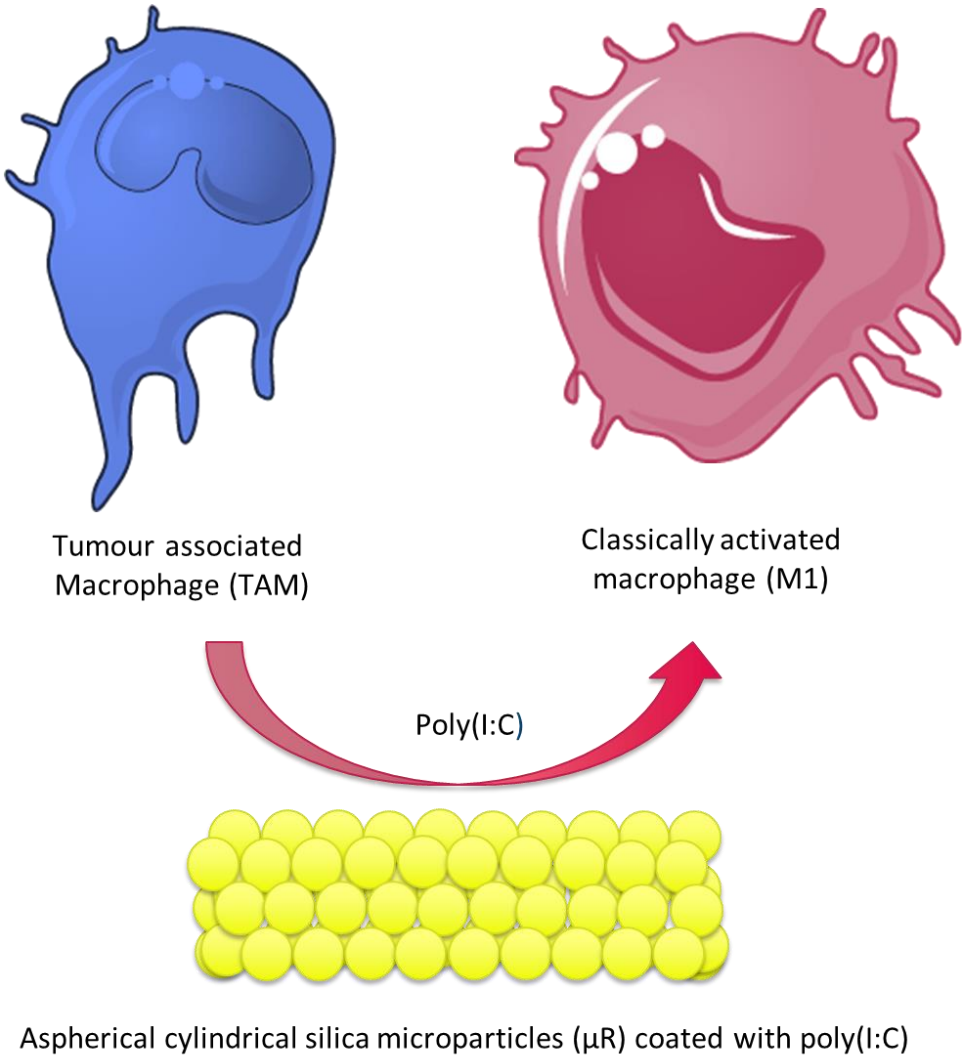

Figure 8. Schematic representation of the process of macrophage repolarization.µRs (yellow) are coated with poly(I:C) to elicit a change in macrophage phenotype from a TAM phenotype to an M1 phenotype. The cell images depicted in this figure have been adapted from https://smart.servier.com/?s=monocyte.

2 Materials and Methods

2.1 Materials

Cell media (RPMI1640, R0883; DMEM, D6546), fetal calf serum (FCS, F7524), penicillin/streptomycin (P433), glutamine (G7513), MTT (3-[4,5-dimethylthiazol-2-yl]-2,5-diphenyltetrazolium bromide; M5655), DMSO (dimethyl sulfoxide; D8418-100ml), crystal violet (C0775-25G), D-PBS (D8537-500ML), accutase (A6964) were obtained from Sigma-Aldrich. Follistatin like 1 (FSL-1, tlrl-fsl), Pam_3CSK_4 (tlrl-pms) were obtained from Invivogen (Toulouse, France). Materials were obtained from Sigma-Aldrich (Darmstadt, Germany) or Carl Roth (Karlsruhe, Germany) if not mentioned otherwise.

2.2 Buffers

Phosphate-buffered saline (PBS):

8 g NaCl
0.2 g KCl
1.44 g Na_2HPO_4
0.24 g KH_2PO_4

The substances were solved in distilled water, and the pH was adjusted to 7.4. The solution was filled up to 1000 ml with distilled water and was autoclaved.

Fluorescence-activated cell sorting wash (FACSwash) solution:

2.5% FCS and 0.05% NaN_3 in PBS

2.3 Cell culture

The growth conditions for all cells were 37°C and 5% CO_2.

2.3.1 Cell lines

A549 cells were cultivated in RPMI1640 supplemented with 10% FCS, 100 U/mL penicillin, 100 µg/mL streptomycin, and 2 mM glutamine. Cells were washed with PBS buffer and detached with trypsin-EDTA for passaging and seeding. Culture medium was added to stop the reaction. Cells were centrifuged for 5 min at 300 *g* and were resuspended in a medium.

2.3.2 Reporter cell lines

HEK-Dual™ hTLR2 (hkd-htlr2ni), HEK-Blue™ hTLR2 (hkb-htlr2), THP1-XBlue™ (thpx-sp), and HEK-Blue™ IL-1R (hkb-il1r) reporter cells were obtained from Invivogen. Cells were maintained according to the supplier's recommendation. HEK-Dual™ hTLR2, HEK-Blue™ hTLR2, and HEK-Blue™ IL1R reporter cells were preserved in DMEM supplemented with 10% heat-inactivated (30 min at 65°C) FCS, 2 mM glutamine, 50 U/mL penicillin G, 50 µg/mL streptomycin, and 100 µg/ml Normocin™ (ant-nr-1, Invivogen). Selection antibiotics were added from starting passage 3, 100 µg/ml Hygromycin B Gold (ant-hg-1, Invivogen) and 50 µg/ml of Zeocin™ (ant-zn-1, Invivogen) to HEK-Dual™ hTLR2 medium, 1x HEK-Blue™ Selection (hb-sel, Invivogen) were added to HEK-Blue™ hTLR2, whereas HEK-Blue™

IL1R were incubated with 200 µg/ml of Hygromycin B Gold, 1 µg/ml Puromycin (ant-pr-1, Invivogen), and 100 µg/ml of Zeocin™. THP1-XBlue™ were preserved in RPMI1640 supplemented with 10% heat-inactivated FCS, 2 mM glutamine, 50 U/mL penicillin G, 50 µg/mL streptomycin, and 100 µg/ml Normocin™. From passage 3, the growth medium was complemented with 200 µg/ml of Zeocin™. The measurement medium did not contain Normocin and selection antibiotics as described previously (Hoppstädter et al., 2021).

2.3.3 Primary cells

Primary murine bone marrow-derived macrophages (BMMs)

Mice were held in a 12/12-hr light/dark cycle with food and water *ad libitum*. BMMs were obtained from C57BL/6 wild type (WT) or NLRP3 knockout (KO) mice (The Jackson Laboratory, approval number 2.4.2.2.-06/2020). The cells were isolated according to the previously described method (Hoppstädter et al., 2019). Briefly, femurs and tibias were flushed with RPMI1640 medium supplemented with 10% FCS, 100 U/mL penicillin, and 100 µg/mL streptomycin. Possible containing erythrocytes were lysed with hypotonic buffer after centrifuging. Obtained cells were cultured overnight in RPMI1640 supplemented with 10% FCS, 100 U/mL penicillin, 100 µg/mL streptomycin, 2 mM glutamine, and mouse macrophage-colony stimulating factor (M-CSF, 130-101-704, Miltenyi Biotec) in a 150-cm² flask. The next day, non-adherent cells were collected and cultivated in a 150-cm² flask for five days. On day six after isolation, cells were detached with accutase and seeded in 96-well plates for MTT assay, Live-cell microscopy-based analysis, and IL-1β secretion analysis (20,000 cell/well) overnight.

Primary peripheral blood human monocyte-derived macrophages (HMDMs) generation

The isolation of PBMCs from buffy coats of healthy adult blood donors (Blood Donation Center, Klinikum Saarbrücken, Germany) was authorized by the local Ethics Committee (permission no. 173/18, State Medical Board of Registration, Saarland, Germany). For PBMCs isolation, density gradient centrifuging was used by deploying Lymphocyte Separation Medium 1077 (C-44010, Promocell, Heidelberg, Germany) and Leucosep tubes (227290, Greiner Bio-One, Kremsmünster, Austria) according to the company's suggestion. After several washing steps with PBS and cell counting, monocytes were separated through magnetic cell sorting using anti-CD14 microbeads (130-050-201, Miltenyi Biotec, Bergisch Gladbach, Germany) and LS Columns (130-042-401, Miltenyi Biotec). The beads amount was changed to 10% of the recommended amount by the supplier. The isolated monocytes were seeded as required for the experiments and differentiated into macrophages for 5 d in RPMI1640 supplemented with 10% FCS, 100 U/mL penicillin G, 100 µg/mL streptomycin, 2 mM glutamine, and 20 ng/mL human M-CSF (130-096-492, Miltenyi Biotec) at 37°C and 5% CO2 (**Table 1**).

Table 1: *HMDM maintaining condition*

Type of analysis	Plate format	Seeding density [cells/well]	Differentiation+ Polarization [d]	Treatment time [h]
IL1-β secretion	96-well	20,000	5	24
MTT assay	96-well	50,000	5	24
Crystal violet	96-well	50,000	5	48
flow cytometry (µR uptake)	24-well	250,000	5+2	1/3
flow cytometry (surface protein expression)	12-well	244,000	5+1	48
microscopy	24-well	200,000	5+2	1/3
live-cell microscopy (µR uptake)	96-well	40,000	5+2	1/3
live-cell microscopy (cytotoxicity)	96-well	40,000	5	24
mRNA expression	6-well	600,000	5+1	4

2.3.4 Tumor condensed medium (TCM) generation

0.5 million A549 cells were seeded in a 75 cm² flask for 3 d, then the medium was aspirated, the cells were washed twice with PBS, and 20 ml medium was added. After 2 d, the supernatant was collected, sterile filtered, and utilized immediately.

2.3.5 Polarization of HMDMs

HMDMs in the differentiation medium were left without any supplementation (M0) or were supplemented with 20 ng/mL IFN-γ (130-096-484, Miltenyi Biotec) and 100 ng/ml LPS (tlrl-peklps, Invivogen) to obtain M1 phenotype. The TAM phenotype was obtained by maintaining HMDMs in TCM (gained as described previously) supplemented with 20 ng/mL M-CSF, which was generated as described previously. HMDMs were polarized for 24 or 48 h, depending on implemented experiments.

2.3.6 Cell freezing and thawing

Cell lines were resuspended in 4°C RPMI1640 supplemented with 10% DMSO after splitting. Reporter cell lines freezing medium was generated according to supplier'srecommendation. The cell vials were frozen overnight at -80°C in Cryo freezing container. Then the vials were transferred in liquid N_2 for an indefinite time.

For cell thawing, appropriate media were preheated to 37°C, and vials were taken out from liquid N_2 and were thawed rapidly in a water bath. After cells were thawed, cells were suspended in the preheated medium. Next, the cells were centrifuged at 300 *g*, resuspended in maintaining medium, and cultured as noted above.

2.4 MTT assay

Cell viability was determined by incubation with MTT (3-[4,5-dimethylthiazol-2-yl]-2,5-diphenyltetrazolium bromide) as described previously (Diesel et al., 2013). Controls included untreated, with 20% DMSO treated samples, and samples in which µRs were added with the MTT solution or in DMSO after MTT addition. In addition, cell samples

with µRs without adding any MTT solution were performed.

After incubation, the medium was aspirated, and the cells were covered with 0.5 mg/ml MTT solution in medium. After about 60 min of incubation, MTT solution was removed and the formazan crystals were dissolved in DMSO. The absorbance was measured at wavelength of 560 nm in GloMax® microarray reader (Promega Walldorf, Germany). Absorption of treated wells were normalized to the mean of absorption of untreated control.

2.5 Crystal violet assay

To investigate the cytotoxicity of µRs, HMDMs were incubated with varying concentrations of non-fluorescent µRs for a duration of 48 hours. Samples that were either untreated or treated with 20% DMSO were included. The medium was carefully aspirated, the cells were washed with PBS. Then the cells were incubated with 0.1% crystal violet solution (in 20% methanol in water solution) and incubated at room temperature for 20 min under shaking at 400 rpm. The solution was subsequently aspirated and washed with PBS before being resuspended in 99% methanol. The absorption was measured at a wavelength of 560 nm.

2.6 Endotoxin assay

PyroGene™ Recombinant Factor C Endpoint Fluorescent Assay (50-658U; Lonza, Basel, Switzerland) with a detection limit of 0.05-0.005 EU/ml was employed for endotoxin detection according to the manufacturer's recommendations. µRs were tested in concentrations corresponding to the concentrations applied in cell culture (100 and 200 µg/ml). µRs are described to disintegrate within hours in culture media (Tschernig et al., 2018). Therefore, disintegrated µRs were investigated. Spike controls were included in each experiment. µRs were considered as not interacting with the assay, if the difference between endotoxin values of spiked control samples were within the acceptable range (50-200%) as recommended by the manufacturer. A lower concentration can indicate an inhibitory effect on the assay, while a higher concentration can suggest enhancement of the assay results by the samples.

2.7 TLR activation and IL-1β secretion assays

The reporter cells feature stably integrated NF-κB-inducible secreted embryonic alkaline phosphatase (SEAP) reporter gene. HEK-Dual™ hTLR2 reporter cell line is derived from the HEK-Dual™ Null (with the knockout of TLR3 and TLR5) cells. The HEK-Blue™-hTLR2 reporter cell line is derived from HEK293 cells. The THP1-XBlue™ reporter cell line is derived from the human THP-1 monocyte cell line. The expressed PRRs in the employed reporter cell lines are as listed (**Table 2**).

Cells were seeded into 96-well plates, specifically HEK-Dual™ hTLR2, HEK-Blue™-hTLR2 (5×10^5 cells/well), and THP1-XBlue™ (10×10^5 cells/well). The cells were then treated as indicated to assess receptor-dependent activation. Positive controls and untreated controls were included. Following 24 h of incubation, 20 µl supernatant from each well was added to 180 µl Quanti-Blue™ solution (SEAP detection medium; rep-qbs; Invivogen) for 6 h. Subsequently the absorption was measured.

HEK-Blue™ IL1R reporter cells, seeded into 96-well plates (5×10^5 cells/well, 180 µl) maintaining medium without selection antibiotics were incubated with 20 µl HMDM or BMM supernatants for 24 h. Then, 20 µl of the reporter cell supernatants were incubated for three h with 180 µl Quanti-Blue™ solution (SEAP detection medium; rep-qbs; Invivogen). For BMM cells, control supernatants (LPS followed by MSU or ATP) were diluted 1:100 before adding. Standard curves of human or murine IL-1β (rcyec-hil1b, Invivogen and 130-101-681, Miltenyi Biotec) were included. Four-parameter logistic curve fit (Myassays.com) was employed for concentration determination.

SEAP activity was quantified at a wavelength of 600 nm using a microplate reader (GloMax® Discover Microplate Reader, Promega). Cell viability was assessed using the MTT assay after removing the supernatants from the wells.

Table 2: *Reporter cell lines and their expressed receptors*

Reporter cell line	Receptor expression
THP1-XBlue™	TLR1/2, TLR2/6, TLR4, TLR5, TLR8, NOD1/2
HEK-Blue™-hTLR2	TLR1/2, TLR2/6, TLR3, TLR5, NOD1
HEK-Dual™ hTLR2	TLR1/2, TLR2/6, NOD1

2.8 Live cell microscopy-based analysis

2.8.1 Viability

Cells were seeded in a medium with 250 nM IncuCyte® Cytotox Red Reagent (4632, Sartorius, Göttingen, Germany). Then the cells were incubated with different concentrations of µRs. 20x objective, Phase-contrast, and fluorescent scans were taken every 2 h. IncuCyte® Cytotox Red Reagent negative cells per treatment per treatment in % of cell count normalized to untreated control using the IncuCyte® S3 live-cell analysis system with the add-on IncuCyte® Cell-By-Cell Analysis Software Module were used to determine the cell viability.

2.8.2 Uptake

To stain the HMDMs for cell detection and analysis, preheated (37°C) solution of 0.5 µM CellTracker™ Deep Red Dye in an FCS-free medium was employed to maintain HMDMs for 30 min in a cell incubator. After the staining solution was removed, the polarization media were added to HMDMs for 48 h, as described previously. µRs were applied in a concentration of 1 µR/cell for the uptake study. For analysis, untreated and unstained samples of each HMDM phenotype were included. In addition, samples of µRs without cells were included. After µRs were added and plates were centrifuged, the plates were placed immediately into the IncuCyte® instrument (Essen BioScience) for one h under standard growth conditions. For this purpose, a 20x objective was used to take phase-contrast and fluorescent scans every 10 min. To observe which HMDMs took up µRs, which are green-fluorescent, HMDMs that were positive for green and red fluorescence were displayed per time using the IncuCyte® S3 live-cell analysis system. The add-on IncuCyte® Cell-By-Cell Analysis Software Module (% cells/cell count) was employed additionally.

2.9 Messenger ribonucleic acid (mRNA) expression analysis

2.9.1 mRNA isolation and reverse transcription

HMDMs were incubated for four h with poly(I:C)-loaded or unloaded non-fluorescent µRs (0.5 µR/cell), or with 100 ng/ml LPS. Untreated samples were included. M1 cells were not incubated with µRs and were included as a control. Next, cells were washed three times with ice-cold PBS on ice. PBS and Lysis/Binding Buffer (from High Pure RNA Isolation Kit, 11828665001, Roche Diagnostics International, Rotkreuz, Switzerland) were added, and cell suspensions were stored at -80°C. Next, cell suspensions were thawed on ice, and mRNAs were isolated according to the supplier's suggestions. mRNA concentrations were determined with NanoDrop™ Lite Spectrophotometer (Thermo Fisher Scientific, Bonn, Germany).

The High-Capacity cDNA Reverse Transcription Kit (4368813, Applied Biosystems, Foster City, United States) was employed to generate complementary deoxyribonucleic acid (cDNA) from an equivalent quantity of mRNA. In addition, RNase inhibitor (10777-019, Invitrogen) was added. 20 µl cDNA were diluted with 180 µl TE Buffer pH 8.0 for molecular biology (A0386, AppliChem GmbH, Darmstadt, Germany). Samples were stored at 20°C.

2.9.2 Plasmid generation

Primers were designed with Primer-Blast (ncbi.nlm.nih.gov) and Eurofines.genomices.eu. The Human Protein Atlas was used to find out which cells express the gene highly. The selected cDNA and the generated plasmids were employed to produce plasmids for the standard dilution. Products were amplified and controlled with the quantitative real-time polymerize chain reaction (qRT-PCR) method. Product control was done with gel electrophoreses. The products were cleaned with NucleoSpin® Gel and PCR Clean-up kit (740609.250, Macherey-Nagel, Düren, Germany). cDNA concentrations were determined with NanoDrop™ Lite Spectrophotometer (Thermo Fischer Scientific).

2.9.3 Transformation

TOP10 chemically competent *E. coli* bacteria (*Escherichia coli*, C4040-03, Thermo Fischer Scientific) were employed to clone the generated cDNA into pGEMTeasy (A1360, Promega) according to the supplier suggestions. *E. coli* suspension was resuspended in 950 µl sterile LB medium with 100 µg/ml ampicillin. The bacterial suspension was incubated at 37°C and 250 rpm for 1.5 h. Then, 100 µl of bacterial suspension were plated on LB plates (1.5% agar, 100 µg/ml ampicillin). The plates were incubated overnight at 37°C.

2.9.4 Plasmid isolation

The following day, single colonies were selected from the agar plate and cultured in LB Medium (with ampicillin) overnight at 150 rpm and 37°C. Then, High Pure Plasmid Isolation Kit (11754777001, Roche) was employed for plasmid isolation.

2.9.5 qRT-PCR

5xHot FirePol EvaGreen qPCR Mix (08-25-00020, Solis BioDyne, Tartu, Estonia) was used according to the supplier's suggestion. The used primers, their concentration, and the specific reaction conditions are shown in **Table 3**. Each reaction sample had the volume of 20 µl contained a 3 µl plasmid or TE-Puffer for controls, 4 µl 5xHot FirePol EvaGreen qPCR Mix, and water. The suitable primer amounts were established in previous experiments. All samples and standards were analyzed in duplicates. The standard solutions had concentrations between 2000 attomole/µl till 0.0002 attomole/µl.

CFX96 Touch™ Real-Time PCR Detection System (Bio-Rad, Hercules, CA, USA) was employed for the quantitative gene expression analysis. The following program was employed:

Denaturation 15 sec 94°C
Denaturation 20 sec 94°C
Annealing 20 sec
Elongation 20 sec 72°C
Plate read
} Repeat 39 X
Melt curve 55 to 95°C

***Table 3**: Primer sequences for qPCR experiment*

Gene	Accession number	Forward primer sequence	Reverse primer sequence	µL primer [10 µM] / reaction	Annealing T [°C]
RNA18S5	NR_003286.2	AGG TCT GTG ATG CCC TTA GA	GAATGGGGTTCAAC GGGTTA	0.5	61
TNF	NM_000594.4	CTCCACCCATGTGC TCCTCA	CTCTGGCAGGGGCT CTTGAT	0.5	60
CXCL10	NM_001565.4	GAGCCTACAGCAGA GGAACC	AAGGCAGCAAATCA GAATCG	0.5	60
IL-1β	NM_000576.2	GGCTGCTCTGGGAT TCTCTT	AGTCATCCTCATTGC CACTGTAA	0.5	60
CXCL8	NM_000584.4	GAGAAGTTTTTGAA GAGGGCTGA	GCTTGAAGTTTCACT GGCATCT	0.5	60
IFNG	NM_000619.3	TGGAAAGAGGAGAG TGACAGA	ACACTCTTTTGGATG CTCTGGT	0.5	60
CCL2	NM_002982.4	TTGATGTTTTAAGTT TATCTTTCATGG	CAGGGGTAGAACTG TGGTTCA	1	60
VEGFA	NM_001171623.1	CGCTTACTCTCACCT GCTTCTG	GGTCAACCACTCAC ACACACAC	0.5	60

* *RNA18S5:* RNA, 18S ribosomal 5; *CXCL10:* C-X-C Motif Chemokine Ligand 10; *IL-1β:* Interleukin 1 beta; *CXCL8:* C-X-C Motif Chemokine Ligand 8; *VEGFA:* Vascular endothelial growth factor A

2.10 Flow cytometry

2.10.1 µR uptake by HMDMs

HMDMs were incubated with 400 µg/ml (corresponding to 2 µR/cell) green-fluorescent µRs for 20 min or left untreated.

The medium was removed, the cells were washed five times with PBS, and warmed (37°C) FCS-free medium with 0.5 µM CellTracker™ Deep Red Dye (C34565, Thermo Fisher Scientific) was added. The medium was removed after 30 min incubation in a cell incubator, and the HMDMs were washed with ice-cold PBS. For detaching, ice-cold PBS was used, and then the HMDMs were fixed in ice-cold 1% paraformaldehyde (PFA) solution. The samples were measured immediately by employing BD LSRFortessa™BD (Biosciences, San Jose, CA, USA). BD FACSDiva™ software (BD Biosciences) and BD FACSuite™ software was utilized for data analysis. Compensation was done to exclude spillover, and the setting and gates were adjusted previously. For this purpose, untreated samples, and samples with µRs were measured to identify the fluorescence signals.

The CellTracker™ Deep Red Dye with the excitation/emission 630/650 has been chosen because of the absence of spillover in the employed detector for µRs (green, fluorescent) detection (**Figure 9**). For the fluorophore selection, the spectral viewer of Bio-Rad has been employed (https://www.bio-rad-antibodies.com/spectraviewer.html).

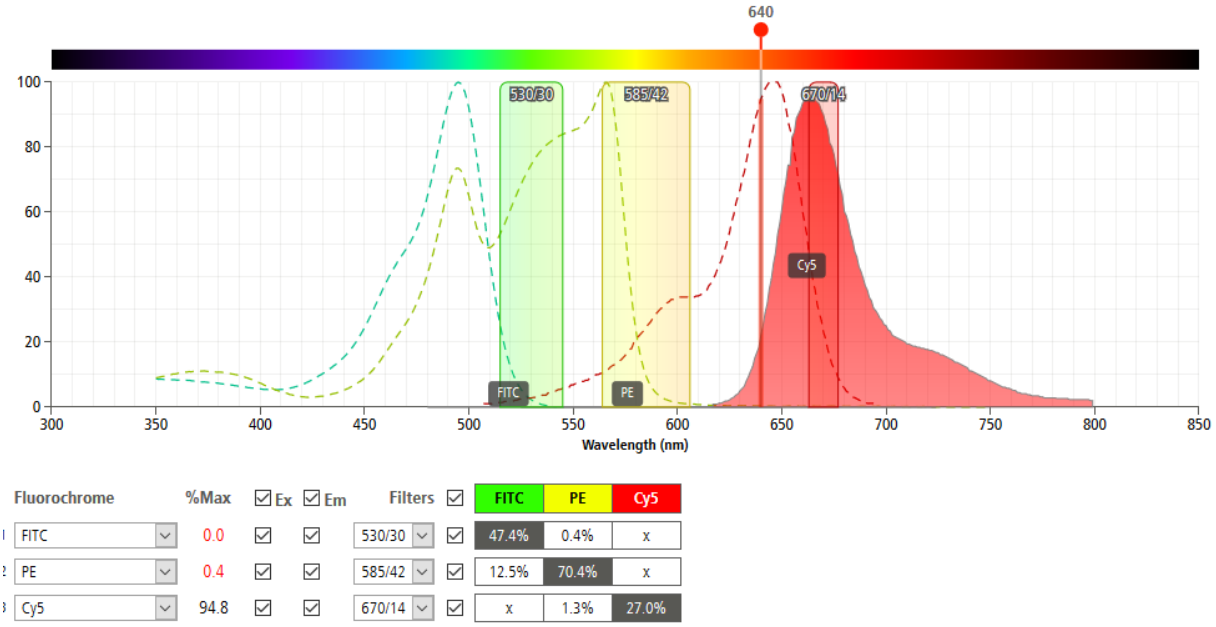

Figure 9. Illustration of the excitation and emission spectra of three fluorophores. µRs were labeled with a fluorophore similar to FITC. The CellTracker™ Deep Red Dye fluorophore is similar to Cy5.

The flow cytometric gating strategy is depicted in **Figure 10**. Initial selection of cells was based on size and granularity, with events characterized by low size (forward scattering area, FSC-A) and low granularity (side scattering area, SSC-A) being excluded as trash. Events exhibiting proportional forward scattering height to area ratios were defined as singlets and selected for further analysis. Fluorescent areas of CellTracker™ Deep Red Dye and FITC were then plotted, allowing for the identification of unstained cells, stained cells, and cells containing µR, or stained cells containing

µR. Gates Q1 and Q2 were selected to include stained cells and stained cells with internalized µR, respectively, for further investigation. The gate P2, which was established using a sample of untreated cells, was used to specifically include cells containing internalized µR in the analysis. The evaluation of µR uptake was based on this plot.

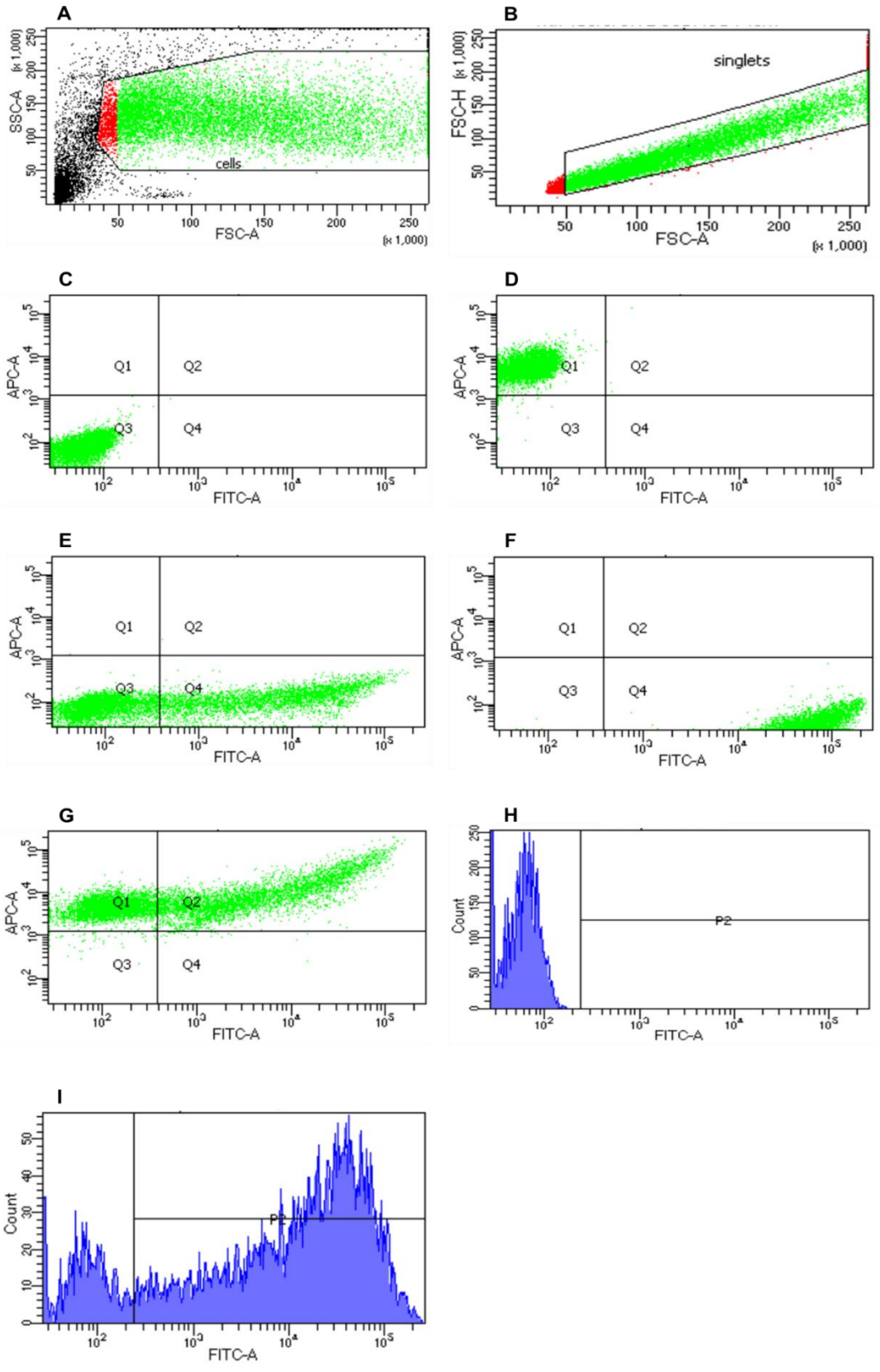

Figure 10 Representative images show the gating strategy for µR uptake investigation by HMDMs. **(A)** Events were selected in FSC-A *vs.* SSC-A plot. **(B)** Singlets were selected in FSC-H *vs.* FSC-A plot. **(C)** APC-A *vs.* FITC-A shows unstained cells in Q3, **(D)** stained cells in Q1, **(E)** unstained cells containing µRs in Q4, **(F)** µRs in Q4, **(G)** and stained cells containing µRs in Q2. Events in Q1 and Q2 were used for evaluation. **(H)** Count *vs*. FITC showed FITC -negative event count and their fluorescence intensity. **(I)** Count *vs*. FITC showed FITC-positive events occurred in P2, 20 min incubation with green-fluorescent µRs (to 2 µR/cell, FITC), stained with CellTracker ™ Deep Red Dye (APC).

2.10.2 Surface protein expression analysis

The fluorophores of the four employed antibodies were selected carefully to avoid spectral overlapping. For the fluorophore selection, the spectral viewer of Bio-Rad has been employed (**Figure 11**). In addition, a compensation experiment was performed to avoid the detection of one fluorophore in multiple detectors. Spillover is the amount of a fluorophore fluorescence signal detected in another detector than the main detector. This spillover needs to be subtracted in a compensation experiment. For this purpose, single stained samples, fluorescence-minus-one (FMO) samples, unstained samples and samples stained with all four antibodies were included.

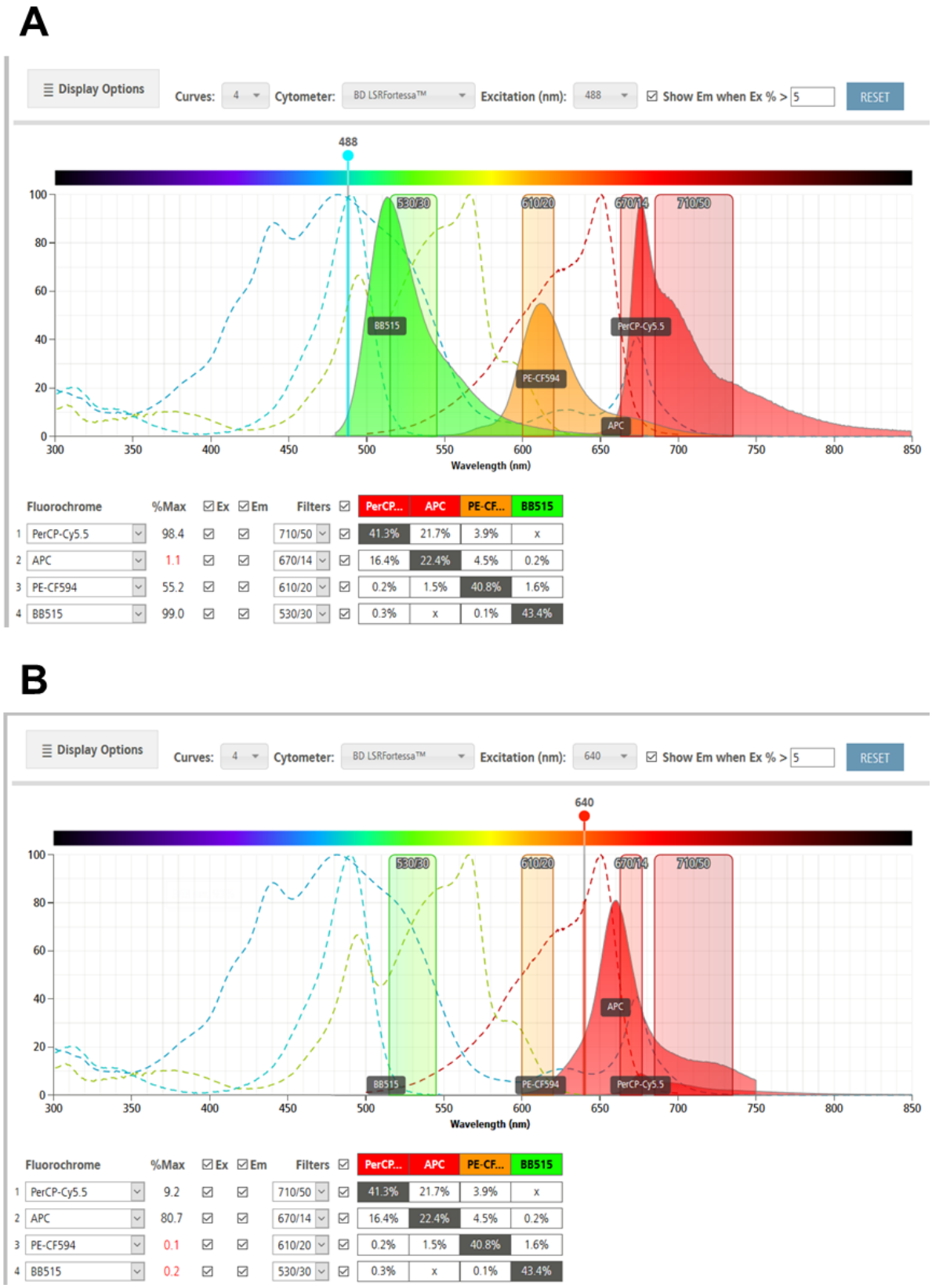

Figure 11. An illustration of the excitation and emission spectra of the four employed fluorophores for marker expression analysis. **(A):** Excitation with 488 nm or **(B)** 640 nm (https://www.bio-rad-antibodies.com/spectraviewer.html).

The surface protein expression of the four investigated markers (**Table 4**) (HLA-DRPerCP-Cy5.5 (552764, Clone: G46-6, BD Biosciences), CD80 BB51 (565008, Clone: L207.4, BD Biosciences), CD163PE-CF594 (562670, Clone: GHI/61, BD Biosciences) and CD14 APC (555399, Clone: M5E2, BD Biosciences)) in the 3 HMDMs phenotype after 1, 2, 3 and 4 days marker expression was investigated.

Table 4: *Markers investigated via flow cytometry in HMDMs and their fluorescent labels.*

Antibody	**CD163-PE-CF594**	**CD14-APC**	**HLA-DR-PerCPCy5.5**	**CD80-BB515**
Excitation Source	Blue 488 nm, Green 532 nm, Yellow/Green 561 nm	Red 633 nm	Blue 488 nm	Blue 488 nm
Excitation Max [nm]	496	650	482	490
Emission Max [nm]	612	660	678	515
Fluorophore brightness	Very bright	bright	Moderate	Very bright

Flow cytometry experiments were performed to analyze the expression of surface proteins. The gating strategy was adjusted and generated based on preliminary experiments (**Figure 12**). gating strategy similar to that used in the uptake study (2.10.1) was developed and adjusted based on the results of the preliminary experiments including compensation. After selecting singlets, plots of the fluorescent signals of the employed antibodies were generated. The plots of unstained samples and FMO samples were used to assess compensation results and detect any spillover. The expression of markers was evaluated by analyzing the plots of cell count against each of the four marker signals.

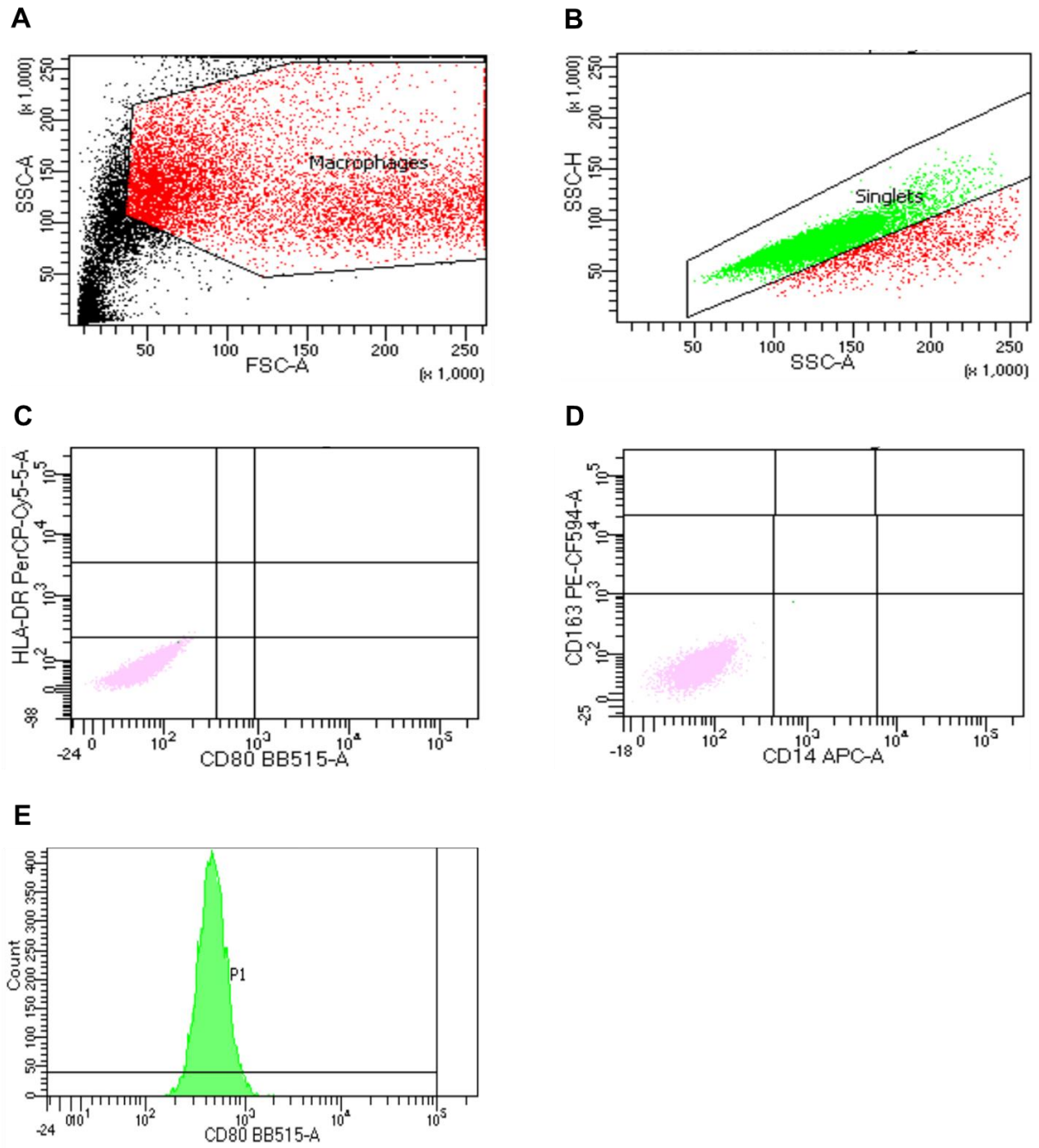

Figure 12. Representative images show the gating strategy for surface marker expression analysis of HMDMs. **(A)** Events were selected in forward scatter-area (FSC-A) *vs.* side scatter-area (SSC-A) plot. **(B)** Singlets were selected in FSC-H *vs.* FSC-A plot. **(C)** HLA-DR *vs.* CD80 and **(D)** CD163 vs. CD14 show left unlabelled cells in the lowest rectangle. Fluorescence signals in the lower three rectangles of each marker were considered as background for x axis and the left three rectangles were considered as background for the y axis. The three middle rectangles include low marker expression, and the three upper rectangles include high marker expression. **(E)** Count *vs*. CD80 showed CD80-positive events and their fluorescence intensity in P1 in antibody-labeled untreated M0 sample.

After 24 h polarization, the medium was changed, and the M0 and TAM HMDMs were incubated with µRs. Poly(I:C)-loaded or unloaded µRs were employed. M1 HMDMs were left untreated as a control. Untreated controls of each phenotype were included.

After 48 h, supernatants were gathered, centrifuged, and stored at -80°C. The maintained HMDMs were washed with ice-cold PBS (3 times) at 4°C and detached in PBS (2.5 mM EDTA). Next, BD Fc Block™Pure (564220, BD Biosciences) in

FACSwash solution was added for 10 min at room temperature. Then, the HMDMs were incubated with antibodies on ice for 30 min under light protection (concentrations according to supplier recommendation). The samples were washed with FACSwash and were fixed with ice-cold 1% PFA solution. The measurement was carried out immediately employing BD LSRFortessa™. During the experiment accomplishment, the samples were stored on ice. BD FACSDiva™ software (BD Biosciences) and BD FACSuite™ software was utilized for data analysis. The marker median fluorescence intensities of singlet cells were analyzed.

2.11 Confocal Laser Scanning Microscope (CLSM)

The movement between planes in the z-stack allowed for clearer visualization of the µR. It was determined that the µR were located within the HMDMs, as demonstrated by cuts through the z-stack and movement of the 3D image. Polarized HMDMs were left untreated or incubated with 2 green-fluorescent µR/cell. After 20 min, the medium was removed, and the cells were washed five times with ice-cold PBS. Then the cells were fixed with ice-cold 4% PFA solution, washed with ice-cold PBS, and permeabilized for 10 min in ice-cold 0.25% tritonX-100 in PBS. The cells were then blocked for 3 h in ice-cold 1% BSA in PBS solution. Next, the cells were stained overnight at 4°C in a humidity chamber under light protection with ice-cold 0.766 µM Phalloidin–Tetramethylrhodamine B isothiocyanate (phalloidin-TRITC, P1951, Sigma-Aldrich) in 1% BSA solution. To stain the cell nucleus, the cells were stained for 20 min with 5 µg/ml DAPI (4′,6-Diamidino-2-phenylindole dihydrochloride, D9542-1MG Sigma-Aldrich) solution (in PBS) on the next day after the cells were washed three times with ice-cold PBS. After the cells were washed twice with PBS and fixed on microscope slides with FluorSave™ Reagent (345789, Calbiochem), they were stored at 4°C in the dark. Images were performed with a Confocal Laser Scanning Microscope (LSM 510 Meta, Zeiss). The images were analyzed, edited, and exported using Zen 3.0 software (blue edition; Zeiss).

2.12 Cylindric-shaped silica microparticles (µRs) manufacturing as drug delivery systems

µRs manufacturing, characterization, and poly(I:C)-release assay were performed by Dr. Thorben Fischer after (Möhwald et al., 2017).

In a filter with a defined length and wide non-fluorescent or fluorescent amorphous silica nanoparticles (NPs, PSI-0.02; PSI-G0.2, Kisker Biotech) were compressed to form µRs (**Figure 13**). 200 nm NPs enter the template membrane's 3 µm wide and 10 µm long pores. The blocking membrane contains 0.1 µm pores. The manufactured µRs were coated with three polymer double-layers for stabilization (dextran sulfate (DS), 10 HS 10 kDa (TdB Labs, Uppsala, Sweden) and branched polyethyleneimine 25 kDa (PEI), Sigma Aldrich). For some experiments, µRs were coated with poly(I:C) (tlrl-pic; HMW, Invivogen , Toulouse, France) as described previously (Fischer et al., 2021a; Fischer et al., 2021b).

The µRs were stored as a powder and suspended in water (LAL Reagent Water; W50-1000; Lonza) (dulbecco’s phosphate-buffered saline (D-PBS) for HMDM MTT assay) at a concentration of 50 µg/µl before the experiment. For µR suspending, an ultrasonic bath and vortex mixer were employed alternately for 30 seconds each. After the µRs

were suspended completely, the µRs were used immediately for experiments or were stored at -20°C. If the µRs were thawed, ultrasonic bath and vortex Mixer were employed twice. Manual counting by using a Neubauer counting chamber and Carl Zeiss™ Axiovert 40 CFL Microscope (Carl Zeiss™, Jena, Germany) or LUNA-FL™ Dual Fluorescence Cell Counter (Logos biosystems, Villeneuve d'Ascq France) were employed for µRs counting. The average concentration of 2.5 million µRs per 1 mg was considered for applying µRs in experiments, alternatively to counting (**Table 5**). Each time before using on cells, the µRs were vortexed, and after applying, the plates were centrifuged immediately by 100 *g* for 30 seconds. The µRs were not disintegrated if not stated otherwise. The µRs were kept for four days at 37°C in RPMI1640 supplemented with 100 U/mL penicillin and 100 µg/mL streptomycin to generate disintegrated µRs.

Table 5: *µR concentration conversion.*

µR [µg/ml]	**100**	**200**	**400**	**600**	**800**
Treatment [µRs/cell]	0.5	1	2	3	4

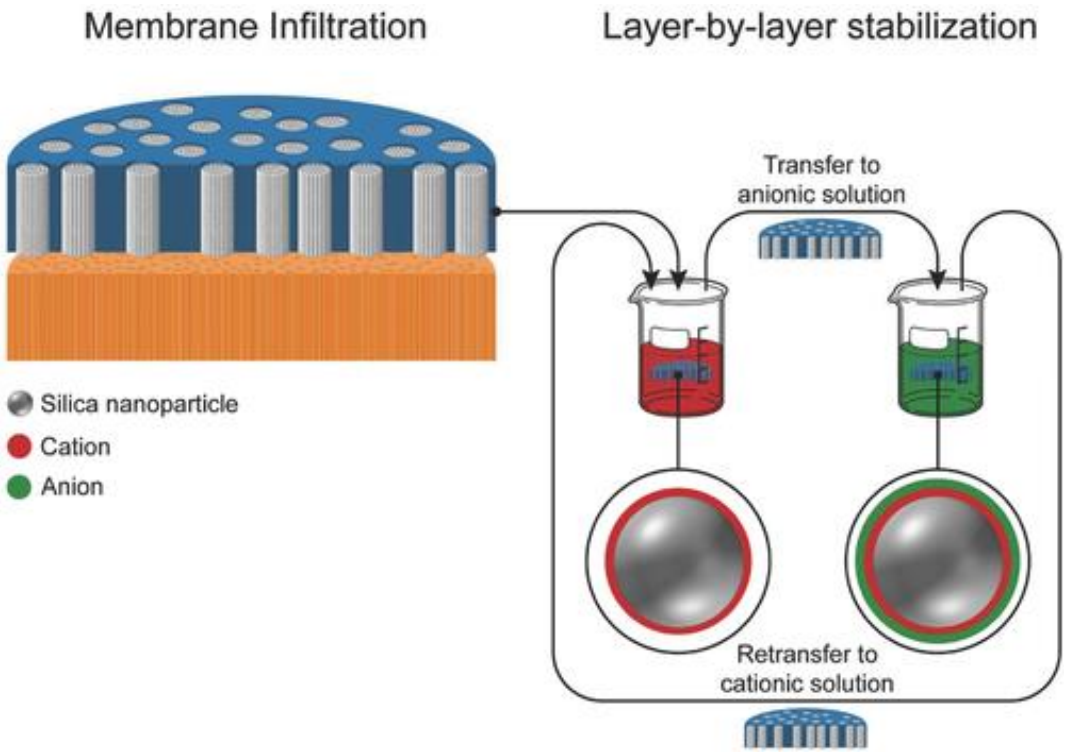

Figure 13. Cylindric-shaped silica microparticles (µRs) manufacturing as drug delivery systems (Möhwald et al., 2017).

The release of poly(I:C) from µRs was determined using a salt mixture that replicated the physiological conditions of a phagolysosome, following Stefaniak et al. (Stefaniak et al., 2005). The investigation was conducted as described previously (Fischer et al., 2021a). Specifically, µRs were incubated in 0.5 ml of salt solution at 37°C under shaking conditions for a defined period of time. Next, the solution was centrifuged at 20,000 *g* for 15 min, after which the supernatant was mixed with SYBR® Gold (S11494, Invitrogen). The fluorescence was measured at a wavelength of 485 nm.

2.13 Statistics

Column and line charts or box charts as $25^{th}/75^{th}$ percentile boxes are presented as means ± SEM (standard error of the mean) geometric medians(Mouasni et al.), means (square), measurement points (rhomb), and 1.5 interquartile range (whiskers). Means ± SD (standard deviation) are indicated. The data normality was investigated by applying the Shapiro-Wilks test. P-values determination was assessed using ANOVA with post hoc Bonferroni correction for normally distributed data or Mann-Whitney U test with Bonferroni correction for not normally distributed data. The Grubbs' test was utilized to specify outliers. The OriginPro 2019 software (OriginLab, Northampton, MA, USA) was employed for statistical analyses and illustrations. Treatment vs. untreated: $^{*}p < 0.05$, $^{**}p < 0.01$, $^{***}p < 0.001$; loaded µRs vs. unloaded µRs: $^{+}p < 0.05$, $^{++}p < 0.01$, $^{+++}p < 0.001$, TAM vs. M0: $^{\circ}p < 0.05$, $^{\circ\circ}p < 0.01$, $^{\circ\circ\circ}p < 0.001$.

3 Results

3.1 Flow cytometry, live-cell microscopy-based analysis, and CLSM confirmed the µR uptake through HMDMs

The uptake of µR by different HMDM phenotypes was examined using flow cytometry, live-cell microscopy-based analysis, and CLSM. Flow cytometry provides precise, quantitative analysis. Flow cytometric analysis showed that one TAM HMDM took up the greatest number of µRs indicated by the highest FITC MFI (median fluorescence intensity), followed by M1 HMDMs (**Figure 14 A**). Analysis of the percentage of cells positive for µR showed that significantly more TAM HMDMs took up µR than M1 HMDMs (78% of TAM, 73% M0, and 57% M1 HMDMs were positive for µR) (**Figure 14 B**). Normalized percentages to M0 are shown.

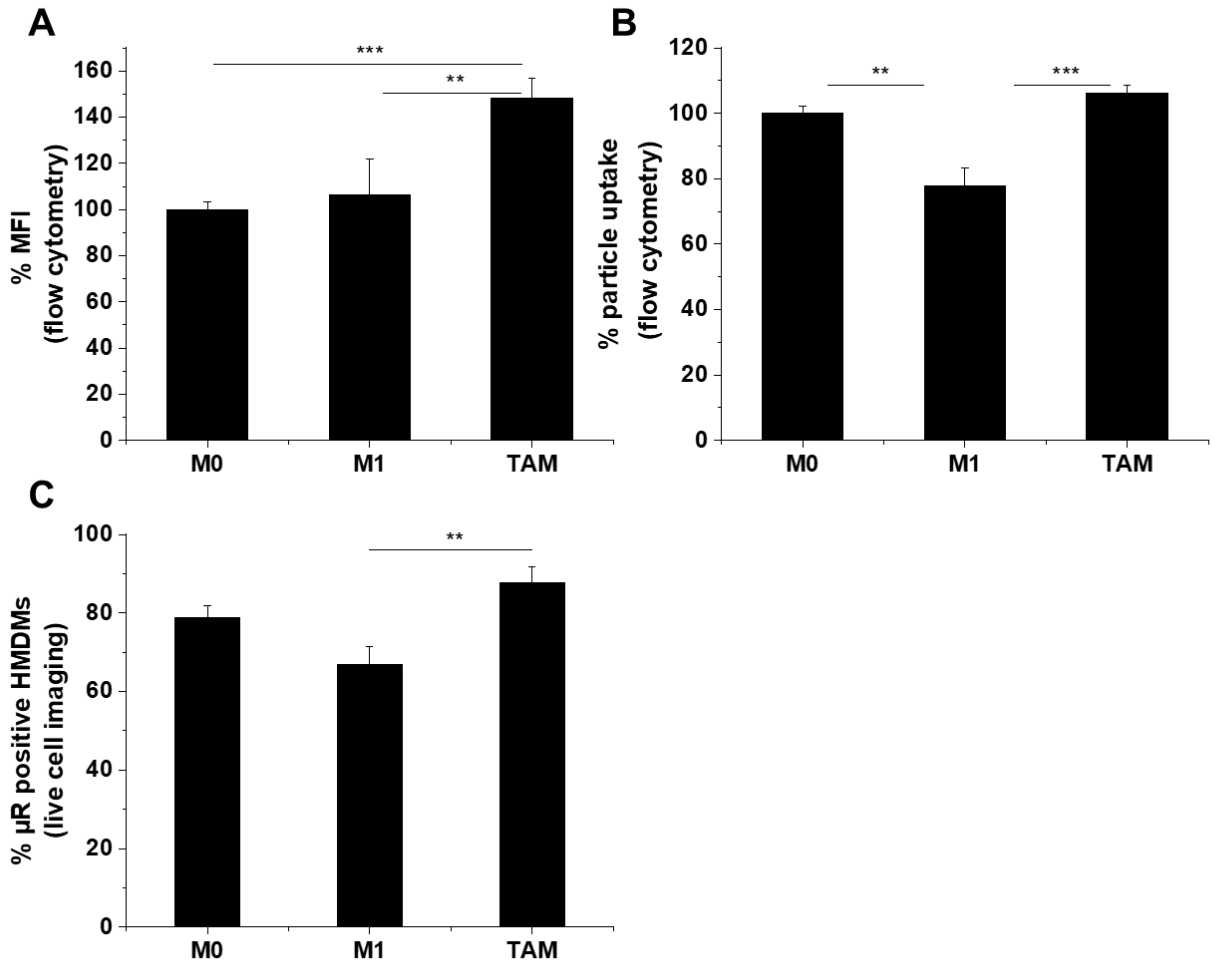

Figure 14. Excellent µR uptake through HMDMs. **(A, B)**: For flow cytometric analysis, M0 M1, and TAM HMDMs were incubated for 20 min with green-fluorescent µRs (400 µg/ml, corresponding to 2 µR/cell, FITC) and stained with CellTracker ™ Deep Red Dye (APC). **(A)**: Mean of normalized FITC MFI of M1 and TAM cells relative to M0 (100%) of CellTracker ™ Deep Red Dye positive events. **(B)**: Percentage of FITC positive cells in CellTracker™ Deep red Dye positive HMDMs normalized to FITC positive M0 (100%), (n = 5, duplicates). **(C)**: Live-cell microscopy-based analysis. Mean of µR-positive (high green) and CellTracker™ positive (high red) HMDMs in % of cell count (1 µR/cell, 20 min, n = 4, triplicates).

Live-cell microscopy-based analysis allows for quantitative analysis with live detection. The results obtained from flow cytometry were corroborated by live-cell microscopy-based analysis, which showed that M1 HMDMs took up fewer µR than TAM HMDMs and M0 HMDMs with a significant difference between TAM HMDMs and M1 HMDMs

(**Figure 14 C**). 88% of TAM HMDMs, 79% M0, and 67% M1 were positive for internalized µR after 20 min of incubation. These findings demonstrate similar results for the phenotypes in both techniques. Live-cell microscopy-based analysis revealed that most of the internalization occurs within a short time frame following the addition of µR (**Figure 15**).

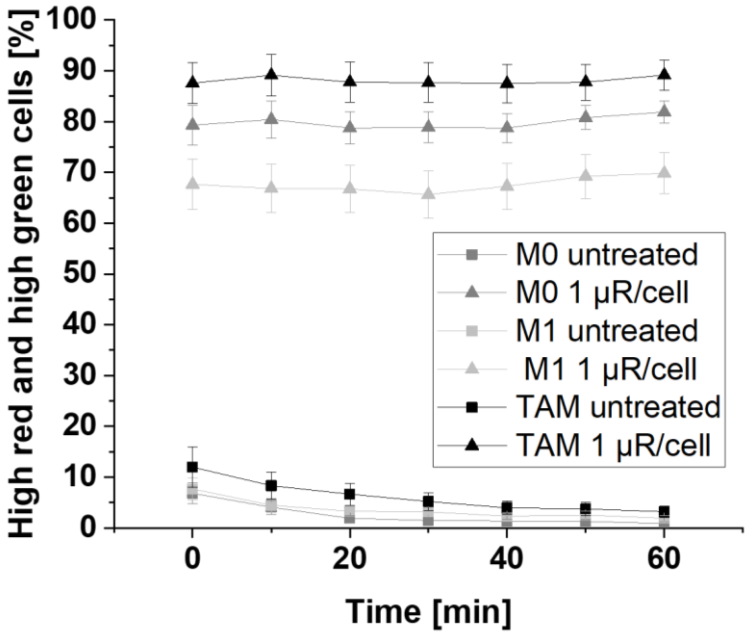

Figure 15. Pronounced µR uptake through HMDMs within minutes. Live-cell microscopy-based analysis. Mean of µR-positive (high green) and CellTracker™ positive (high red) HMDMs in % of cell count, starting immediately after µR addition (time point 0, 1 µR/cell, n = 4, triplicates).

CLSM allows for confirmation that the µR are present within the cells. CLSM analysis, which allows for the imaging of each layer separately through the acquisition of z-stacks, was performed to confirm the presence of µR within the cells. Merged images of 50 planes of the z-stacks are shown (**Figure 16**). TAM HMDMs had a high level of µR uptake, followed by M0 HMDMs, in agreement with the results from the other methods. In addition, the CLSM images demonstrated morphological differences between the HMDM phenotypes, M0 HMDMs were spherical and larger in size, while M1 HMDMs were smaller and TAM HMDMs were on average more elongated. Further, the images showed that HMDMs formed clumps surrounding µRs.

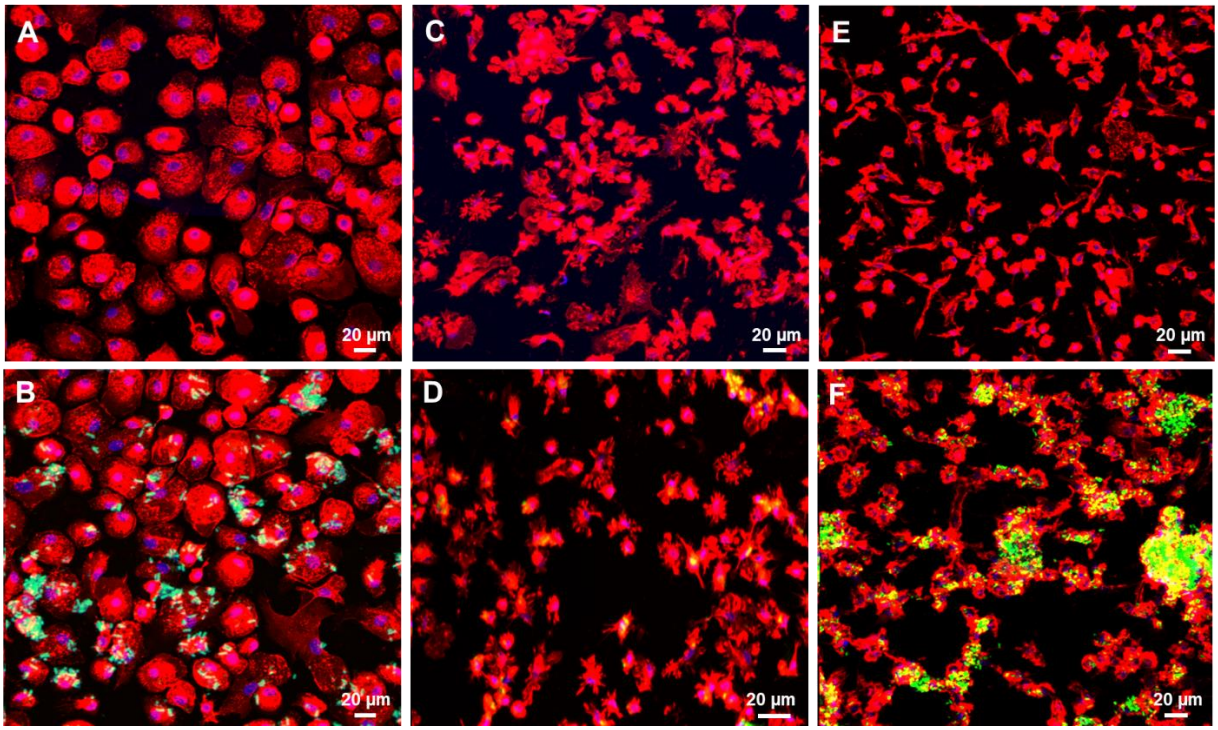

Figure 16. CLSM confirmed µR uptake by HMDMs. TAM HMDMs take up more µRs than M0 and M1 HMDMs. Merged CLSM images of HMDMs without treatment (above) or after incubation with µRs (below) (20 min, 400 µg/ml, corresponding to 2 µR/cell). **(A, B):** M0, **(C, D)** M1, and **(E, F)** TAM HMDMs. Red: F-actin stained with phalloidin-TRITC, blue: Nucleus stained with DAPI, green: µRs. Representative images are shown (n = 3, duplicates).

Separation of the channels in the imaging analysis allowed the identification of stained cell structure and µR locations (**Figure 17**). A large number of intact µRs were observed. µR fragments were detected particularly within the cells. The µR fragments provide insight into the distribution and potential degradation of µRs within the samples. In general, cells that internalize µRs tend to uptake multiple particles.

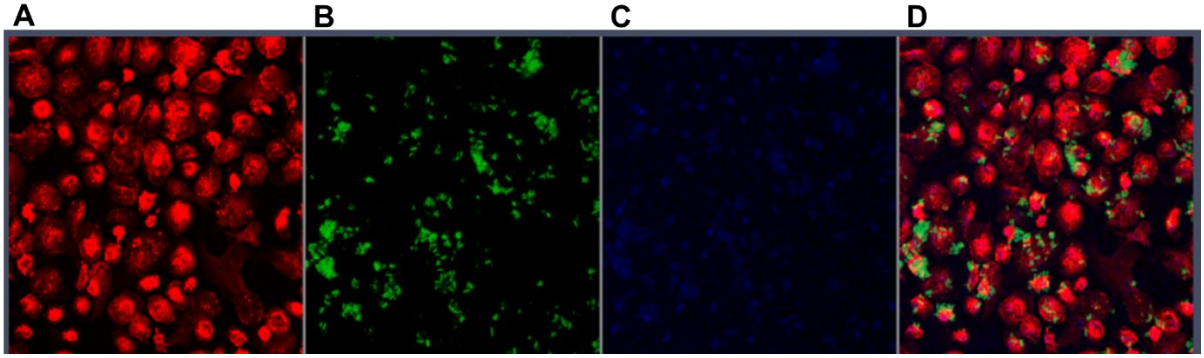

Figure 17. Representative CLSM image of M0 HMDMs incubated with 400 µg/ml µR (2 µR/cell) for 20 min. **(A)** Red: F-actin stained with phalloidin-TRITC, **(B)** green: µRs **(C)** blue: Nucleus stained with DAPI, **(D)** merged image (n = 3, duplicates).

A thorough analysis revealed that the majority of the µR were present inside the cells, rather than on the surface of the cells. However, a minority of the µR were found to be partially outside of the fixed HMDMs, which indicates that the cells are in uptake process (**Figure 18**). In the 3D image, several particles are covered by phalloidin-TRITC and show yellow color, which indicates that they are inside the cells (**Figure 18**

C, D). Each image contained 50 planes which can considered individually (**Figure 19**).

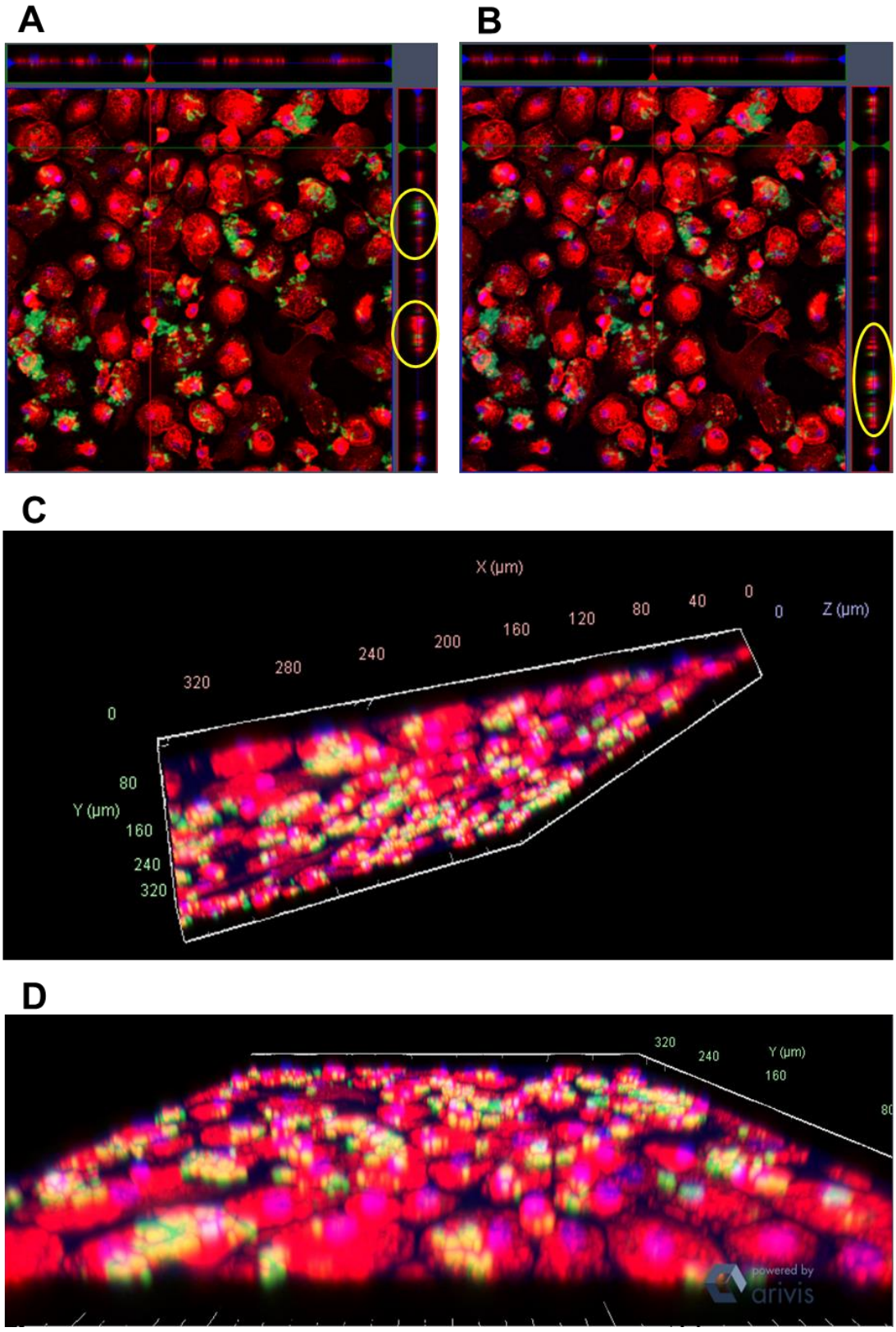

Figure 18. Representative CLSM image of M0 HMDMs incubated with 400 µg/ml µR (2 µR/cell) for 20 min showing different z-stacks and 3D images. **(A, B)** Different planes of a z-stack are visualized through cuts made through the z-stack. Yellow circles indicate examples of µR located on the same plane as cells. **(C)** Upper side **(D)** and the downside of the 3D image. Red: F-actin stained with phalloidin-TRITC, blue: Nucleus stained with DAPI, green: µRs (n = 3, duplicates).

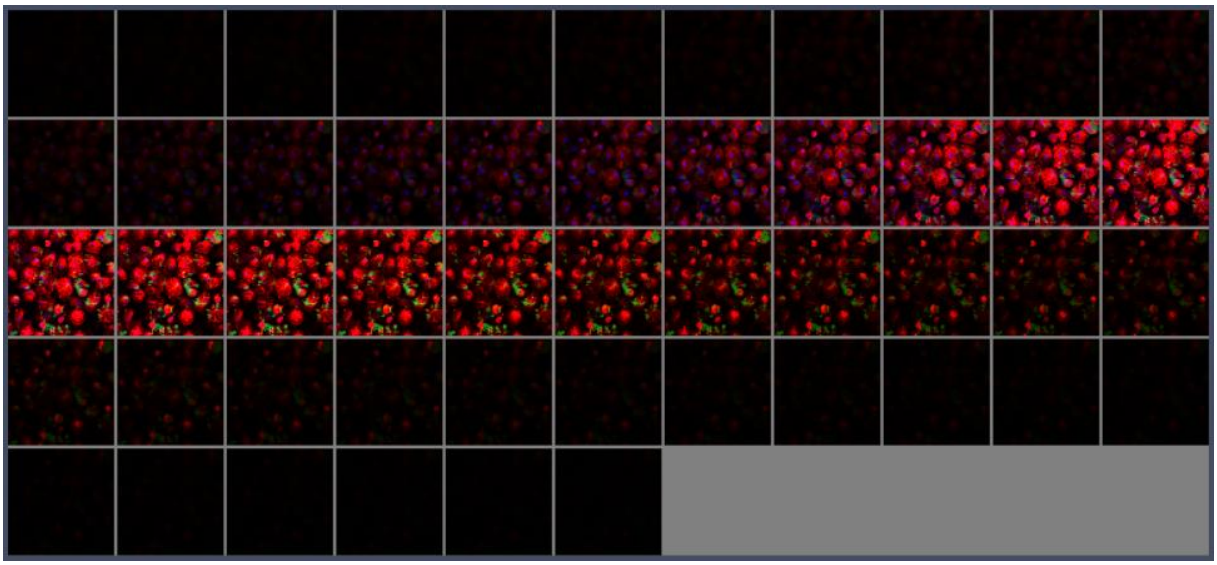

Figure 19. Representative CLSM z-stacks of an M0 HMDM image incubated with 400 µg/ml µR (2 µR/cell) for 20 min (50 planes).Red: F-actin stained with phalloidin-TRITC, blue: Nucleus stained with DAPI, green: µRs (n = 3, duplicates).

3.2 Poly(I:C)-release from µRs

The release of poly(I:C) was determined over 96 hours (by Dr. Thorben Fischer). After 4 h, 22 ng of poly(I:C) per mg of µR was released, and after 48 h, 182 ng of poly(I:C) per mg of µR was released (**Figure 20**, **Table 6**). These timepoints were used for investigating the effect of poly(I:C)-loaded µR on gene or protein expression in HMDMs. It should be noted that the number of µRs per mg varied between batches. It can be estimated that a concentration of poly(I:C) in picograms per cell may be released in cells after the uptake of approximately one µR during incubation, based on the fact that 1 mg of batch 8 contained more than 280 million µRs.

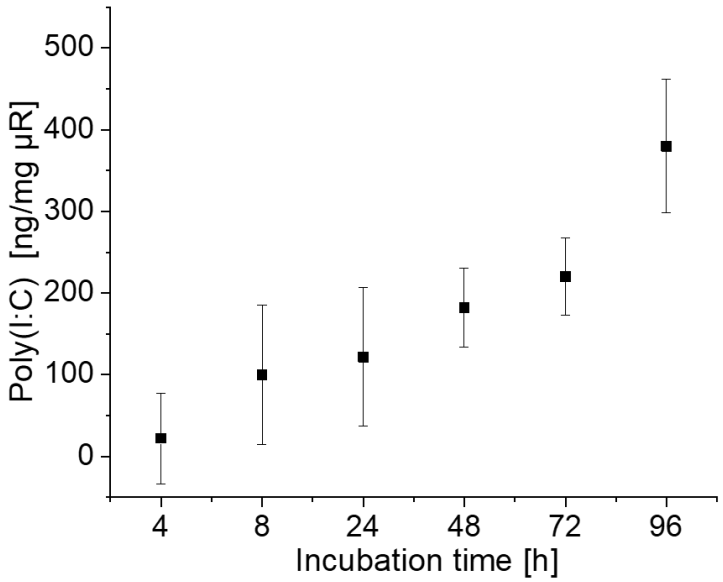

Figure 20. Release study of poly(I:C)- from µRs in phagolysosomal simulant fluid. µRs were gently shaken at 37°C for the indicated time, centrifuged at 20,000 *g* for 15 min, and the supernatants were mixed with SYBR® Gold. Fluorescence ± SD at 485 nm (n=1, triplicates).

Table 6: *Poly(I:C)-release from µRs in phagolysosomal simulant fluid*

Incubation time [h]	Poly(I:C) [ng/mg µRs]
4	22.00
8	99.94
24	121.60
48	182.23
72	220.14
96	379.66

3.3 Poly(I:C)-loaded as well as the unloaded µRs polarize HMDMs to an M1-similar phenotype

To investigate the ability of poly(I:C) targeted delivery using µRs to repolarize HMDMs towards an M1-like phenotype, poly(I:C)-loaded µRs were applied. Flow cytometry experiments were performed to analyze the expression of surface proteins.

The high expression of the surface proteins HLA-DR and CD80 in M1 macrophages and CD163 and CD14 in TAMs were confirmed through our investigation. The expression of markers was investigated after one, two, three, and four days and indicated that polarization was achieved after one day and increased thereafter (**Figure 21**). There was no evidence of any alteration in the activity of HMDMs during this period. Even after one day, differences in marker expression between the investigated HMDM phenotypes were observed. M1 markers were more highly expressed in M1 HMDMs, while M2 markers were more highly expressed in M0 and TAM HMDMs. These findings indicate that distinct polarization patterns can be identified within a short time frame and that HMDMs remain expressing the surface proteins even after four days of polarization.

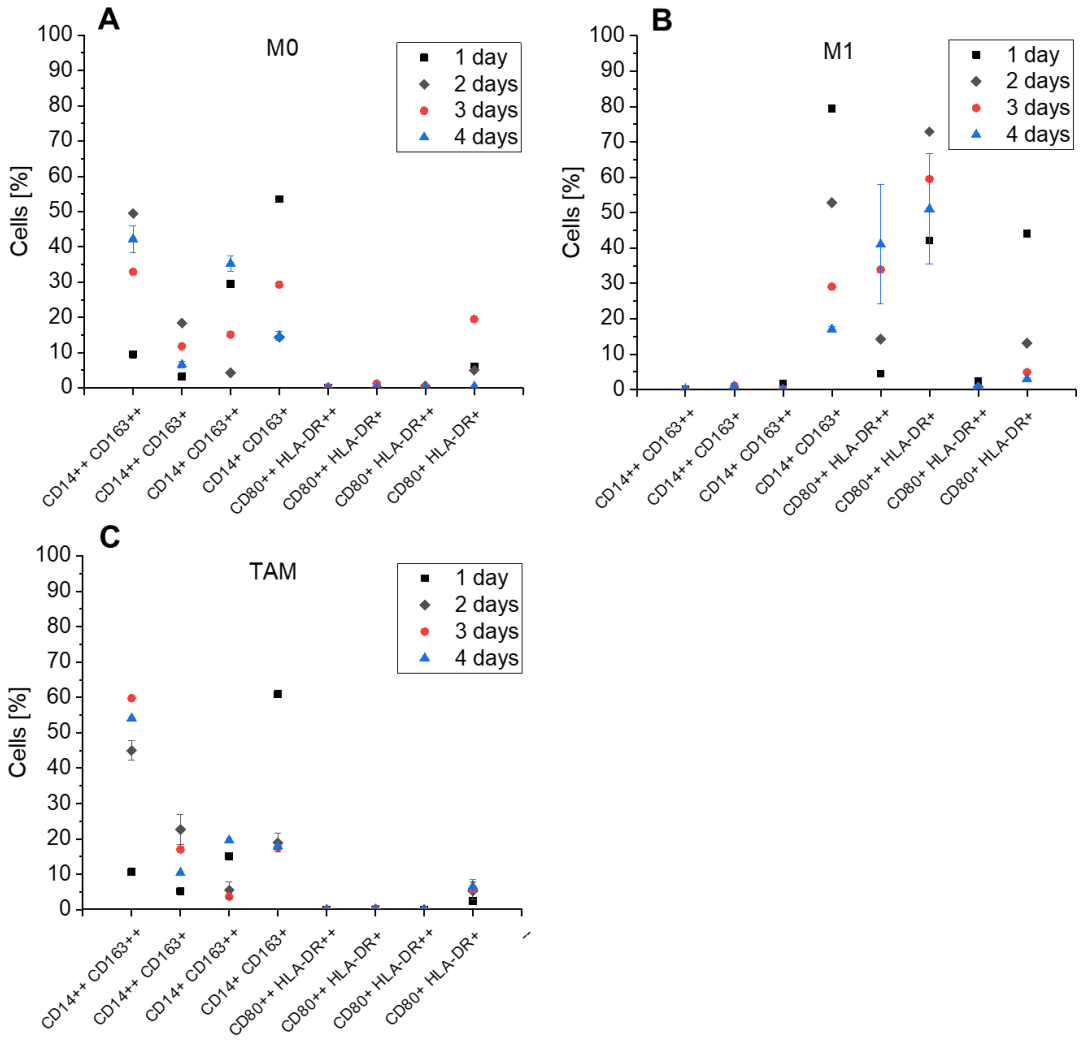

Figure 21. Marker expression over four days of polarization in M0, M1, and TAM HMDMs. Cells in percent expressing CD163, CD14, CD80, and HLA-DR markers were divided into low (+) and high (++) expressing (n=1, 1(-2) replicates). Marker expression in untreated M1 HMDMs compared to M0 confirmed successful polarization: Consistent to **Figure 22** the untreated M1 HMDM phenotypes higher expressed CD80 and HLA-DR, whereas CD163 and CD14 were lower expressed on M1 HMDMs surface compared to unpolarized M0 and TAM macrophages (**Figure 23**).

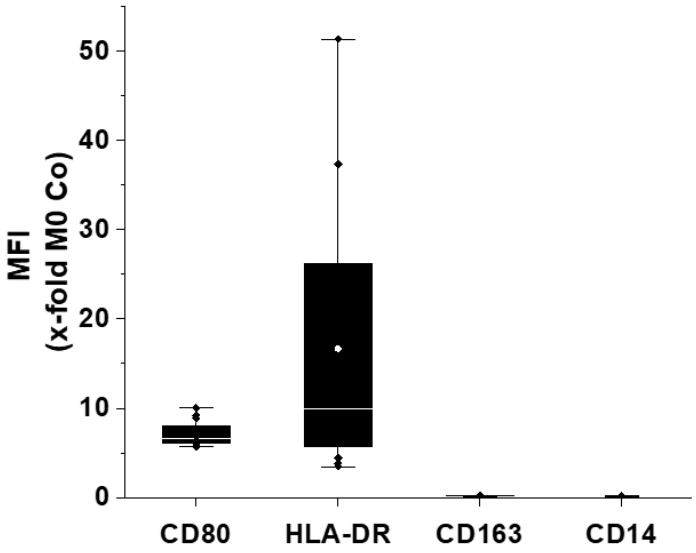

Figure 22. High M1-marker (CD80 and HLA-DR) and low M2 markers (CD163 and CD14) expression in untreated M1 HMDMs according to flow cytometry. Mean MFI x-fold untreated M0 HMDMs (n=4, triplicates).

The effect of poly(I:C)-loaded and unloaded µRs on marker expression was evaluated. Incubation with poly(I:C)-loaded µR resulted in the following effects: An increase in HLA-DR expression in M0 and TAM HMDMs. The increase was significant in M0 HMDMs samples. Further, it leaded to a clearly significant increase of CD80 in M0 and TAM HMDMs compared to untreated samples and unloaded µRs samples. In addition, it caused a significant decrease in CD14 expression and a significant decrease in CD136 expression in M0 HMDMs. Considering poly(I:C) release experiment (**Figure 20**) and µR number per mg (1 mg of batch 8 contained more than 280 million µRs), it can be assumed that about 80 pg were released in 48 h in one well.

The expression of CD163 and CD14 markers was more variable in TAM HMDMs than in M0 HMDMs due to differences between different donors. An unexpected revelation was polarization of M0 and TAM towards the M1 phenotype by unloaded µR.

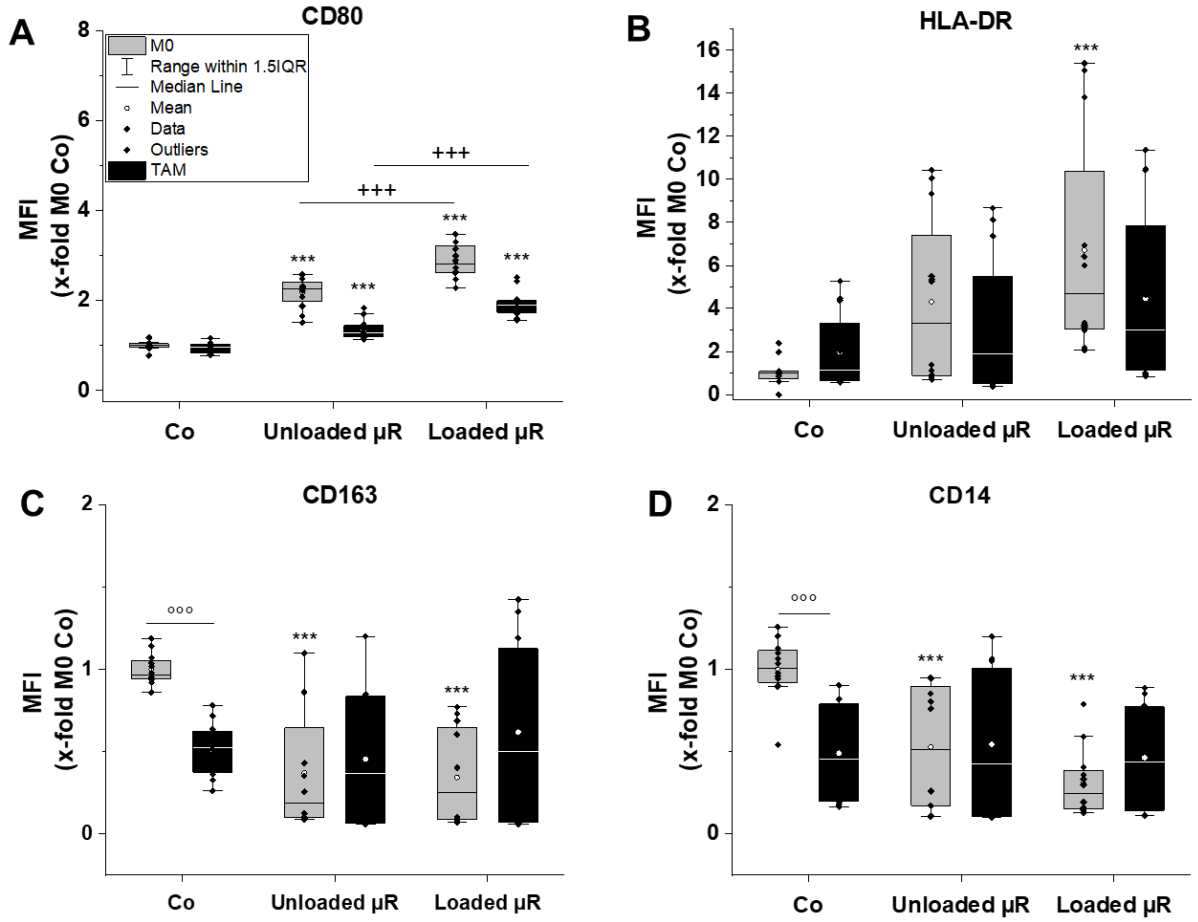

Figure 23. M1-markers CD80 and HLA-DR increased, and M2 markers CD163 and CD14 decreased in M0 and TAM HMDMs after µR incubation. Expression of surface marker **(A)** CD80, **(B)** HLA-DR, **(C)** CD163, and **(D)** CD14 in M0 (grey), or TAM (black) HMDMs determined by flow cytometry. Incubation with 0.5 non-fluorescent µR/cell (poly(I:C)-loaded µR = Loaded µR or unloaded µR). Mean MFI x-fold untreated M0 HMDMs (n = 4, triplicates).

It has been demonstrated that TLR3 agonists such as poly(I:C) can induce the production of different cytokines, including CXCL10, CXCL8, IL-1β, and TNF. TNF can also be induced through TLR4 agonists (Hoppstädter et al., 2019; Reimer et al., 2008).

In this study, poly(I:C)-loaded µRs resulted in a significant induction of *CXCL10* mRNA in M0 and TAM HMDMs and in TAMs also compared to unloaded µRs after 4 h incubation (**Figure 24**). The further investigated inflammatory genes *TNF*, *CCL2*, *CXCL8*, and *IL-1β* were also induced significantly compared to untreated controls, whereas *CCR2* expression decreased. The decrease was significantly in TAMs. the induction of *IFNG*, a cytokine with antimicrobial, antiviral, and antitumor activities (Ivashkiv, 2018), was not significantly changed after incubation with poly(I:C)-loaded µRs. The changes in gene expression induced by µRs were similar to those induced by LPS control, except for the *CCL2* gene, which was slightly reduced by LPS but increased by µR. In addition, the *CXCL10* mRNA was significantly higher in LPS-treated samples compared to µR-treated samples.

VEGFA expression, a growth factor induces proliferation and migration (Li and Zhu, 2023), was unexpectedly increased through poly(I:C)-loaded µRs compared to

untreated control. More the expectation according, *VEGFA expression* was lower compared to unloaded µRs.

The gene expression analysis confirmed that incubation with µRs resulted in a shift of M0 and TAM HMDMs toward M1 phenotype, comparable to the protein expression analysis. However, also unloaded µRs stimulate cytokine production in HMDMs, with the magnitude of response being dependent on the specific cytokine.

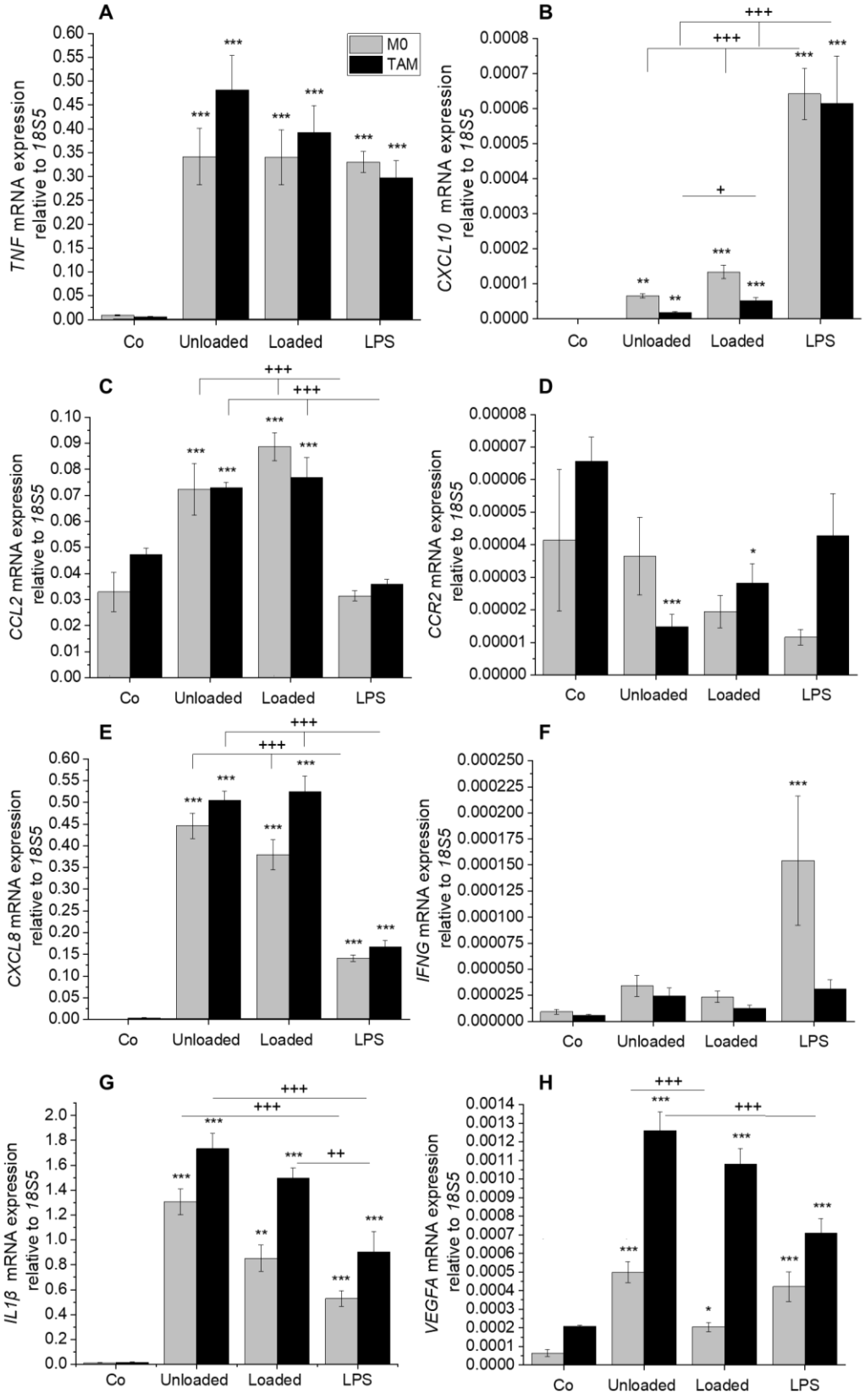

Figure 24. µRs affect mRNA expression in HMDMs according to qPCR. Mean mRNA expression (relative to 18S) in M0 (grey) and TAM (white) HMDMs after incubation with 0.5 µR/cell poly(I:C)-loaded µRs = Loaded, unloaded µRs. untreated samples (Co), or 100 ng/ml LPS; (n=3, triplicates).

3.4 Screening µRs for inflammatory activation

To ensure the absence of unspecific inflammatory effects due to µRs contamination, endotoxin assay was performed. The applied test allowed a quantitative detection with a detection limit of 0.005 EU/ml, which is higher than many available LAL assays.

The experiment included several intact µR batches at concentrations of 100 and 200 µg/ml, with 4 µR batches tested in duplicate (n=1). No detectable endotoxin contamination was found (data not shown). The test was performed with disintegrated µRs, using 9 µR batches at concentrations of 100 and 200 µg/ml, tested in duplicate (n=2). Whereas the intact µR did not interfere with the endotoxin assay, the results of the spike controls indicated that the disintegrated µRs could potentially interfere with the assay.

Since particulates are known to activate PRRs (Diesel et al., 2013), reporter cell assays were conducted to determine whether PRRs are activated by µRs and to obtain hints about which PRRs are involved in the activation process. Employed TLR agonists as positive control showed high cell activation. To further investigate a possible role of particle shape on activation, several µR batches were tested after disintegration. The employed µR concentrations were not toxic for the used cells (**Figure 25**).

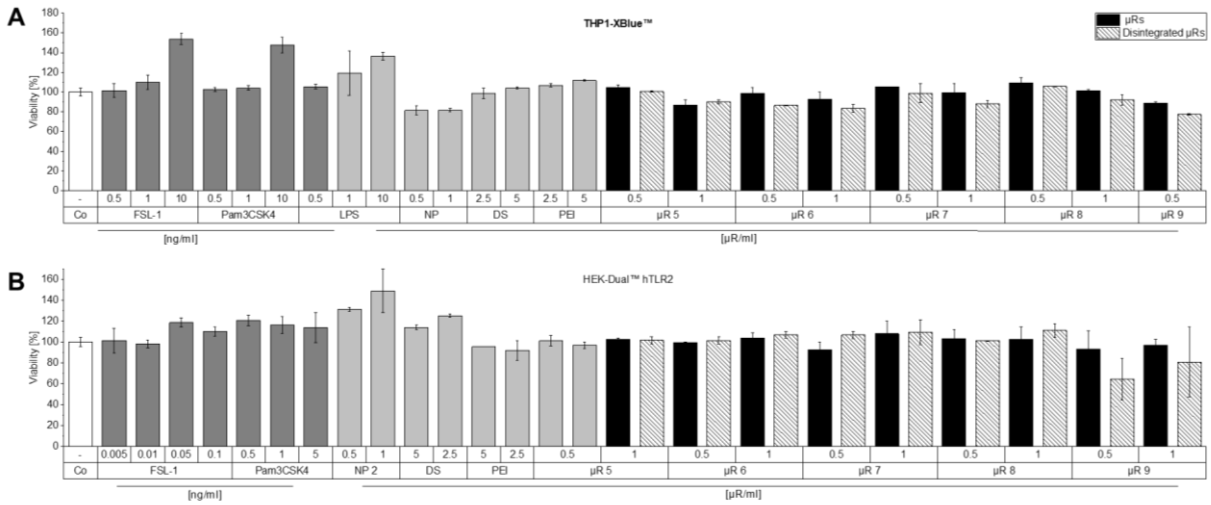

Figure 25. THP1-XBlue™ and HEK-Dual™ hTLR2 cells viability employing MTT assay.**(A)**: THP1-XBlue™ and **(B)** HEK-Dual™ hTLR2 cells were left untreated (Co), or incubated with FSL-1, Pam_3CSK_4, or LPS (ng/ml); components of silica µRs in an amount, which corresponds to 0.5 or 1 µR/cell. Silica nanoparticles (NPs): 100 µg/ml, 200 µg/ml; dextran sulfate (DS) and branched polyethyleneimine (PEI): 2.5 and 5 µg/ml; with 100 or 200 µg/ml µRs (0.5 and 1 µR/cell) of different production batches (µR 5-9). Mean absorption normalized to untreated controls (Co, 100%). Intact µRs (black) or disintegrated (shaded); n = 1, duplicates.

The sensitivity of the assay was tested using increasing concentrations of these agonists (**Figure 26**). The THP1-XBlue™ cells showed the highest sensitivity to LPS, followed by FSL-1, and Pam_3CSK_4 in terms of mass concentration. µR coating substances DS and PEI did not activate THP1-XBlue™ cells at the concentrations tested. The NPs activated the THP1-XBlue™ cells in a concentration-dependent manner. THP1-XBlue™ cells were activated dependent from µR batch to different extinct.

Among the reporter cell lines tested, HEK-Blue™-hTLR2 cells showed the highest

sensitivity to the TLR2 agonist FSL-1. Similar to THP1-XBlue™ cells, DS and PEI did not activate the HEK-Blue™-hTLR2 cells at the concentrations tested and the NPs activated the cells in a concentration-dependent manner. In contrast to THP1-XBlue™ cells, all investigated µR batches activated HEK-Blue™-hTLR2 almost similarly to the untreated control, whereby the HEK-Blue™-hTLR2 cells are more sensitive and specific regarding TLR2 agonists.

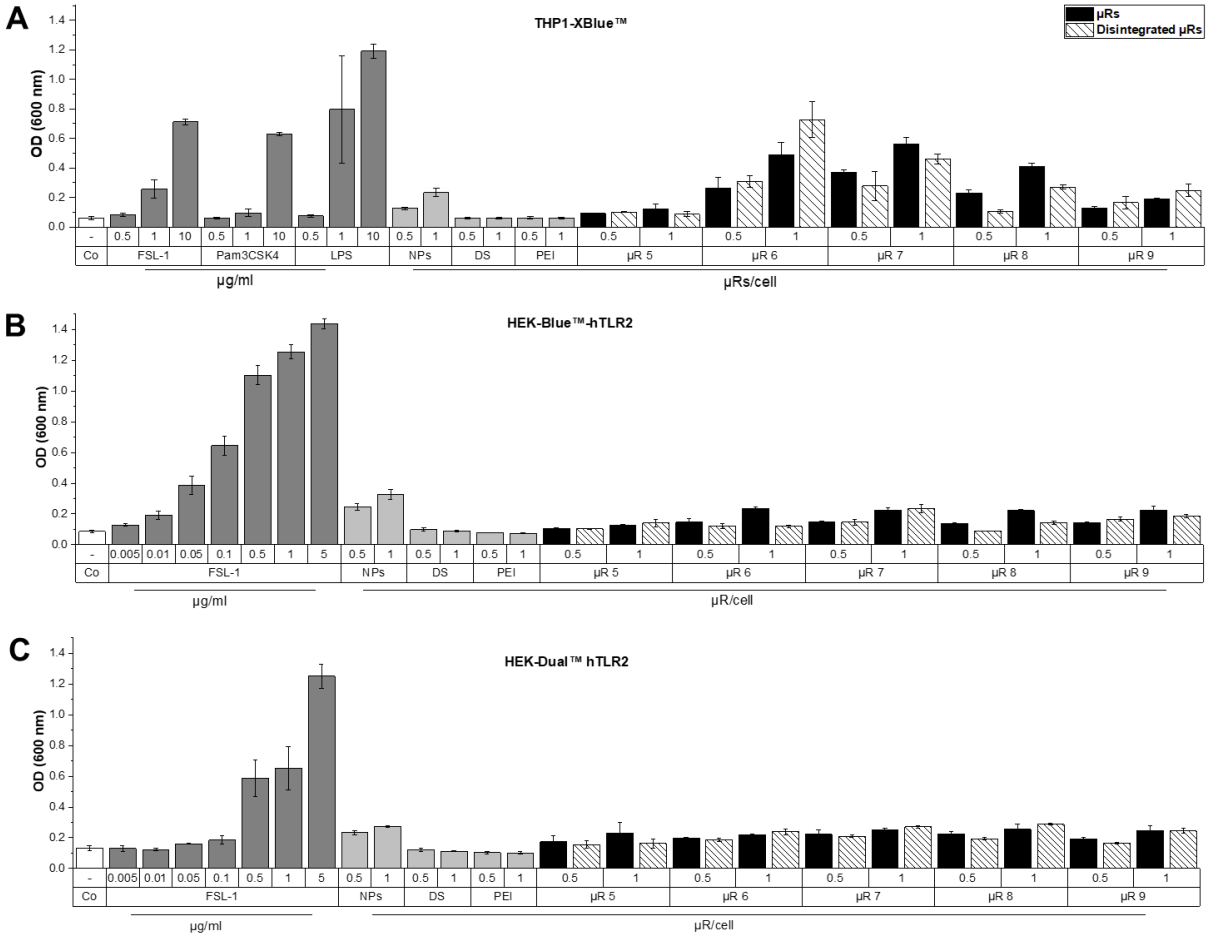

Figure 26. µRs activate TLRs in the reporter cell lines **(A)** THP1-XBlue™, **(B)** HEK-Blue™-hTLR2, and **(C)** HEK-Dual™ hTLR2. **(A-C):** Cells were either left untreated (Co) or were incubated with positive controls: **(A)** FSL-1, Pam_3CSK_4, and LPS (ng/ml), **(B, C)** FSL-1 (ng/ml). **(A-C):** Components of silica µRs; Silica nanoparticles (NPs), dextran sulfate (DS), and branched polyethyleneimine (PEI) in an amount that corresponds to 0.5 or 1 µR/cell (NPs: 100 µg/ml, 200 µg/ml; DS and PEI: 2.5 and 5 µg/ml). 100 or 200 µg/ml µRs (0.5 and 1) of different batches (µR 5 - µR 9). µRs were measured as intact µRs (black bars) or disintegrated (striped bars), mean ± SD (n = 1, duplicates).

In the experiments conducted, the HEK-Dual™ hTLR2 cells showed the second highest sensitivity to the TLR2 agonist FSL-1 compared to the other investigated reporter cell lines. The tested components had similar effects on the cells like on HEK-Blue™-hTLR2. Since there was no recognizable different between the two investigated HEK cells, it can be concluded that TLR3 and TLR5 are not involved in the inflammatory activation.

In summary, almost no activation of TLRs was induced through µRs in the HEK reporter cell lines, while in the THP1-XBlue™ cells, the activation was more pronounced. Thus, beside no detection of endotoxin (recombinant factor C assay, absence of TLR4 activation), also TLR2 activation may be excluded. With this the

inflammatory HMDMs activation through bacterial contamination can be defined as improbable. Moreover, the results showed no clear trend in the differences between the intact µR and the disintegrated µR in terms of activation.

3.5 µRs induced IL-1β secretion in HMDMs

To determine whether NLRP3 inflammasome formation, leading to IL-1β cytokine secretion, is induced by µR incubation due to their particulate nature, the concentration of IL-1β in the supernatant was measured. For this purpose, HMDM supernatants were incubated with HEK-Blue™ IL1R reporter cells (**Figure 28**), which express human and murine interleukin-1 cytokines (IL1-α and IL-1β). LPS treatment did not result in IL-1β secretion, while treatment with LPS followed by monosodium urate crystals (MSU), as a positive control, promoted IL-1β secretion, as reported in the literature (Piancone et al., 2018).

In general, IL-1β decreased viability of HEK-Blue™ IL1R reporter cells, as expected (**Figure 27 A**). The viability of the HEK-Blue™ IL1R reporter cells is slightly affected by HMDM supernatant treated with µR (**Figure 27 B**).

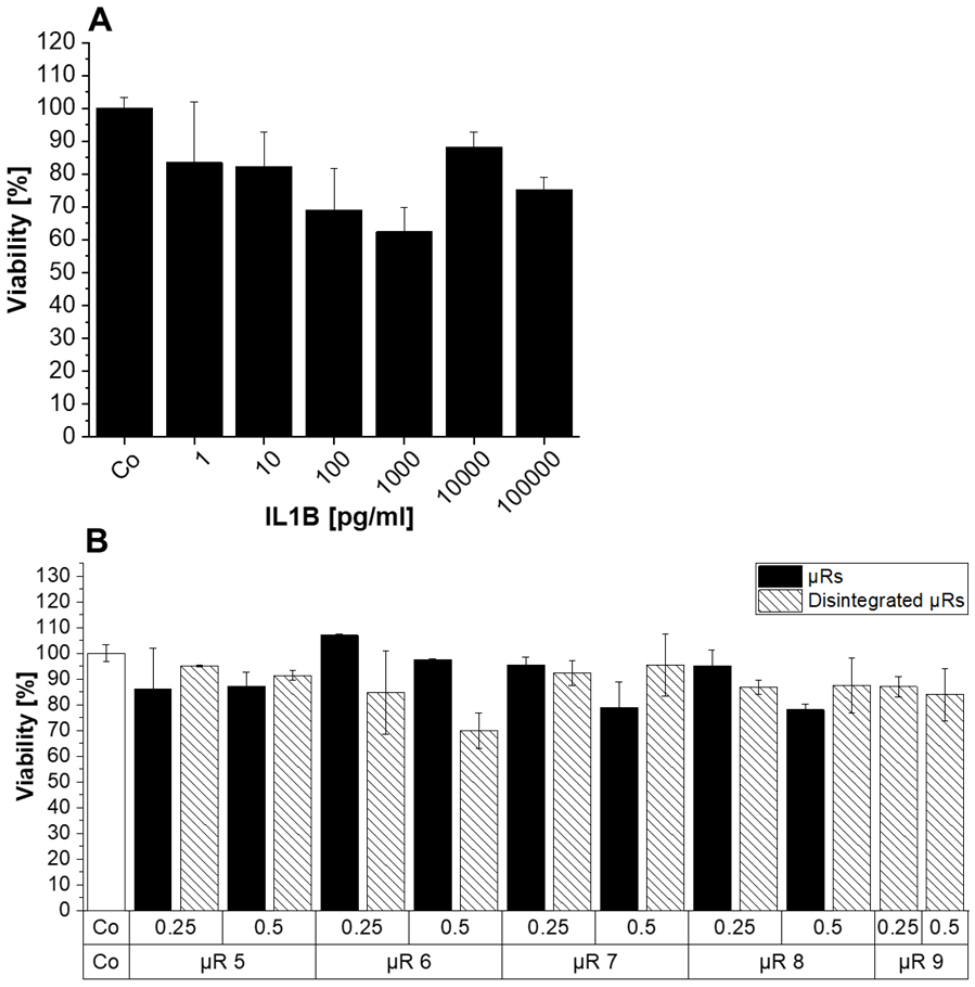

Figure 27. HEK-Blue™ IL1R reporter cell viability after incubation with IL-1β standard dilution **(A)** and HMDM supernatant for 24 h **(B)**. MTT results of HEK-Blue™ IL1R reporter cells after incubation with HMDM supernatants: Cells were left untreated (Co) **(B):** Cells were incubated with 0.25 or 0.5 µR/cell of different batches (µR 5- µR 9). µRs were measured as intact µRs (black bars) or disintegrated (striped bars), mean ± SD (n = 1, duplicates).

Several µR batches were investigated in intact and disintegrated forms at two different concentrations. All of the investigated batches induced higher IL-1β secretion compared to the untreated control, but to a different extent. Generally, there was no clear difference in the IL-1β secretion between intact and disintegrated µRs.

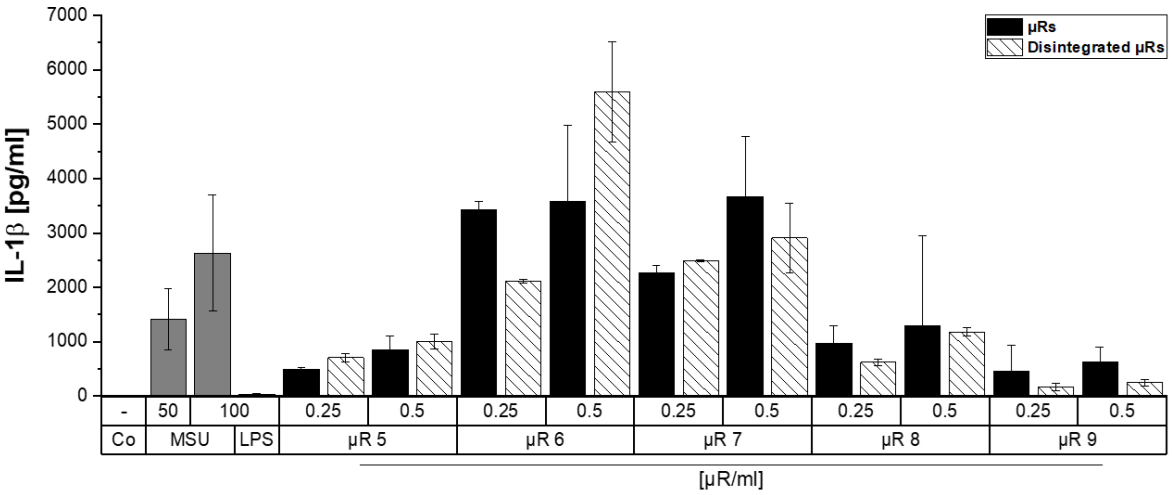

Figure 28. IL-1β secretion in HMDMs after µR incubation. IL-1β [pg/ml] was measured in HEK-Blue™ IL1R reporter cells after incubation with HMDM supernatant for 24 h. Cells were left untreated (Co), treated with LPS (100 ng/ml) for 18 h alone or followed by monosodium urate crystals (50 and 100 µg/ml) for 6 h, or incubated with 0.25 or 0.5 µR/cell of different batches (µR 5- µR 9). µRs were measured as intact µRs (black bars) or disintegrated (striped bars), mean ± SD (n = 1, duplicates).

3.6 IL-1β secretion in BMMs induced by µRs

For further investigation if NLRP3 inflammasome is involved in the inflammatory reaction following µR incubation, NLRP3 KO and WT cells were incubated with µR and IL-1β concentrations in supernatants were compared employing HEK-Blue™ IL1R reporter cells (**Figure 29**). The IL-1β secretion in BMMs was lower than in HMDMs, except for supernatants from the positive control treatments of LPS followed by ATP, and LPS, which had to be diluted for measurement. LPS followed by ATP induced higher IL-1β secretion in WT than NLRP3 KO BMMs. The IL-1β secretion in C57BL/6 NLRP3 KO BMMs followed LPS and ATP treatment suggests that NLRP3 inflammasome was not completetly shut down.

The µRs induced IL-1β secretion in WT and NLRP3 KO BMMs, with a higher induction in C57BL/6 WT BMMs. The IL-1β secretion induced by µR was highly donor-dependent, resulting in a high standard deviation, especially in WT BMMs. The NPs induced no remarkable IL-1β secretion.

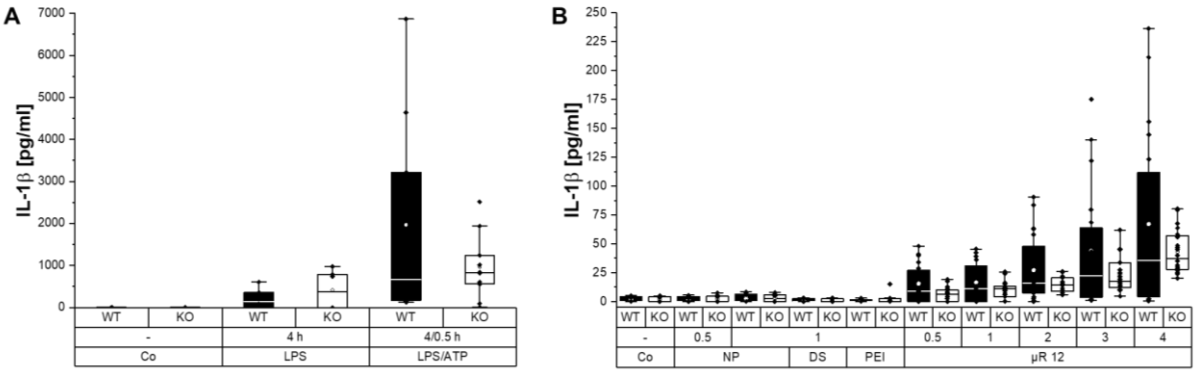

Figure 29. IL-1β secretion in BMMs after µR incubation. IL-1β [pg/ml] as measured in HEK-Blue™ IL1R reporter cells after µR incubation with C57BL/6 WT or C57BL/6 NLRP3 KO BMMs supernatant for 24 h. **(A)**: Cells were left untreated (Co) or were treated with the first stimulus LPS (100 ng/ml) for four h followed by a second ATP (3 mM) for 30 min. n = 2-4, duplicates. **(B):** Cells were left untreated (Co) or incubated with 0.5, 1, 2, 3, or 4 µR (µR 12). Treatment with components of µRs in an amount which corresponds to 0.5 or 1 µR /cell (Silica nanoparticles (NPs): 100 µg/ml, 200 µg/ml; dextran sulfate (DS) and branched polyethyleneimine (PEI): 5 µg/ml), mean ± SD (n = 4-6, duplicates).

3.7 Cytotoxic effect of µRs on viability

Due to the observed high inflammatory activation by µRs, which is known to be toxic and induce pyroptosis (Swanson et al., 2019), the µR cytotoxicity was thoroughly investigated using the MTT assay, crystal violet, and live-cell microscopy-based analysis. The MTT assay is a method based on mitochondrial function, the crystal violet assay is based on cell detachment, and the live-cell microscopy-based analysis is based on membrane permeability.

According to the results of the MTT assay, the viability of M0 HMDMs was above 80% for a concentration of 0.5 µR/cell after 24 and 48 h of incubation, regardless of the µR batch investigated. However, the viability was significantly reduced. There was no remarkable increase between 24 and 48 h incubation (**Figure 30**). Live-cell microscopy-based analysis indicated that the viability of HMDMs was at 80% after incubation with 0.5 µR/cell, although the curve was steeper. The crystal violet assay showed that 62% of the HMDMs were viable after incubation with 1 µR/cell for 48 hours.

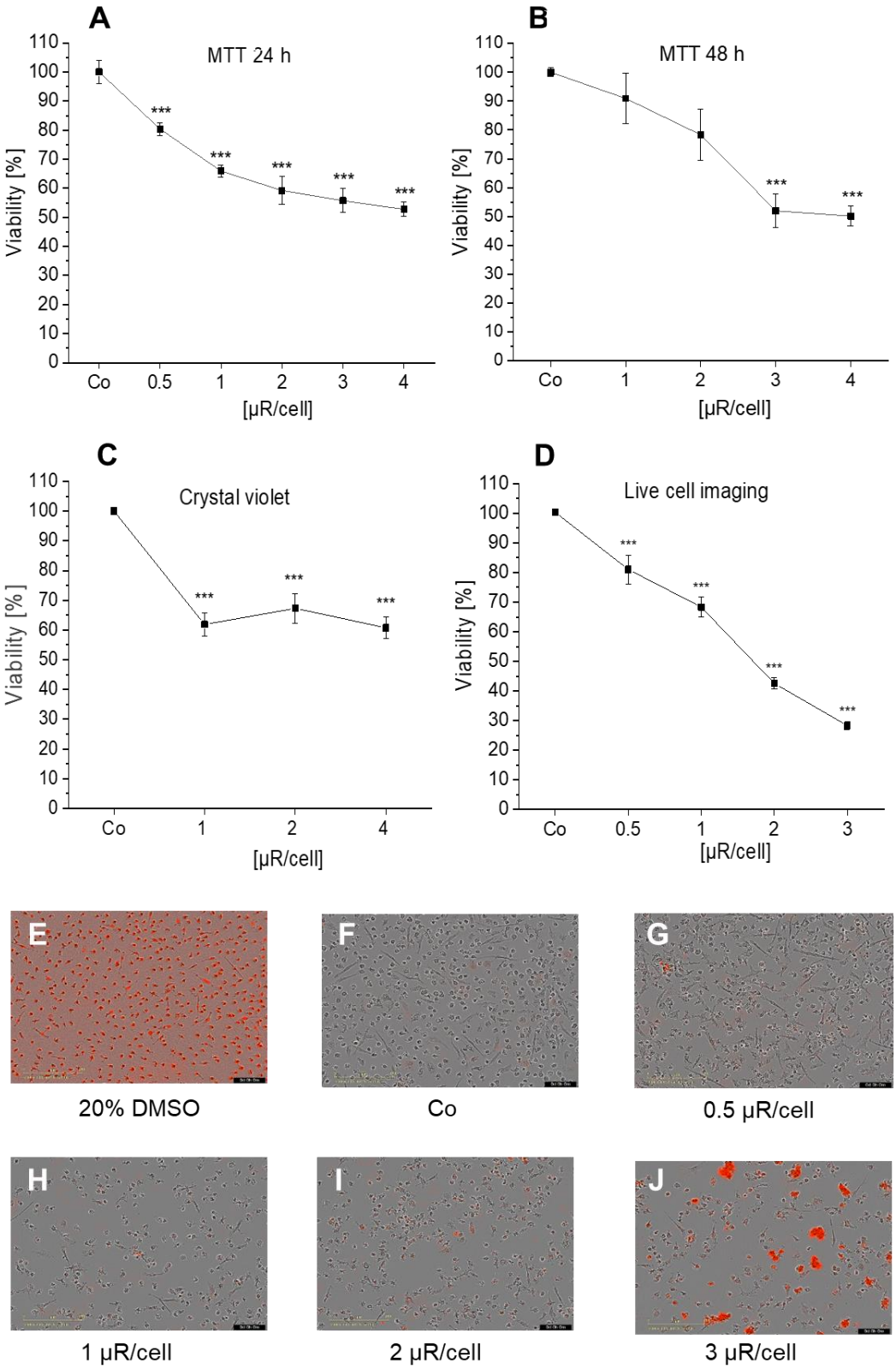

Figure 30. M0 HMDM viability affected by high µRs concentrations as determined by **(A, B)** MTT assay, **(C)** crystal violet, and **(D-J)** live cell imaging. HMDMs were left untreated (Co) or incubated with **(A)** µRs for 24 h (n = 3-5), quadruplicates, 4 µR batches). **(B):** µR incubation for 48 h (n = 2-4, triplicates, 1 µR batch). Mean absorption normalized to Co. **(D-J):** For analysis with IncuCyte® S3 live-cell analysis system, HMDMs were incubated with µRs and IncuCyte® Cytotox Red Reagent. **(C):** µRs incubated for 48 h with µRs (n = 2, triplicates, 1 µR batch). Mean absorption normalized to Co. **(D):** Mean percentage of IncuCyte® Cytotox Red Reagent negative (=viable) cells after 48 h per cell count normalized to Co (n = 4, triplicates, 1 µR batch). **(E – J):** Representative live cell microscopy images.

to determine whether the NLRP3 activation is involved in cytotoxic effects, cytotoxicity tests was conducted with WT and NLRP3 KO BMMs.

Controls with LPS followed by ATP significantly decreased the viability of WT BMMs (**Figure 31 A**). A higher viability of NLRP3 KO BMMs after treatment with µRs and ATP control was observed (**Figure 31 B**). Consistent with the findings in this study that µRs induced an inflammatory response and pyroptosis, µRs affected the viability of WT BMMs higher than NLRP3 KO BMMs.

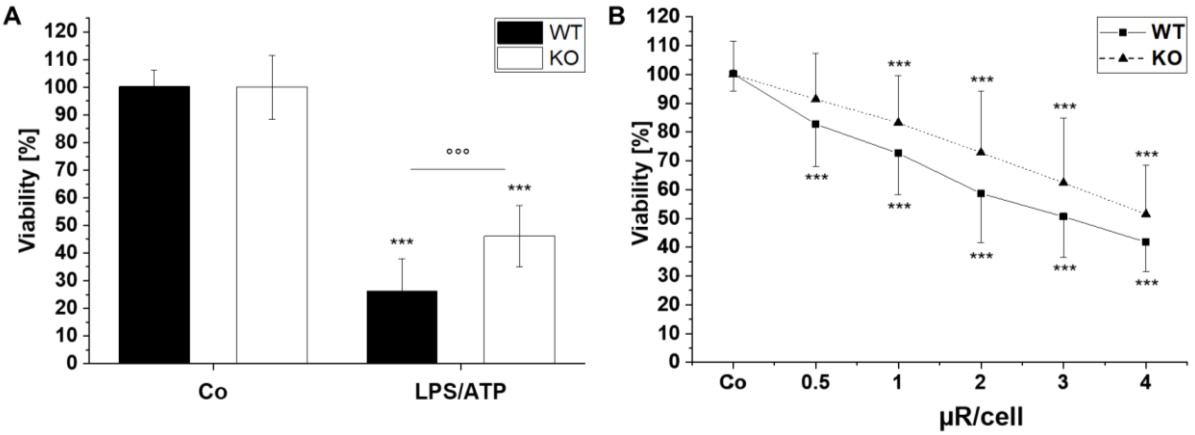

Figure 31. C57BL/6 WT BMM and NLRP3 KO C57BL/6 BMM viability as determined by MTT assay. **(A)**: Controls were treated with the first stimulus LPS (100 ng/ml) for four h followed by ATP (3 mM) for 30 min. **(B)**: Cells were left untreated (Co) or incubated with µRs (0.5, 1, 2, 3, and 4 µR/cell). Means of absorption normalized to untreated control (Co) ± SD in percent, 2 µR batches, 24 h **(A):** WT: n = 2-6, duplicates, KO: n = 2-4, duplicates, **(B)** WT: n = 9, triplicates, KO: n = 6, triplicates.

A live cell imaging assay was performed for 48 h, with measurements taken every 4 h (**Figure 32**). The viability increased during the first 4 h and did not continue to increase thereafter. µRs were less toxic in the live cell imaging assay compared to the MTT assay. The difference between 1 and 2 µR/cell was considerably smaller in the live cell imaging assay than between the other concentrations. The live-cell imaging assay clearly showed a higher viability of NLRP3 KO BMMs compared to WT BMMs.

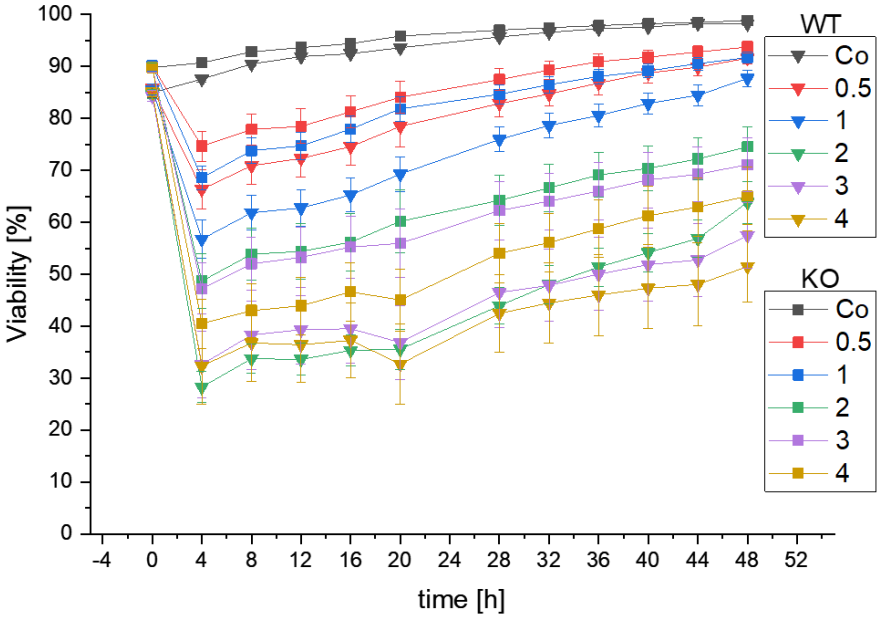

Figure 32. WT and NLRP3 KO BMMs viability within four h after incubation with µRs according to live-cell imaging after incubation.BMMs were left untreated (Co) or incubated with µRs (0.5, 1, 2, 3, and 4 µR/cell) and stained with IncuCyte® Cytotox Red Reagent. Mean percentage of IncuCyte® Cytotox Red Reagent negative (=viable) cells per cell count, 48 h, n = 4, 2 batches (triplicates).

3.8 Particles manufactured of different materials induce TLR activation

To further investigate to what extent the coating polymers are involved in the inflammatory effect of µRs, µRs were manufactured with agarose coating instead of DS and PEI (**Figure 33**). However, the *TNF* and *IL-1β* mRNA expression was higher by agarose-coated µRs than dextran sulfate and branched polyethyleneimine-coated µRs.

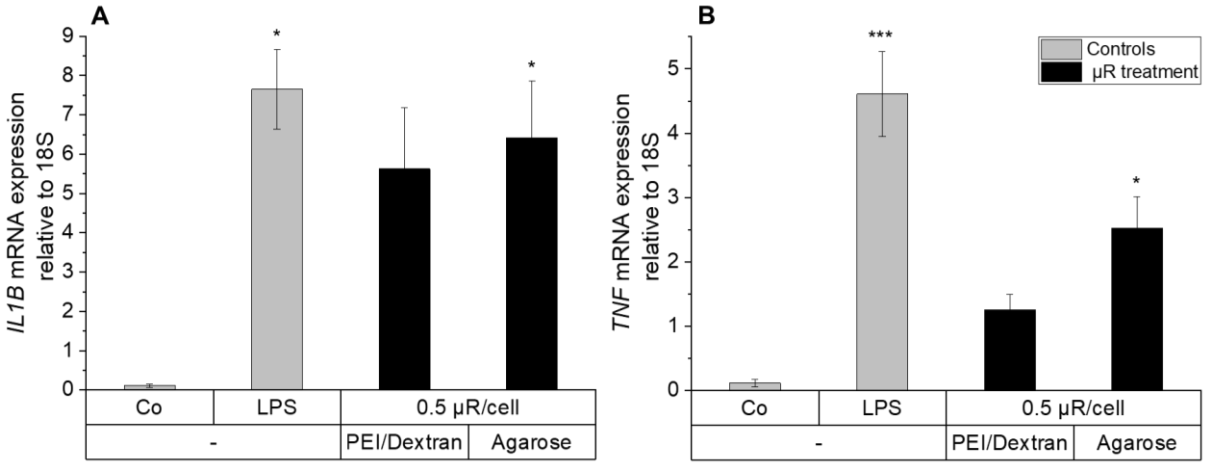

Figure 33. Agarose-coated µRs induced higher inflammation than dextran sulfate and branched polyethyleneimine-coated µRs in HMDMs according to qPCR. **(A)**: Mean *TNF* and **(B)** *IL-1β* mRNA expression (relative to 18S) in HMDMs after incubation with 0.5 µR/cell unloaded µRs coated with dextran sulfate (Dextran) and branched polyethyleneimine (PEI). Untreated samples (Co) or 100 ng/ml LPS, (n=1, triplicates).

To determine whether the material and/or shape of particles are responsible for cytotoxic and inflammatory effects, several materials commonly used for particle manufacturing were incubated with THP1-XBlue™ (**Figure 34**). The materials were not tested for bacterial contamination. The components of gelatin rods (GNPR) gelatin and gelatin nanoparticles (GNP) did not activate TLR, while GNPR did. Poly(lactic-co-glycolic acid) nanoparticles (PLGANP) did not cause any activation. Agarose induced huge activation, in contrast to polyvinyl acetate (PVA), DS, PEI, and poloxamer 188 (P 188).

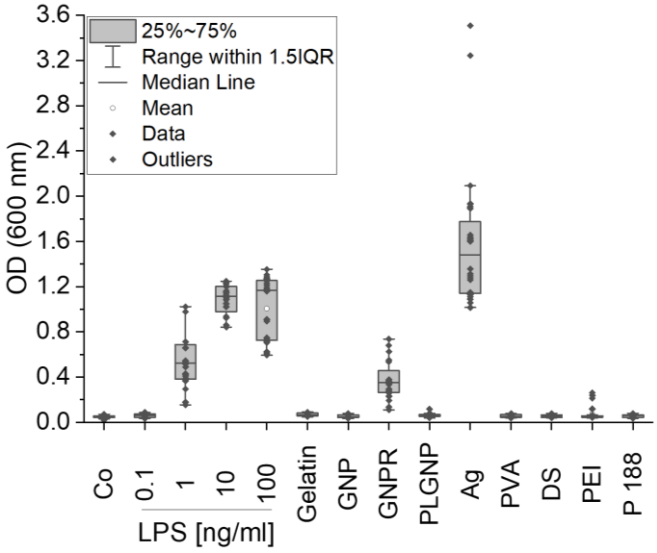

Figure 34. Different polymers do not cause TLRs activation, but microparticles do.THP1-XBlue™ cells were left untreated (Co) or were incubated with gelatin, gelatin nanoparticles (GNP) gelatin microparticles consist of gelatin nanoparticles (GNPR, 0.5 µR/cell), poly(lactic-co-glycolic acid) nanoparticles (PLGANP) in an amount corresponding to about 0.5 µR/cell (100 µg/ml), and polymers Agarose (Ag), polyvinyl acetate (PVA), dextran sulfate (DS), branched polyethylenimine (PEI), and poloxamer 188 (P 188) were employed in an amount corresponding to about 0.5 µR/cell (2 µg/ml). As positive control cells were treated with LPS. After 24 h incubation, 20 µl of the supernatant was added to 180 µl Quanti-Blue™ solution and incubated for the indicated time. Absorption at 600 nm is shown (n = 3, technical triplicates).

4 Discussion

4.1 µR uptake by HMDMs

Previous studies have demonstrated the uptake of the µRs by murine alveolar macrophages after 24 h employing CLSM (Möhwald et al., 2017). This study showed that HMDMs also took up µRs. One notable finding was that the uptake of µRs by HMDMs occurred within minutes and did not increase thereafter, whereas previous literature showed the µRs uptake at least 4 h after incubation in differentiated THP-1 cells using CLSM (Fischer et al., 2021a). This finding suggests that the process of µR internalization by cells may be efficient and involve multiple particles at once. It is possible that after several minutes, all µR were taken up, so the uptake did not increase further. Another interesting observation was that a TAM HMDM took up more µRs than an M1 or an M0 HMDM, and more TAM HMDMs took up µRs compared to M1 HMDMs. This is consistent with previous findings that showed that the particle uptake were higher in TAMs and M2 HMDMs compared to M1 HMDMs (Hoppstädter et al., 2015). This study adds value by using three different methods to investigate uptake, and the results obtained from all three methods were consistent. These findings suggest that the employed µRs are appropriate as a drug-delivery system for targeted delivery to macrophages, particularly TAM macrophages, and potentially for cancer treatment. Previous study indicated the high presence of monocyte-derived macrophages in human NSCLC, that highlighted the eligibility of HMDMs cell model for lung cancer macrophage targeting research (Leader et al., 2021). Further, particles in micrometer range, as large as the µRs, can reach the deep lung. Whereby particles bigger than ~ 0.5 µm can only be taken by specialized phagocytes (Jaumouillé and Grinstein, 2011).

Additionally, the CLSM investigation confirmed the µR' internalization and the morphological differences between macrophage phenotypes, as previously described in the literature (Edin et al., 2013; McWhorter et al., 2013; Rey-Giraud et al., 2012; Rostam et al., 2017). M0 HMDMs were generally round and larger, while M1 HMDMs were smaller and TAM HMDMs were elongated on average. Moreover, especially in TAM cell' CLSM images the cells were building clumps and surrounding the µR, which gives hinted at the fact that HMDMs moved in the direction of µR.

4.2 HMDM repolarization through µRs

Previous studies have utilized poly(I:C) at concentrations in the microgram per milliliter range in HMDMs (Lundberg et al., 2007; Lyons et al., 2015; Maeda et al., 2019), even when poly(I:C) was delivered intracellularly to HMDMs using lipofectamine (Reimer et al., 2008). This is likely due to the fact that poly(I:C) is an agonist of the intracellular, endosomal TLR3, and thus, intracellular delivery is advantageous (O'Neill et al., 2013). Furthermore, studies have demonstrated that transfected poly(I:C) can induce TNF protein expression within 8 h, which remains after 12 h and 24 h in HMDMs. In contrast, adding poly(I:C) to the cell culture medium only resulted in a low increase in TNF expression after 24 h. Poly(I:C) can induce a similar inflammatory response to LPS in HMDMs, but with different kinetics (Reimer et al., 2008). A previous study successfully employed arginine-based nano complexes for specific poly(I:C) delivery and M2-like HMDMs repolarization toward an M1-like phenotype (Dacoba et al., 2020). Further poly(I:C) was employed as a nanocomplex in clinical trials (Márquez-Rodas et al., 2020).

In this study, flow cytometry was utilized to confirm differences in marker expression among human macrophage phenotypes and confirmed that TAM HMDMs polarized by TCM are suitable as TAM model because of the similarity to *ex vivo* TAMs (Hoppstädter et al., 2021). Specifically, M1 markers CD80 and HLA-DR, as well as M2 markers CD163 and CD14 were identified in different macrophage phenotypes. The differences in M1 marker expression between untreated M1 HMDMs compared to untreated M0 and TAM HMDMs were much greater than the differences in the expression of M2 markers. The polarization of M0 HMDMs into M1 HMDMs using poly(I:C)-loaded µRs was successful as all markers were significantly shifted towards an M1-like phenotype. This shift was different from the shift observed with unloaded µRs, indicating an effect of poly(I:C). TAM HMDMs were also slightly shifted towards a M1-like phenotype, albeit to a lesser extent. Compared to previous studies employing poly(I:C), the drug concentration was very low. A previous study incubated HMDMs with 1 µg/ml or 10 µg/ml poly(I:C) with or without lipofectin. In this study the poly(I:C) release from applied poly(I:C)-loaded µRs was likely to be about 80 pg in total per well during the marker expression analysis (48 h incubation), which corresponds to very low concentrations. With this, this repolarization of HMDMs toward an M1-like phenotype was successful using µRs with very low concentration of poly(I:C).

Previous research has shown that intracellular poly(I:C) treatment increases inflammatory gene expression, such as *CXCL10*, in HMDMs after 4 h treatment with 1 µg/ml or 10 µg/ml poly(I:C) and lipofectamine, with a low increase after 8 and 12 h. The *CXCL10* increase was at least 100-fold higher when compared to adding poly(I:C) to the cell culture. LPS incubation was found to have the highest inflammatory gene expression after 4 h (Reimer et al., 2008). In this study the poly(I:C) release from applied poly(I:C)-loaded µRs was likely to be about 24 pg in total per well during the marker expression analysis (4 h incubation). Despite the low released concentration, the expression of most of investigated inflammatory genes increased, which pointed out the good drug delivery properities of µRs. For further evaluation, several incubation times or improved poly(I:C) release may clarify the effectiveness of µRs as drug delivery system and may show increase of the inflammatory effect of poly(I:C)-loaded µRs.

However, the detected unloaded µR' inflammatory effect may be due to µRs properties like shape, size and material. A previous study demonstrated that treatment with silica particles increased TNF, IL-10, and MCP1 proteins in NR8383 rat alveolar macrophages at concentrations between 50 and 250 µg/mL (Mao et al., 2021). The particle properties are known to have a crucial impact on particle effects (Salvioni et al., 2019). Thus, further investigation for causes of µR' inflammatory induction were needed.

4.3 Endotoxin determination of µRs

To find out the cause of the µR' inflammatory effect, TLR activation was investigated. According to literature, nano- and microparticles can alter gel formation, enzyme reactions, and assays based on absorption and fluorescence measurements. Therefore, it is important to thoroughly test established endotoxin detection methods for their suitability in nanomaterial testing (Kucki et al., 2014; Li and Boraschi, 2016; Li et al., 2017a). This study showed that the highly sensitive fluorescent-based assay had

low robustness for endotoxin detection in disintegrated µRs, as the spike controls spread. Nevertheless, there was no evidence of contamination in the intact µR.

Endotoxin contamination is challenging to remove, especially from small batches of nanomaterials (Magalhães et al., 2007). Therefore, it is essential to produce pyrogen-free nanomaterials for use in drug delivery systems.

To conclude, the results of this study suggest that there was no evidence of endotoxin contamination in the intact µRs. The detection was performed with a detection limit of 0.05-0.005 EU/ml. Additionally, we discovered that the disintegrated µR samples interacted with the endotoxin assay used in this study, which suggest the high interaction potential of smale particles compared to the bigger, intact µR with the employed endotoxin assay. Since µR disintegrate incide of cells, disintegrated µR testing should be considered.

4.4 TLRs activation through µRs

Reporter cell lines expressing TLR4 were employed in the literature as bioassays for detecting bacterial contamination and inflammatory response. Different pyrogens and particles are able to induce inflammatory activation (Li and Boraschi, 2016; Li et al., 2017b; Smulders et al., 2012). In previous research, the HEK-Blue™-hTLR2 and HEK-Blue™-hTLR4 cell lines were used to investigate the inflammatory effect of several herbal extracts (Schink et al., 2018). Utilizing different reporter cell lines could provide more information on the signal transduction pathway induced by the applied µRs and further explain the inflammatory activation through unloaded µRs. Further, reporter cell line assay offers the possibility to study the effect of disintegrated particles on TLR, in contrast to endotoxin assay.

A previous study showed that 50 µg/ml 100 nm silica nanoparticles induced TNF production in THP-1 cells. It was also found that smaller silica particles, in nanogram range, elicit a synergistic inflammatory response by co-incubation with TLR agonist (Diesel et al., 2013). Additionally, smaller particles were described in the literature as more likely to induce inflammation than bigger particles in the micrometer range in immune phagocytes (Baranov et al., 2021).

In this work, it was assumed that viral contamination occurs less likely than bacterial contamination, and HEK293 cells were not expected to take up µRs, in contrast to THP1-XBlue™. Thus, it is more likely to detect signals with the PRRs located on the cell surface in HEK293 and PRRs detecting bacterial components, not with the endosomal-located PRRs activated by viral material (O'Neill et al., 2013). There were no significant differences in activation between the two HEK293 cell lines after incubation with the µRs. This suggests that TLR5 and TLR3 may not be essential for the cell response to µR particles. Since the highly sensitive to TLR 2 agonists, HEK293 were hardly activated by µR, TLR2 is unlikely to be involved in µR inflammatory activation.

THP1-XBlue™ cells express TLR4 and the cells reacted similarly sensitive to the LAL assay, the frequently used endotoxin test (Smulders et al., 2012). Since the endotoxin test was negative, it is unlikely that TLR4 is responsible for the inflammatory activation through µR. It is worth noting that THP1-XBlue™ cells were less sensitive to the

TLR2/6 agonist FSL-1 than HEK-Blue™-hTLR2 and HEK-Dual™ hTLR2 cells. This suggests that TLR1/2 and TLR2/6 may not be responsible for the response of THP1-XBlue™ cells to µRs. After an intensive investigation for bacterial contamination, it can be concluded that the µR-induced inflammation in HMDMs is not due to bacterial contamination.

4.5 µR cytotoxicity in HMDMs and the influence of inflammation

Polyethyleneimine is a cationic polymer that has been widely used as a coating for particle-based drug delivery systems (Lin et al., 2019). Dextran sulfate has also been utilized for the same purpose (Lamichhane et al., 2016).

Silica crystals have been shown to induce NLRP3 inflammasome activation and inflammation activation in HMDMs and BMMs by detecting IL-1β secretion (Hornung et al., 2008). Amorphous silica particles have been found to be less toxic than crystalline silica particles, possibly due to their more rapid clearance. There is also evidence that different sizes of silica particles can have different immunotoxic effects (Murugadoss et al., 2017). The inflammatory and cytotoxic effects of silica particles have been widely studied (Kusaka et al., 2014). Silica can induce an inflammatory response, with inflammasome activation and IL-1β secretion being dependent on particle size. The highest activation was observed with silica particles ranging in diameter from 30 to 1000 nm, compared to those ranging in diameter from 3000 to 10000 nm in C57BL/6N BMMs (Kusaka et al., 2014). Silica particles have also been shown to induce lysosomal destabilization and cell death. Cytotoxic effects were observed at a concentration of ~ 0.03 mg/ml (the lowest investigated concentration), with a relationship between particle size and cell death similar to that observed for IL-1β secretion (Kusaka et al., 2014). Further studies have investigated the effects of particle shape, size, and type on TNF secretion, with rough particles and those with high aspect ratios being found to be particularly effective at inducing inflammasome activation and cell death in THP-1 (Baranov et al., 2021; Caicedo et al., 2013).

Particles generally have been shown to activate the NLRP3 inflammasome. Phagocytosis of particles has been identified as a mechanism for NLRP3 inflammasome activation, which occurs after particle uptake in macrophages (Muñoz-Planillo et al., 2013). The uptake of particles, both self-produced particles like uric acid and foreign particles like silica, leads to lysosomal disruption and the leakage of its contents into the cytoplasm, which is a key mechanism for NLRP3 activation (Hornung et al., 2008; Swanson et al., 2019). IL-1β secretion is a pyroptosis-related protein and an effector for inflammasome activation (Bergsbaken et al., 2009). It has been shown that pyroptosis is caspase-1-dependent but not caspase-11-dependent in BMMs (Broz et al., 2010). It was found that caspase-1 is responsible for CXCL8 processing, in addition to IL-1β, in BMMs (Ghonime et al., 2014). Further study observed the uptake of approximately 30 nm and 500 nm silica particles by RAW-ASC, a murine monocyte cell line expressing ASC (apoptosis-associated speck-like protein containing a CARD domain). The protein is involved in inflammatory and apoptotic signaling pathways by binding NLRP proteins with procaspase-1 (Compan et al., 2015). The uptake led to cell membrane rupture, mitochondrial lysis, and pyroptosis (Yin et al., 2022). Previous research has also indicated that amorphous silica particles (12 nm) can induce inflammatory gene expression in murine macrophages (Napierska et al., 2010).

In this study employed particles at even higher concentrations (up to approximately 0.09 mg/ml). The detection of IL-1β in HMDMs suggested inflammation-related cytotoxicity induction by µRs. The results from the reporter cell line suggest that the particulate nature of the µRs is responsible for their immune activation potential.

In this study, various viability assays were employed to investigate the mechanism of cytotoxicity in primary cells. Crystal violet assay is based on the detachment of cells from the surface to which they are attached. Microscopic analysis showed that µR were taken up by HMDMs and they might move toward the µRs, which may weaken the cell's attachment to the plate surface. Therefore, it was expected that cell detachment would lead to high toxicity in the crystal violet assay. The MTT assay indicated that the cytotoxic effect of the µRs did not show a proportional relationship between time and cytotoxic impact, as there was no increase in cytotoxicity after 48 h of incubation compared to 24 h incubation. Thus, it can be suggested that the cytotoxicity occurred during the uptake mechanism. The elevated decrease in HMDM viability observed in the live-cell microscopy-based assay with increasing µR concentrations may be due to the internalization of the IncuCyte® Cytotox Red Reagent along with the µR during uptake.

According to the above-mentioned literature, the µR' cytotoxicity effects in HMDMs might be induce by inflammatory activation and pyroptosis. In addition, lysosomal distribution following internalization of µRs may also contribute to the cytotoxic effects. The µR were employed in nontoxic concentration in the performed bioassays.

4.6 µR cytotoxicity in BMMs and the influence of inflammation

NLRP3 inflammasome formation leads to the production of pro-caspase-1 and pro- IL-1β, which can subsequently lead to IL-1β secretion and pyroptosis, among other effects. Both one-step and canonical NLRP3 activation are possible. Pyroptosis can also be induced through cytosolic LPS by activating caspase 11 in mice or caspase 4 and 5 in humans (Swanson et al., 2019). It has been reported that in human monocytes and mouse bone marrow-derived dendritic cells one-step NLRP3 activation can be induced, in contrast to macrophages (He et al., 2016). It has been observed that the phagocytosis of long, aspherical particles by macrophages leads to lysosomal destabilization and inflammasome activation (Baranov et al., 2021).

In this study it was observed that µRs induced lower IL-1β secretion in NLRP3 KO BMMs than in WT BMMs. This suggests that IL-1β secretion induced by µRs is dependent on NLRP3 expression to some extent. WT BMMs had lower viability than NLRP3 KO BMMs after incubation with µRs. This difference suggests that a part of the µR toxicity is due to NLRP3 inflammasome activation. The uptake of the µRs may activate the NLRP3 without priming with TLR agonists, as phagocytosis was reported to induce inflammasome activation (Hornung et al., 2008; Nakayama, 2018).

The toxicity in WT BMMs was lower than in HMDMs, which is consistent with the known sensitivity of these cell types as discussed in literature (Agbanoma et al., 2012; Hoppstädter et al., 2016). The IL-1β secretion was significantly higher in HMDMs than in BMMs. Comparing the NPs samples to µRs samples of BMMs indicates that the shape of the µRs is involved in the inflammatory activation.

To conclude, the results from BMM assays confirm the further findings, indicating that the activation of the NLRP3 inflammasome plays a role in the cytotoxicity and inflammatory activation of µRs. However, since NLRP3 KO BMMs also produced IL-1β, it has revealed that the NLRP3 inflammasome is not the sole cause of the inflammatory effects of µRs.

4.7 Investigation of different polymers' effects on TLR activation

IL-1β secretion in WT and NLRP3 KO BMMs indicated a role of the µR shape in IL-1β secretion and NLRP3 activation, whereby the reporter cell experiments provided no clear evidence of µR shape influence on inflammation. In literature, it has been shown, that particles with high aspect ratios induce inflammasome activation and cell death in THP-1 (Baranov et al., 2021; Caicedo et al., 2013). For detailed analysis, in this study, polymers, nanoparticles, and microparticles inflammatory effects were investigated.

The investigation of different polymers indicated that the polymers tested did not elicit inflammation, despite agarose which clearly activate inflammation. The TLR activation assay suggested that the inflammatory of agarose-coated microparticles may be attributed to agarose, but DS and PEI might not be involved in the effect, which confirmed the further results. the gelatin microparticles (GNPRs) with an elongated shape caused low levels of inflammation, which is a first hint on the role of particle shape in inflammatory macrophage activation. However, as elucidated in this study, a meticulous assessment of potential contaminations must be conducted, considering various material properties.

5 Summary and conclusion

In this study, the rapid uptake of µRs by HMDMs was observed, with a particularly high number of TAM macrophages showing uptake of the µRs. Additionally, it was found that one TAM macrophage took up a higher number of µRs than an M0 and an M1 HMDM. Moreover, incubation with µRs partially repolarized HMDMs to an M1-like phenotype when loaded with poly(I:C). Thus, µRs are appropriate drug delivery system to target macrophages and specially TAMs. Further, the inflammatory effects of poly(I:C)-loaded µRs and repolarizing of M0 and TAMs macrophages toward an M1-like phenotype was successful observed. Despite the low drug release and thus the resulting low poly(I:C) concentration, the inflammatory effect of poly(I:C)-loaded µRs were higher than this through unloaded µRs on many of the investigated genes and proteins.

It was also shown that the involvement of PRRs and the NLRP3 inflammasome are not the only cause of the inflammatory response following the incubation with µRs. To further clarify the effect of poly(I:C), it is suggested that careful evaluation of the materials used to be conducted in future studies to ensure using a non-active material as the drug delivery system. To optimize the use of this novel drug delivery system, it may be beneficial to explore the use of silica nanoparticles or other materials with reduced inflammatory effects as components of the drug delivery system. Generally, in depth analysis of particulate drug delivery systems has to be performed regarding material characteristics and possible bacterial contamination.

To conclude, this study indicated that µRs are promising drug delivery system for macrophage targeting, thus it is beneficial to modify and characterize it further. Thus, this study is the foundation for further investigation of the particulate drug delivery system. Additionally, the inflammasome involvedness in cell response toward particulate drug delivery system was highlighted.

6 References

Agbanoma, G., Li, C., Ennis, D., Palfreeman, A. C., Williams, L. M., and Brennan, F. M. "Production of TNF-α in Macrophages Activated by T Cells, Compared with Lipopolysaccharide, Uses Distinct Il-10–Dependent Regulatory Mechanism". *The Journal of Immunology* (2012), 188, 1307-1317. doi:10.4049/jimmunol.1100625.

Al-Fityan, S., Diesel, B., Fischer, T., Ampofo, E., Schomisch, A., Mashayekhi, V., Schneider, M., and Kiemer, A. K. "Nanostructured Microparticles Repolarize Macrophages and Induce Cell Death in an in Vitro Model of Tumour-Associated Macrophages". *Pharmaceutics* (2023), 15, 1895. doi:10.3390/pharmaceutics15071895.

Anfray, C., Ummarino, A., Andón, F. T., and Allavena, P. "Current Strategies to Target Tumor-Associated-Macrophages to Improve Anti-Tumor Immune Responses". *Cells* (2019), 9, 46. doi:10.3390/cells9010046.

Bajpai, G., and Lavine, K. J. "Isolation of Macrophage Subsets and Stromal Cells from Human and Mouse Myocardial Specimens". *Journal of visualized experiments: JoVE* (2019), 10.3791/60015. doi:10.3791/60015.

Baranov, M. V., Kumar, M., Sacanna, S., Thutupalli, S., and Van Den Bogaart, G. "Modulation of Immune Responses by Particle Size and Shape". *Frontiers in Immunology* (2021), 11, 607945. doi:10.3389/fimmu.2020.607945.

Boorsma, C. E., Draijer, C., and Melgert, B. N. "Macrophage Heterogeneity in Respiratory Diseases". *Mediators of Inflammation* (2013), 2013, 769214. doi:10.1155/2013/769214.

Broz, P., Von Moltke, J., Jones, J. W., Vance, R. E., and Monack, D. M. "Differential Requirement for Caspase-1 Autoproteolysis in Pathogen-Induced Cell Death and Cytokine Processing". *Cell host & microbe* (2010), 8, 471-483. doi:10.1016/j.chom.2010.11.007.

Caicedo, M. S., Samelko, L., Mcallister, K., Jacobs, J. J., and Hallab, N. J. "Increasing Both Cocrmo-Alloy Particle Size and Surface Irregularity Induces Increased Macrophage Inflammasome Activation in Vitro Potentially through Lysosomal Destabilization Mechanisms". *J Orthop Res* (2013), 31, 1633-1642. doi:10.1002/jor.22411.

Chambers, M., Rees, A., Cronin, J. G., Nair, M., Jones, N., and Thornton, C. A. "Macrophage Plasticity in Reproduction and Environmental Influences on Their Function". *Frontiers in immunology* (2021), 11, 607328-607328. doi:10.3389/fimmu.2020.607328.

Chávez-Galán, L., Olleros, M. L., Vesin, D., and Garcia, I. "Much More Than M1 and M2 Macrophages, There Are Also Cd169+ and Tcr+ Macrophages". *Frontiers in Immunology* (2015), 6, 263. doi:10.3389/fimmu.2015.00263.

Compan, V., Martín-Sánchez, F., Baroja-Mazo, A., López-Castejón, G., Gomez, A. I., Verkhratsky, A., Brough, D., and Pelegrín, P. "Apoptosis-Associated Speck-Like Protein Containing a Card Forms Specks but Does Not Activate Caspase-1 in the Absence of Nlrp3 During Macrophage Swelling". *J Immunol*

(2015), 194, 1261-1273. doi:10.4049/jimmunol.1301676.

Dacoba, T. G., Anfray, C., Mainini, F., Allavena, P., Alonso, M. J., Torres Andón, F., and Crecente-Campo, J. "Arginine-Based Poly(I:C)-Loaded Nanocomplexes for the Polarization of Macrophages toward M1-Antitumoral Effectors". *Frontiers in Immunology* (2020), 11, 1412. doi:10.3389/fimmu.2020.01412.

Dai, J., Yang, P., Cox, A., and Jiang, G. "Lung Cancer and Chronic Obstructive Pulmonary Disease: From a Clinical Perspective". *Oncotarget* (2017), 8, 18513-18524. doi:10.18632/oncotarget.14505.

De Waele, J., Verhezen, T., Van Der Heijden, S., Berneman, Z. N., Peeters, M., Lardon, F., Wouters, A., and Smits, E. L. J. M. "A Systematic Review on Poly(I:C) and Poly-Iclc in Glioblastoma: Adjuvants Coordinating the Unlocking of Immunotherapy". *Journal of Experimental & Clinical Cancer Research* (2021), 40, 213. doi:10.1186/s13046-021-02017-2.

Diesel, B., Hoppstädter, J., Hachenthal, N., Zarbock, R., Cavelius, C., Wahl, B., Thewes, N., Jacobs, K., Kraegeloh, A., and Kiemer, A. K. "Activation of Rac1 Gtpase by Nanoparticulate Structures in Human Macrophages". *European Journal of Pharmaceutics and Biopharmaceutics* (2013), 84, 315-324. doi:10.1016/j.ejpb.2012.12.015.

Edin, S., Wikberg, M. L., Rutegård, J., Oldenborg, P.-A., and Palmqvist, R. "Phenotypic Skewing of Macrophages in Vitro by Secreted Factors from Colorectal Cancer Cells". *PloS one* (2013), 8, e74982-e74982. doi:10.1371/journal.pone.0074982.

Fischer, T., Tschernig, T., Drews, F., Brix, K., Meier, C., Simon, M., Kautenburger, R., and Schneider, M. "Sirna Delivery to Macrophages Using Aspherical, Nanostructured Microparticles as Delivery System for Pulmonary Administration". *European Journal of Pharmaceutics and Biopharmaceutics* (2021a), 158, 284-293. doi:10.1016/j.ejpb.2020.11.024.

Fischer, T., Winter, I., Drumm, R., and Schneider, M. "Cylindrical Microparticles Composed of Mesoporous Silica Nanoparticles for the Targeted Delivery of a Small Molecule and a Macromolecular Drug to the Lungs: Exemplified with Curcumin and Sirna". *Pharmaceutics* (2021b), 13, 844. doi:10.3390/pharmaceutics13060844.

Franceschi, C., Bonafè, M., Valensin, S., Olivieri, F., De Luca, M., Ottaviani, E., and De Benedictis, G. "Inflamm-Aging: An Evolutionary Perspective on Immunosenescence". *Annals of the New York Academy of Sciences* (2000), 908, 244-254. doi:10.1111/j.1749-6632.2000.tb06651.x.

Ghonime, M. G., Shamaa, O. R., Das, S., Eldomany, R. A., Fernandes-Alnemri, T., Alnemri, E. S., Gavrilin, M. A., and Wewers, M. D. "Inflammasome Priming by Lipopolysaccharide Is Dependent Upon Erk Signaling and Proteasome Function". *The Journal of Immunology* (2014), 192, 3881-3888. doi:10.4049/jimmunol.1301974.

Guilbaud, E., Gautier, E. L., and Yvan-Charvet, L. "Macrophage Origin, Metabolic Reprogramming and Il-1 Signaling: Promises and Pitfalls in Lung Cancer". *Cancers (Basel)* (2019), 11, 298. doi:10.3390/cancers11030298.

Guilliams, M., and Van De Laar, L. "A Hitchhiker's Guide to Myeloid Cell Subsets: Practical Implementation of a Novel Mononuclear Phagocyte Classification System". *Frontiers in Immunology* (2015), 6, 406. doi:10.3389/fimmu.2015.00406.

Hartmann, G., and Krieg, A. M. "Cpg DNA and Lps Induce Distinct Patterns of Activation in Human Monocytes". *Gene Therapy* (1999), 6, 893. doi:10.1038/sj.gt.3300880.

He, Y., Hara, H., and Núñez, G. "Mechanism and Regulation of Nlrp3 Inflammasome Activation". *Trends in Biochemical Sciences* (2016), 41, 1012-1021. doi:10.1016/j.tibs.2016.09.002.

Hoppstädter, J., Dembek, A., Höring, M., Schymik, H. S., Dahlem, C., Sultan, A., Wirth, N., Al-Fityan, S., Diesel, B., Gasparoni, G., Walter, J., Helms, V., Huwer, H., Simon, M., Liebisch, G., Schulz, M. H., and Kiemer, A. K. "Dysregulation of Cholesterol Homeostasis in Human Lung Cancer Tissue and Tumour-Associated Macrophages". *EBioMedicine* (2021), 72, 103578. doi:10.1016/j.ebiom.2021.103578.

Hoppstädter, J., Diesel, B., Linnenberger, R., Hachenthal, N., Flamini, S., Minet, M., Leidinger, P., Backes, C., Grässer, F., Meese, E., Bruscoli, S., Riccardi, C., Huwer, H., and Kiemer, A. K. "Amplified Host Defense by Toll-Like Receptor-Mediated Downregulation of the Glucocorticoid-Induced Leucine Zipper (Gilz) in Macrophages". *Frontiers in immunology* (2019), 9, 3111-3111. doi:10.3389/fimmu.2018.03111.

Hoppstädter, J., Hachenthal, N., Valbuena-Perez, J. V., Lampe, S., Astanina, K., Kunze, M. M., Bruscoli, S., Riccardi, C., Schmid, T., Diesel, B., and Kiemer, A. K. "Induction of Glucocorticoid-Induced Leucine Zipper (Gilz) Contributes to Anti-Inflammatory Effects of the Natural Product Curcumin in Macrophages". *The Journal of Biological Chemistry* (2016), 291, 22949-22960. doi:10.1074/jbc.M116.733253.

Hoppstädter, J., Seif, M., Dembek, A., Cavelius, C., Huwer, H., Kraegeloh, A., and Kiemer, A. K. "M2 Polarization Enhances Silica Nanoparticle Uptake by Macrophages". *Frontiers in pharmacology* (2015), 6, 55-55. doi:10.3389/fphar.2015.00055.

Hornung, V., Bauernfeind, F., Halle, A., Samstad, E. O., Kono, H., Rock, K. L., Fitzgerald, K. A., and Latz, E. "Silica Crystals and Aluminum Salts Activate the Nalp3 Inflammasome through Phagosomal Destabilization". *Nature Immunology* (2008), 9, 847-856. doi:10.1038/ni.1631.

Ivashkiv, L. B. "Ifnγ: Signalling, Epigenetics and Roles in Immunity, Metabolism, Disease and Cancer Immunotherapy". *Nature Reviews Immunology* (2018), 18, 545-558. doi:10.1038/s41577-018-0029-z.

Jang, H., Kim, E. H., Chi, S.-G., Kim, S. H., and Yang, Y. "Nanoparticles Targeting Innate Immune Cells in Tumor Microenvironment". *International Journal of Molecular Sciences* (2021), 22, 10009.

Jaumouillé, V., and Grinstein, S. "Receptor Mobility, the Cytoskeleton, and Particle Binding During Phagocytosis". *Current Opinion in Cell Biology* (2011), 23, 22-29. doi:doi.org/10.1016/j.ceb.2010.10.006.

Kirchenbaum, G., Hanson, J., Roen, D., and Lehmann, P. "Detection of Antigen-Specific T Cell Lineages and Effector Functions Based on Secretory Signature". *Journal of Immunological Sciences* (2019), 3, 14-20. doi:10.29245/2578-3009/2019/2.1168.

Kucki, M., Cavelius, C., and Kraegeloh, A. "Interference of Silica Nanoparticles with the Traditional Limulus Amebocyte Lysate Gel Clot Assay". *Journal of Innate Immunity* (2014), 20, 327-336. doi:10.1177/1753425913492833.

Kusaka, T., Nakayama, M., Nakamura, K., Ishimiya, M., Furusawa, E., and Ogasawara, K. "Effect of Silica Particle Size on Macrophage Inflammatory Responses". *PLoS One* (2014), 9, e92634. doi:10.1371/journal.pone.0092634.

Lamichhane, S., Anderson, J., Remund, T., Kelly, P., and Mani, G. "Dextran Sulfate as a Drug Delivery Platform for Drug-Coated Balloons: Preparation, Characterization, in Vitro Drug Elution, and Smooth Muscle Cell Response". *Journal of Biomedical Materials Research - Part B Applied Biomaterials* (2016), 104, 1416-1430. doi:10.1002/jbm.b.33494.

Leader, A. M., Grout, J. A., Maier, B. B., Nabet, B. Y., Park, M. D., Tabachnikova, A., Chang, C., Walker, L., Lansky, A., Le Berichel, J., Troncoso, L., Malissen, N., Davila, M., Martin, J. C., Magri, G., Tuballes, K., Zhao, Z., Petralia, F., Samstein, R., D'amore, N. R., Thurston, G., Kamphorst, A. O., Wolf, A., Flores, R., Wang, P., Müller, S., Mellman, I., Beasley, M. B., Salmon, H., Rahman, A. H., Marron, T. U., Kenigsberg, E., and Merad, M. "Single-Cell Analysis of Human Non-Small Cell Lung Cancer Lesions Refines Tumor Classification and Patient Stratification". *Cancer Cell* (2021), 39, 1594-1609.e1512. doi:10.1016/j.ccell.2021.10.009.

Li, F., and Zhu, W. "Linc00460 Promotes Angiogenesis by Enhancing Nf-Kb-Mediated Vegfa Expression in Cervical Cancer Cells". *Biochemical and Biophysical Research Communications* (2023), 671, 146-152. doi:doi.org/10.1016/j.bbrc.2023.05.063.

Li, Y., and Boraschi, D. "Endotoxin Contamination: A Key Element in the Interpretation of Nanosafety Studies". *Nanomedicine* (2016), 11, 269-287. doi:10.2217/nnm.15.196.

Li, Y., Fujita, M., and Boraschi, D. "Endotoxin Contamination in Nanomaterials Leads to the Misinterpretation of Immunosafety Results". *Frontiers in Immunology* (2017a), 8, 472. doi:10.3389/fimmu.2017.00472.

Li, Y., Shi, Z., Radauer-Preiml, I., Andosch, A., Casals, E., Luetz-Meindl, U.,

Cobaleda, M., Lin, Z., Jaberi-Douraki, M., Italiani, P., Horejs-Hoeck, J., Himly, M., Monteiro-Riviere, N. A., Duschl, A., Puntes, V. F., and Boraschi, D. "Bacterial Endotoxin (Lipopolysaccharide) Binds to the Surface of Gold Nanoparticles, Interferes with Biocorona Formation and Induces Human Monocyte Inflammatory Activation". *Nanotoxicology* (2017b), 11, 1157-1175. doi:10.1080/17435390.2017.1401142.

Lin, S. F., Jiang, P. L., Tsai, J. S., Huang, Y. Y., Lin, S. Y., Lin, J. H., and Liu, D. Z. "Surface Assembly of Poly(I:C) on Polyethyleneimine-Modified Gelatin Nanoparticles as Immunostimulatory Carriers for Mucosal Antigen Delivery". *Journal of Biomedical Materials Research - Part B Applied Biomaterials* (2019), 107, 1228-1237. doi:10.1002/jbm.b.34215.

Liu, Y.-C., Zou, X.-B., Chai, Y.-F., and Yao, Y.-M. "Macrophage Polarization in Inflammatory Diseases". *International Journal of Biological Sciences* (2014), 10, 520-529. doi:10.7150/ijbs.8879.

Lundberg, A. M., Drexler, S. K., Monaco, C., Williams, L. M., Sacre, S. M., Feldmann, M., and Foxwell, B. M. "Key Differences in Tlr3/Poly I:C Signaling and Cytokine Induction by Human Primary Cells: A Phenomenon Absent from Murine Cell Systems". *Blood* (2007), 110, 3245-3252. doi:10.1182/blood-2007-02-072934.

Lyons, C., Fernandes, P., Fanning, L. J., Houston, A., and Brint, E. "Engagement of Fas on Macrophages Modulates Poly I:C Induced Cytokine Production with Specific Enhancement of Ip-10". *PLoS ONE* (2015), 10, e0123635. doi:10.1371/journal.pone.0123635.

Maeda, A., Digifico, E., Andon, F. T., Mantovani, A., and Allavena, P. "Poly(I:C) Stimulation Is Superior Than Imiquimod to Induce the Antitumoral Functional Profile of Tumor-Conditioned Macrophages". *European Journal of Immunology* (2019), 49, 801-811. doi:10.1002/eji.201847888.

Magalhães, P., Lopes, A., Mazzola, P., Rangel-Yagui, C., Penna, T., and Pessoa, A. "Methods of Endotoxin Removal from Biological Preparations: A Review". *Journal of pharmacy & pharmaceutical sciences : a publication of the Canadian Society for Pharmaceutical Sciences, Société canadienne des sciences pharmaceutiques* (2007), 10, 388-404.

Márquez-Rodas, I., Longo, F., Rodriguez-Ruiz, M. E., Calles, A., Ponce, S., Jove, M., Rubio-Viqueira, B., Perez-Gracia, J. L., Gómez-Rueda, A., López-Tarruella, S., Ponz-Sarvise, M., Álvarez, R., Soria-Rivas, A., De Miguel, E., Ramos-Medina, R., Castañon, E., Gajate, P., Sempere-Ortega, C., Jiménez-Aguilar, E., Aznar, M. A., Calvo, A., Lopez-Casas, P. P., Martín-Algarra, S., Martín, M., Tersago, D., Quintero, M., and Melero, I. "Intratumoral Nanoplexed Poly I:C Bo-112 in Combination with Systemic Anti-Pd-1 for Patients with Anti-Pd-1-Refractory Tumors". *Sci Transl Med* (2020), 12. doi:10.1126/scitranslmed.abb0391.

Mcwhorter, F. Y., Wang, T., Nguyen, P., Chung, T., and Liu, W. F. "Modulation of Macrophage Phenotype by Cell Shape". *Proceedings of the National Academy of Sciences of the United States of America* (2013), 110, 17253-

17258. doi:10.1073/pnas.1308887110.

Möhwald, M., Pinnapireddy, S. R., Wonnenberg, B., Pourasghar, M., Jurisic, M., Jung, A., Fink-Straube, C., Tschernig, T., Bakowsky, U., and Schneider, M. "Aspherical, Nanostructured Microparticles for Targeted Gene Delivery to Alveolar Macrophages". *Advanced Healthcare Materials* (2017), 6, 1700478. doi:10.1002/adhm.201700478.

Mouasni, S., Gonzalez, V., Schmitt, A., Bennana, E., Guillonneau, F., Mistou, S., Avouac, J., Ea, H. K., Devauchelle, V., Gottenberg, J.-E., Chiocchia, G., and Tourneur, L. "The Classical Nlrp3 Inflammasome Controls Fadd Unconventional Secretion through Microvesicle Shedding". *Cell Death & Disease* (2019), 10, 190. doi:10.1038/s41419-019-1412-9.

Murugadoss, S., Lison, D., Godderis, L., Van Den Brule, S., Mast, J., Brassinne, F., Sebaihi, N., and Hoet, P. H. "Toxicology of Silica Nanoparticles: An Update". *Archives of Toxicology* (2017), 91, 2967-3010. doi:10.1007/s00204-017-1993-y.

Nahrendorf, M., Swirski, F. K., Aikawa, E., Stangenberg, L., Wurdinger, T., Figueiredo, J.-L., Libby, P., Weissleder, R., and Pittet, M. J. "The Healing Myocardium Sequentially Mobilizes Two Monocyte Subsets with Divergent and Complementary Functions". *The Journal of experimental medicine* (2007), 204, 3037-3047. doi:10.1084/jem.20070885.

Nakayama, M. "Macrophage Recognition of Crystals and Nanoparticles". *Front Immunol* (2018), 9, 103. doi:10.3389/fimmu.2018.00103.

Napierska, D., Thomassen, L. C. J., Lison, D., Martens, J. A., and Hoet, P. H. "The Nanosilica Hazard: Another Variable Entity". *Particle and Fibre Toxicology* (2010), 7, 39. doi:10.1186/1743-8977-7-39.

O'neill, L. a. J., Golenbock, D., and Bowie, A. G. "The History of Toll-Like Receptors — Redefining Innate Immunity". *Nature Reviews Immunology* (2013), 13, 453. doi:10.1038/nri3446.

Ovais, M., Guo, M., and Chen, C. "Tailoring Nanomaterials for Targeting Tumor-Associated Macrophages". *Advanced Materials* (2019), 31, 1808303. doi:10.1002/adma.201808303.

Palmieri, E. M., Menga, A., Martín-Pérez, R., Quinto, A., Riera-Domingo, C., De Tullio, G., Hooper, D. C., Lamers, W. H., Ghesquière, B., Mcvicar, D. W., Guarini, A., Mazzone, M., and Castegna, A. "Pharmacologic or Genetic Targeting of Glutamine Synthetase Skews Macrophages toward an M1-Like Phenotype and Inhibits Tumor Metastasis". *Cell Reports* (2017), 20, 1654-1666. doi:doi.org/10.1016/j.celrep.2017.07.054.

Paranjpe, M., and Müller-Goymann, C. C. "Nanoparticle-Mediated Pulmonary Drug Delivery: A Review". *Int J Mol Sci* (2014), 15, 5852-5873. doi:10.3390/ijms15045852.

Piancone, F., Saresella, M., Marventano, I., La Rosa, F., Santangelo, M. A.,

Caputo, D., Mendozzi, L., Rovaris, M., and Clerici, M. "Monosodium Urate Crystals Activate the Inflammasome in Primary Progressive Multiple Sclerosis". *Frontiers in immunology* (2018), 9, 983-983. doi:10.3389/fimmu.2018.00983.

Reimer, T., Brcic, M., Schweizer, M., and Jungi, T. W. "Poly(I:C) and Lps Induce Distinct Irf3 and Nf-Kb Signaling During Type-I Ifn and Tnf Responses in Human Macrophages". *Journal of Leukocyte Biology* (2008), 83, 1249-1257. doi:doi:10.1189/jlb.0607412.

Rey-Giraud, F., Hafner, M., and Ries, C. H. "In Vitro Generation of Monocyte-Derived Macrophages under Serum-Free Conditions Improves Their Tumor Promoting Functions". *PloS one* (2012), 7, e42656-e42656. doi:10.1371/journal.pone.0042656.

Ringleb, J., Strack, E., Angioni, C., Geisslinger, G., Steinhilber, D., Weigert, A., and Brune, B. "Apoptotic Cancer Cells Suppress 5-Lipoxygenase in Tumor-Associated Macrophages". *J Immunol* (2018), 200, 857-868. doi:10.4049/jimmunol.1700609.

Romaszko, A. M., and Doboszyńska, A. "Multiple Primary Lung Cancer: A Literature Review". *Advances in Clinical and Experimental Medicine* (2018), 27, 725-730. doi:10.17219/acem/68631.

Rostam, H. M., Reynolds, P. M., Alexander, M. R., Gadegaard, N., and Ghaemmaghami, A. M. "Image Based Machine Learning for Identification of Macrophage Subsets". *Scientific Reports* (2017), 7, 3521. doi:10.1038/s41598-017-03780-z.

Salvioni, L., Rizzuto, M. A., Bertolini, J. A., Pandolfi, L., Colombo, M., and Prosperi, D. "Thirty Years of Cancer Nanomedicine: Success, Frustration, and Hope". *Cancers (Basel)* (2019), 11, 1855. doi:10.3390/cancers11121855.

Schink, A., Neumann, J., Leifke, A. L., Ziegler, K., Fröhlich-Nowoisky, J., Cremer, C., Thines, E., Weber, B., Pöschl, U., Schuppan, D., and Lucas, K. "Screening of Herbal Extracts for Tlr2- and Tlr4-Dependent Anti-Inflammatory Effects". *PLoS One* (2018), 13, e0203907. doi:10.1371/journal.pone.0203907.

Sedighzadeh, S. S., Khoshbin, A. P., Razi, S., Keshavarz-Fathi, M., and Rezaei, N. "A Narrative Review of Tumor-Associated Macrophages in Lung Cancer: Regulation of Macrophage Polarization and Therapeutic Implications". *Translational lung cancer research* (2021), 10, 1889-1916. doi:10.21037/tlcr-20-1241.

Seif, M., Philippi, A., Breinig, F., Kiemer, A. K., and Hoppstädter, J. "Yeast (Saccharomyces Cerevisiae) Polarizes Both M-Csf- and Gm-Csf-Differentiated Macrophages toward an M1-Like Phenotype". *Inflammation* (2016), 39, 1690-1703. doi:10.1007/s10753-016-0404-5.

Smulders, S., Kaiser, J.-P., Zuin, S., Van Landuyt, K. L., Golanski, L., Vanoirbeek,

J., Wick, P., and Hoet, P. H. M. "Contamination of Nanoparticles by Endotoxin: Evaluation of Different Test Methods". *Particle and Fibre Toxicology* (2012), 9, 41. doi:10.1186/1743-8977-9-41.

Stefaniak, A. B., Guilmette, R. A., Day, G. A., Hoover, M. D., Breysse, P. N., and Scripsick, R. C. "Characterization of Phagolysosomal Simulant Fluid for Study of Beryllium Aerosol Particle Dissolution". *Toxicology in Vitro* (2005), 19, 123-134. doi:10.1016/j.tiv.2004.08.001.

Swanson, K. V., Deng, M., and Ting, J. P. Y. "The Nlrp3 Inflammasome: Molecular Activation and Regulation to Therapeutics". *Nature Reviews Immunology* (2019), 19, 477-489. doi:10.1038/s41577-019-0165-0.

Tschernig, T., Fischer, T., Grissmer, A., Beckmann, A., Meier, C., Lipp, P., and Schneider, M. "Silica Nanoparticles of Microrods Enter Lung Epithelial Cells". *Biomedical reports* (2018), 9, 156-160. doi:10.3892/br.2018.1117.

Turvey, S. E., and Broide, D. H. "Innate Immunity". *Journal of Allergy and Clinical Immunology* (2010), 125, S24-S32. doi:10.1016/j.jaci.2009.07.016.

Valbuena Perez, J. V., Linnenberger, R., Dembek, A., Bruscoli, S., Riccardi, C., Schulz, M. H., Meyer, M. R., Kiemer, A. K., and Hoppstädter, J. "Altered Glucocorticoid Metabolism Represents a Feature of Macroph-Aging". *Aging Cell* (2020), 19, e13156. doi:10.1111/acel.13156.

Wofford, K. L., Cullen, D. K., and Spiller, K. L. "Modulation of Macrophage Phenotype Via Phagocytosis of Drug-Loaded Microparticles". *Journal of Biomedical Materials Research Part A* (2019a), 107, 1213-1224. doi:10.1002/jbm.a.36617.

Wofford, K. L., Singh, B. S., Cullen, D. K., and Spiller, K. L. "Non-Genetic Reprogramming of Monocytes Via Microparticle Phagocytosis for Sustained Modulation of Macrophage Phenotype". *bioRxiv* (2019b), 674598. doi:10.1101/674598.

Wynn, T. A., Chawla, A., and Pollard, J. W. "Macrophage Biology in Development, Homeostasis and Disease". *Nature* (2013), 496, 445. doi:10.1038/nature12034.

Xue, J., Schmidt, S. V., Sander, J., Draffehn, A., Krebs, W., Quester, I., De Nardo, D., Gohel, T. D., Emde, M., Schmidleithner, L., Ganesan, H., Nino-Castro, A., Mallmann, M. R., Labzin, L., Theis, H., Kraut, M., Beyer, M., Latz, E., Freeman, T. C., Ulas, T., and Schultze, J. L. "Transcriptome-Based Network Analysis Reveals a Spectrum Model of Human Macrophage Activation". *Immunity* (2014), 40, 274-288. doi:10.1016/j.immuni.2014.01.006.

Yamasaki, K., and Eeden, S. F. V. "Lung Macrophage Phenotypes and Functional Responses: Role in the Pathogenesis of Copd". *International journal of molecular sciences* (2018), 19, 582. doi:10.3390/ijms19020582.

Yang, L., and Zhang, Y. "Tumor-Associated Macrophages: From Basic Research to Clinical Application". *Journal of Hematology & Oncology* (2017), 10, 58.

doi:10.1186/s13045-017-0430-2.

Yin, H., Fang, L., Wang, L., Xia, Y., Tian, J., Ma, L., Zhang, J., Li, N., Li, W., Yao, S., and Zhang, L. "Acute Silica Exposure Triggers Pulmonary Inflammation through Macrophage Pyroptosis: An Experimental Simulation". *Frontiers in Immunology* (2022), 13, 874459. doi:10.3389/fimmu.2022.874459.

Zhou, J., Tang, Z., Gao, S., Li, C., Feng, Y., and Zhou, X. "Tumor-Associated Macrophages: Recent Insights and Therapies". *Frontiers in Oncology* (2020), 10, 188. doi:10.3389/fonc.2020.00188.

7 Appendix

7.1 Abbreviation

Ag	agarose
ATP	adenosine triphosphate
BMMs	primary murine bone marrow-derived macrophages
CCL2	C-C motif chemokine ligand 2
CCR2	C-C motif chemokine receptor 2
cDNA	complementary deoxyribonucleic acid
CLSM	confocal laser scanning microscope
CSF1R	colony stimulating factor 1 receptor
CXCL8	C-X-C motif chemokine ligand 8
CXCL10	C-X-C motif chemokine ligand 10
DAMPs	damage-associated molecular patterns
DAPI	4,6-diamidino-2-phenylindole dihydrochloride
DS	dextran sulphate
DMSO	dimethyl sulfoxide
D-PBS	dulbecco's phosphate-buffered saline
(ds)RNA	synthetic double-stranded ribonucleic acid
e. coli	*Escherichia coli*
FACSwash	fluorescence-activated cell sorting wash
FCS	fetal calf serum
FMO	fluorescence-minus-one
FSC-A	forward scatter-area
GNP	gelatin and gelatin nanoparticles
GNPR	gelatin rods
HMDMs	primary peripheral blood human monocyte-derived macrophages
IFNG	interferon gamma
IL-1β	interleukin 1 beta
IL4	interleukin 4
IL10	interleukin 10

IL18	interleukin 18
IRAKs	IL1R-associated kinases
KO	knockout
LAL-Test	limulus amebocyte lysate
LPS	lipopolysaccharide
M-CSF	macrophage-colony stimulating factor
MFI	median fluorescence intensity
μRs	aspherical silica microparticles
mRNA	messenger ribonucleic acid
MSU	monosodium urate crystals
MTT	3-[4,5-dimethylthiazol-2-yl]-2,5 diphenyltetrazolium bromide
MYD88	myeloid differentiation primary-response protein 88
NLRP3	NOD-, LRR- and pyrin domain-containing protein 3
NPs	amorphous silica nanoparticles
NSCLC	non-small cell lung cancer
PAMPs	pathogen-associated molecular patterns
PBMCs	human peripheral blood mononuclear cells
PBS	phosphate-buffered saline
PEI	branched polyethyleneimine
PFA	paraformaldehyde
Phalloidin-TRITC	phalloidin–tetramethylrhodamine B isothiocyanate
qRT-PCR	quantitative real-time polymerase chain reaction
PMA	phorbol 12-myristate 13-acetate
PLGANP	poly(lactic-co-glycolic acid) nanoparticles
poly(I:C)	polyinosinic:polycytidylic acid
poly-ICLC	polyinosinic:polycytidylic acid with carboxymethylcellulose and poly-L-lysine
pro- IL-1β	pro-interleukin 1 beta
PRRs	pattern recognition receptors
PVA	polyvinyl acetate
P 188	poloxamer 188

RNA18S5	RNA, 18S ribosomal 5
SCLC	small cell lung cancer
SD	standard deviation
SDS	sodium dodecyl sulfate
SEAP	secreted embryonic alkaline phosphatase
SEM	standard error of the mean
siRNA	small interfering RNA
SSC-A	side scatter-area
TAMs	tumor-associated macrophages
TCM	tumor condensed medium
TLRs	Toll-like receptors
TLR 1/2	Toll-like receptor 1/2
TNF	tumor necrosis factor
TRAFs	adaptor molecules tumor necrosis factor (TNF) receptor-associated factors
VEGFA	vascular endothelial growth factor A
WT	wild type

7.2 List of figures

7.3 List of tables

7.4 Supplement

Table 7: *The concentration of applied µR batches in each experiment*

µR batch	1 Mio µR in 1 µl	loaded	Cell/well	Medium/well [ml]	µR/cell	plate	µg/ml	experiments
1	18	+	- 20k 50k, 100k	0.2 0.2	- 0.25, 0.5 -	96	100, 200 23, 45 100, 200	Endotoxin test HMDMs for IL1-B assay Reporter cell lines
2	-	-	- 50k	0.2 0.2		96	100, 200 Up 100	Endotoxin test MTT HMDMs (48 h)
3	5.5	+	-	0.2		96	100, 200	Endotoxin test
4	23,1	-	40k	0.2	Up 0.5	96	Up 115	HMDMs cytotoxicity IncuCyte
5	166		- 20k 50k, 100k	0.2	- 0.25, 0.5 -	96	100, 200 208, 415 100, 200	Endotoxin test HMDMs for IL1-B assay Reporter cell lines
6	100	-	- 20k 50k, 100k	0.2	- 0.25, 0.5 -	96	100, 200 125, 250 100, 200	Endotoxin test HMDMs for IL1-B assay Reporter cell lines
7	104	-	- 20k 50k, 100k	0.2	- 0.25, 0.5 -	96	100, 200 130, 260 100, 200	Endotoxin test HMDMs for IL1-B assay Reporter cell lines
8	14.8	-	244k 600k 50k, 100k 20k 20k 20k	1 2 0.2 0.2	0.5 0.5 - 0.25, 0.5 Up 0.5 Up 0.5	12 6 96 96	90 111 100, 200 37, 74 Up 74	Marker expression qPCR Reporter cell lines HMDMs for IL1-B assay MTT THP-1

9	14	+	244k 600k 50k, 100k 20k 20k	1 2 0.2	0.5 0.5 - 0.25, 0.5 Up 0.5	12 6 96	85 105 100, 200 35, 70 Up 70	Marker expression qPCR Reporter cell lines HMDMs for IL1-B assay MTT C57BL/6 WT BMMs
10	35.7	-	20k	0.2	0.5	96	Up 90	MTT cell lines (THP-1, RAW 264.7, A549) MTT C57BL/6 WT BMMs 129/SV WT BMMs
11	17.4 10.2	-	40k 20k	0.2	1 0.5	96	175 26	Phagoc. IncuCyte BMMs for ILR reporter cells MTT, IncuCyte C57BL/6
12	13.2	-	20k	0.2	0.5	96	19	BMMs for ILR reporter cells MTT, IncuCyte C57BL/6 BMMs MTT 129/SV WT BMMs
17		-	50k	0.2	-	96	Up 100	MTT HMDMs
18		-	50k	0.2	-	96	Up 100	MTT HMDMs
22		-	50k	0.2	-	96	Up 100	MTT HMDMs
23		-	50k	0.2	-	96	Up 100	MTT HMDMs (48)

8 Publication

8.1 Journal publication

Hoppstädter J, Dembek A, Höring M, Schymik H S, Dahlem C, Sultan A, Wirth N, **Al-Fityan S**, Diesel B, Gasparoni G, Walter J, Helms V, Huwer H, Simon M, Liebisch G, Schulz M H, and Kiemer A K. “Dysregulation of Cholesterol Homeostasis in Human Lung Cancer Tissue and Tumor-associated Macrophages”. *EBioMedicine* (2021), 72, 103578. doi.org/10.1016/j.ebiom.2021.103578.

Al-Fityan S*, Diesel B*, Fischer T, Ampofo E, Schomisch A, Mashayekhi V, Schneider M, and Kiemer, A K. “Nanostructured Microparticles Repolarize Macrophages and Induce Cell Death in an In Vitro Model of Tumour-Associated Macrophages”. *Pharmaceutics* (2023), 15, 1895. doi:10.3390/pharmaceutics15071895.
* These authors contributed equally to the work.

8.2 Conference publication

Fischer T, **Al-Fityan S**, Dembek A, Diesel B, Kiemer A K, and Schneider M. Development of a Novel Drug Carrier System for Specific Targeting of Human Macrophages, HIPS Symposium, Saarbrücken, 14 June 2018

Al-Fityan S, Fischer T, Diesel B, Schneider M and Kiemer A K. Novel Drug Carrier Systems for the Specific Repolarization of human Macrophages, HIPS Symposium, Saarbrücken, 27 – 28 June 2019

Al-Fityan S, Diesel B, Fischer T, Schneider M, and Kiemer A K. Aspherical Silica Microparticles as a Drug Delivery System: Effects on Viability and Primary Human Macrophages Polarization, Nanosafety 2020 virtual conference, 05 – 07 October 2020

9 Acknowledgment

الْحَمْدُ لِلَّهِ قَبْلَ كُلِّ أَحَدٍ وَالْحَمْدُ لِلَّهِ بَعْدَ كُلِّ أَحَدٍ وَالْحَمْدُ لِلَّهِ عَلَى كُلِّ حَالٍ

I would like to extend my deepest gratitude to Professor Alexandra K. Kiemer for providing me with the invaluable opportunity to complete my dissertation as part of her research group. Your guidance, support, and belief in me throughout my academic journey have been instrumental in my success. Thank you for your constant guidance and support.

I am deeply thankful to Professor Marc Schneider for agreeing to serve as the second examiner for my dissertation. Your contributions to the project, expertise, and insights have been invaluable and greatly appreciated. Thank you for your invaluable support and guidance.

I am deeply grateful to Dr. Britta Diesel for her support throughout my research journey. I am thankful for your guidance as my supervisor, the stimulating conversations, and the constant encouragement and assistance provided.

I am grateful to Dr. Thorben Fischer for his collaboration on this project as a PhD student under the guidance of Professor Marc Schneider. Thank you for providing the particles and for the many stimulating conversations and exchange of ideas.

I also want to thank the members of the Pharmaceutical Biology research group for the cooperation.

I am deeply grateful to my parents for instilling in me a love for science and a strong work ethic that has sustained me throughout my academic journey. Your encouragement and support have been invaluable, and I am grateful to have had such wonderful role models at the personal and professional levels who have taught me the importance of moral values above all else. Thank you for your guidance and support.

I am also deeply thankful to my husband for his unwavering support and encouragement during my dissertation. Your patience, understanding, and empathy have been essential, and I am grateful for your companionship during long and challenging days. Your constant listening and encouragement have helped me to persevere through the challenges of this journey.

I am grateful to my sisters, family, and friends for their moral support. I am also thankful to have met such wonderful people in Saarbrücken who have supported me morally and for making me feel like I have a second family.

Lastly, I am grateful to the higher power for guiding and protecting me throughout this journey. Without their guidance, none of this would have been possible.